NASA Conference Publication 10037

CO Oxidation Catalysts for Long-Life CO_2 Lasers

Compiled by
David R. Schryer
Langley Research Center
Hampton, Virginia

Collected papers and abstracts from an International Conference sponsored by the National Aeronautics and Space Administration and the Royal Signals and Radar Establishment and held at Langley Research Center
Hampton, Virginia
October 17-19, 1989

October 1989

National Aeronautics and Space Administration

TABLE OF CONTENTS

SESSION III: FUNDAMENTALS

SESSION IV: EXPERIMENTAL TECHNIQUES I

SESSION V: EXPERIMENTAL TECHNIQUES II

SESSION VI: LASER-CATALYST INTEGRATION AND APPLICATIONS

Pulsed-Discharge CO_2 Lasers

David V. Willetts
Royal Signals and Radar Establishment
United Kingdom

This abstract and paper not available at time of printing.

ABSTRACT: REVIEW OF NOBLE-METAL REDUCIBLE OXIDE (NMRO)

CATALYSTS AND CATALYSIS OF CO OXIDATION

Richard K. Herz
AMES/Chemical Engineering, B-010
University of California, San Diego
La Jolla, California 92093

INTRODUCTION

This paper presents a review of work on a class of materials referred to as "noble-metal reducible oxide catalysts" or "NMRO" catalysts by Schryer and coworkers at NASA Langley. This class of materials typically consists of an element in a metallic state (the "noble" metal) dispersed over a metal oxide which can be reduced to some extent under reaction or pretreatment conditions. The noble metals include Au, Ag, and the Pt-group metals, as well as other metals in some cases. The class also includes materials in which the noble metal is oxidized under some conditions, materials in which the some of the metal oxide may become completely reduced under some conditions, and complex materials composed of more than two metals or oxides.

An essential aspect of the NMRO materials of interest is that the combination of metal and reducible oxide has a synergistic effect. The materials have unique catalytic activity and/or selectivity characteristics which are not a simple addition of the characteristics of the separate materials. Synergistic effects have been demonstrated over Pt/SnO_2 CO oxidation catalysts and Pt/TiO_2 CO hydrogenation catalysts, for example. There are three ways in which the two types of components in MNRO materials can participate: (a) one component may substantially alter the properties of the other component, (b) the two components may each provide independent catalytic functions in a complex reaction mechanism, and/or (c) a unique site with a catalytic function may be formed through combination of the two components at the atomic level.

The range of materials considered is wide. At (or beyond) one far extreme, consider bifunctional Pt/Al_2O_3 petroleum reforming catalysts. Al_2O_3 is considered to be a nonreducible oxide. However, exposed Al cations, at sites which might be considered oxygen vacancies in the Al_2O_3 surface, can serve as acidic sites, when hydrated, that promote the isomerization of olefins. This function, combined with the dehydrogenating-hydrogenating function of Pt, forms a material that can catalyze the isomerization of paraffins. Mixed oxide catalysts lie at the other far extreme of the range of materials.

NMRO materials have important applications. Many of the applications involve oxidation or reduction reactions which involve transfer of oxygen atoms. In a noncatalytic application, Pt/SnO_2 and other materials serve as gas detectors. Reducing gases such as CO chemisorb on the metal, reduce the oxide in a stoichiometric reaction, and change the electrical characteristics of the oxide, providing the sensor signal. NMRO materials catalyze CO oxidation in many types of applications, hydrocarbon oxidation in catalytic heaters, CO, H_2 and hydrocarbon oxidation and NO reduction in automotive "three-way" catalysts. Hydrocarbons can be selectively oxidized over NMRO materials. CO and CO_2 can be hydrogenated over NMRO catalysts to form methane and higher hydrocarbons in Fischer-Tropsch processes. Methanol and other oxygenated products can also be formed during CO hydrogenation. In reactions not involving oxygen transfer, NMRO materials catalyze reforming reactions of hydrocarbons. NMRO materials also serve as catalytic electrodes in electrochemical processes and catalyze photochemical processes.

The processes by which noble metals and reducible oxides interact and catalyze reactions are complex and not well understood. This presentation will review previous studies of materials in this class, with special attention to gaining an understanding of low temperature CO oxidation activity. In order to

organize the material, the effect of the metal on the oxide will be discussed first, followed by the effect of the oxide on the metal, the interaction of the metal and oxide to form unique catalytic sites, and the possible ways in which the CO oxidation reaction is catalyzed by the NMRO materials.

METAL EFFECT ON OXIDE

Metals dispersed over metal oxides have been shown to catalyze the reduction of the oxide by CO and H_2 and the reoxidation of the metal by O_2. For H_2 and O_2, the action of the metal probably involves dissociative adsorption of the diatomic molecules. For adsorbed CO, H, and O on the metal, the oxidation and reduction reactions may occur at the interface between the metal and the oxide. Defect sites in the oxide located at the metal-oxide interface may participate in the reaction. In addition, CO and H have been shown to "spillover" from the metal to the oxide.

OXIDE EFFECT ON METAL

The effects of the oxide on the metal are more varied. Choice of the metal oxide affects the dispersion of the reduced metal that can be achieved and the dispersion and distribution of metals between metal particles in bimetallic catalysts. These effects indicate that there are significant interactions between the metal and the oxide support. For small metal particles, the electronic structure and catalytic behavior of the metal atoms may be affected by the oxide.

Except for gold, all of the "noble" metals can be oxidized to some extent under some conditions (e.g., pretreatment conditions if not reaction conditions). Oxide supports tend to stabilize the oxidized form of the supported metal against reduction treatments. Oxidation of large supported metal particles to form an oxide that "wets" the supporting oxide, followed by re-reduction of the noble metal, can lead to redistribution of the supported metal. Under severe oxidizing conditions, compound formation can occur between the oxide form of the supported metal and the oxide support, deactivating the metal.

Oxide or suboxide species can partially or completely cover the surfaces of supported metal particles, as has been shown for Pt/TiO_2. There are several possible mechanisms for this "decoration" of supported metal particles by oxide species. One mechanism can be a gradual growth of the oxide over the surface on the metal particle, or "encapsulaton," that is driven by interfacial energies. Suboxide species may dissolve in the metal under some conditions and then segregate to the surface to decorate the metal under other conditions. Under relatively severe reducing conditions, the oxide may be reduced to the metal and form an alloy with the supported noble metal. Under subsequent oxidizing conditions, segregation may occur to produce oxide species on the surface of the noble metal. Once this decoration occurs, the oxide species may modify the electronic structure and catalytic properties on neighboring noble metal atoms.

FORMATION OF UNIQUE SITES

If alloy formation occurs between the noble metal and the metal from the reduced oxide, unique catalytic sites can be formed, either through modification of the alloyed noble metal atoms or sites involving both types of metal atoms. At this meeting, Hoflund and coworkers will provide evidence for Pt-Sn alloy formation in Pt/SnO_2 catalysts. Other workers have demonstrated enhanced synergistic CO oxidation activity with metal alloys. If reoxidation of the metal alloy occurs under subsequent pretreatment or reaction conditions, the process might lead to redispersion of the noble metal over the supporting oxide as well as decoration of the noble metal by the oxide. The formation of unique sites at the interface between Pt and TiO_x overlayers have been proposed to catalyzed the dissociation of CO during CO hydrogenation to methane and higher hydrocarbons.

NMRO CATALYSIS OF CO OXIDATION

During oxidation of CO by O_2, two basic steps must occur: dissociation of the O_2 molecule and formation of and O-CO bond. Generally, these two steps are considered to occur in separate events. Over the surface of heterogeneous catalysts, then, O_2 must adsorb and dissociate and CO must adsorb next to and react with an O atom.

Over zero-valent noble metals (on inert, nonreducible oxide supports), CO and O2 compete for the same sites on the surface. Low temperature activity is minimal because CO covers the metal surface and inhibits O_2 adsorption. CO dominates the surface because O_2 adsorption has more stringent open site requirements since it must dissociate and because O_2 adsorption probabilities or "sticking coefficients" on bare metal surfaces are at least an order of magnitude lower than CO sticking coefficients.

Over metal oxide surfaces the picture is more complex. However, low temperature CO oxidation activity is also minimal over simple oxide surfaces, primarily because of the strong bonding of oxygen to the surface.

NMRO materials such as Pt/SnO_2 are synergistic combinations with significant low temperature CO oxidation activity. The limiting steps with conventional catalysts involve oxygen: competition between O_2 and CO adsorption over metal catalysts and removal of oxygen bound to oxide catalysts. Thus, we can postulate that one or both of these processes are facilitated over NMRO catalysts: O_2 adsorption and dissociation is enhanced relative to CO adsorption and/or oxygen can be removed from the oxide surface relatively easily. The latter process is a likely candidate to occur over NMRO catalysts since the oxide is relatively easily reducible and noble metals have been shown to catalyze the reduction of oxides.

An obvious way that the former process, O_2 adsorption and dissociation, can be enhanced relative to CO adsorption is provision of separate but neighboring sites for the two molecules. A possibility is that CO adsorbs over the metal in NMRO catalysts and O_2 adsorbs over the oxide or the metal-oxide interface. If this process is important, intimate intermixing of the two catalyst components at the atomic level becomes important. In addition, work by Hoflund and coworkers suggests that alloys between the noble metal and the metal from completely reduced oxide may be important.

In addition to eliminating competition between CO and O_2 by the presence of separate adsorption sites, O_2 dissociation may be facilitated over NMRO catalysts. Experimental studies have shown that the presence of H_2O can affect the behavior and possibly enhance the activity of NMRO catalysts. The way in which H_2O might participate is suggested by the mechanism of homogeneous CO oxidation in the gas phase. In the gas phase, traces of H_2 or H_2O serve as a catalyst of the CO oxidation reaction. O_2 is dissociated by collision with H to form OH and O radicals. CO is oxidized by collision with OH radicals to form CO_2 and H, not by collision with O atoms. Oxide surfaces are usually found in a hydroxylated and protonated state, even when H_2O has not been added to a reactant stream deliberately. Hydroxyl groups and protons on the reducible oxide surface might participate by catalyzing the dissociation of O_2. The possibility that CO is oxidized over NMRO catalysts by surface hydroxyl groups, as in the homogeneous reaction mechanism, must also be considered.

Research on other NMRO catalysts will be considered in relation to CO oxidation for closed cycle CO_2 laser applications and directions of future work will be outlined.

CO-OXIDATION CATALYSTS FOR LONG-LIFE CLOSED-CYCLE CO_2 LASERS

David R. Schryer, Billy T. Upchurch, Robert V. Hess, and George M. Wood
NASA Langley Research Center
Hampton, VA 23665

Barry D. Sidney, John D. Van Norman, and Irvin M. Miller
Science and Technology Corporation
Hampton, VA 23666

Kenneth G. Brown, Jacqueline Schryer, and David R. Brown
Old Dominion University
Norfolk, VA 23508

Gar B. Hoflund
University of Florida
Gainesville, FL 32611

Richard K. Herz
University of California, San Diego
La Jolla, CA 92093

INTRODUCTION

Pulsed CO_2 lasers have several potential remote-sensing applications, both military and non-military, which require long-life operation with high conversion-efficiency and good power-stability. However, two problems are potentially associated with such applications.

One problem is that the electrical discharge normally used to excite pulsed CO_2 lasers generally decomposes some of the CO_2:

$$CO_2 \xrightarrow{\text{Elec. Disch.}} CO + 1/2\ O_2$$

This decomposition is harmful to long-life laser operation both because of the loss of CO_2 and because of the buildup of O_2. The loss of CO_2 results in a corresponding gradual loss of laser power. The buildup of even relatively small concentrations of O_2 molecules can cause rapid power loss and even complete laser failure. Although CO_2 lasers differ somewhat in their tolerance of O_2, it is generally desirable to keep the O_2 concentration below a few tenths of 1 mole-percent. CO has no significant deleterious affect on laser performance at moderate concentrations.

The second problem is the fact that the atmosphere contains a significant concentration, about 300 ppm, of common-isotope CO_2 ($^{12}C^{16}O_2$). If common-isotope CO_2 is used in a CO_2 laser intended for atmospheric transmission, the emission frequencies available to the laser will correspond to the absorption frequencies of the atmospheric CO_2 and poor transmission will result.

The solutions to these two problems are superficially quite simple: (1) continuously remove O_2 as it is formed and replenish CO_2 and (2) use some form of rare-isotope CO_2 (such as $^{12}C^{18}O_2$, $^{13}C^{16}O_2$, or $^{13}C^{18}O_2$) in lasers intended for applications involving atmospheric transmission so that the emission frequencies of such lasers will differ from the absorption frequencies of atmospheric $^{12}C^{16}O_2$. Actual implementation of these two solutions, however, is far from simple.

Removal of O_2 and replenishment of CO_2 can be achieved in certain applications simply by operating the laser open-cycle with a continuous flow-through of fresh laser-gas and the consequent removal of dissociation products. However, for space-based applications or other applications involving weight and/or volume constraints, the amount of gas required for open-cycle operation would be unacceptable and, instead, closed-cycle laser operation with recycling of the laser gases would be imperative. Closed-cycle operation would also be highly desirable for any applications where rare-isotope CO_2 is used for enhanced atmospheric transmission because of the expense of the large volumes of rare-isotope gas which would be required for flow-through operation.

Achievement of closed-cycle operation of pulsed CO_2 lasers requires catalytic recombination of the decomposition products, CO and O_2, to regenerate CO_2.

$$CO + 1/2\ O_2 \xrightarrow{\text{Cat.}} CO_2$$

Candidate catalysts must have high efficiency at steady-state laser conditions which are, generally, 25°C to 100°C and about one atmosphere of total pressure with low partial-pressures of CO and O_2. Some excess CO may be added to the laser-gas mixture but generally it is not. It is desirable that little or no heating of the catalyst be required in order to minimize power consumption.

The catalytic oxidation of CO to CO_2 has been extensively studied at various conditions for a number of catalysts. These include the noble metals and various metal oxides (refs. 1 and 2) and the commercial catalyst, Hopcalite (ref. 3), which is a mixture of CuO and MnO_2 plus small quantities of other oxides. However, few catalysts have sufficiently high activity to allow operation at the low steady-state temperatures and low oxygen partial pressures characteristic of typical pulsed CO_2 lasers.

The most promising catalysts studied to date, whose performance has been verified by actual closed-cycle laser operation, consist of Pt and/or Pd on tin (IV) oxide (refs. 4 and 5). A systemmatic study of (Pt, Pd)/SnO_2 catalysts for use with closed-cycle pulsed CO_2 lasers, including the preparation and testing of improved catalyst formations, has been in progress at the Langley Research Center of NASA (LaRC) for the past several years (refs. 5-16). This study has been expanded by joint research with investigators at Old Dominion University, the University of Florida, the University of California, San Diego, and Science and Technology Corporation (refs. 1, 5-11, 13, 15-21).

TEST FACILITIES

Catalyst research at LaRC is carried out both in laboratory reactors and in a commercial CO_2 TEA laser.

Laboratory Reactors

Laboratory reactors are used for catalyst study under controlled conditions. Several laboratory reactors are presently operational, most of which are flow-through (plug-flow) reactors. In these reactors a test-gas mixture flows through a reactor tube containing a catalyst sample which is situated in a temperature-controlled oven. The gas which enters and exits the reactor tube is quantitatively analyzed with either a gas chromatograph (GC) or mass spectrometer (MS) and from this analysis the amount of CO and O_2 converted to CO_2 by the catalyst sample is determined. For many tests the test-gas mixtures used are purchased premixed in a high-purity He carrier, typically 1.00 percent CO and 0.50 percent O_2 plus 2.00 percent Ne (as an internal calibration standard for gas analysis). For some tests the gas mixtures are blended in the laboratory using high-purity component gases and calibrated flow controllers.

All except one of the reactors are used with common-isotope gases and use GC's for gas analysis. These GC's are fully automated so that tests with common-isotope gases can be conducted in the flow-through reactors continuously around-the-clock. One flow-through reactor is used with rare-isotope gases and uses an MS for gas analysis.

Studies performed in the flow-through reactors are (1) parametric studies to determine the effect of such parameters as catalyst mass, temperature, reactor residence-time, pretreatment conditions, etc., on the performance of a given catalyst material, (2) comparison of different catalyst compositions (such as Pt/SnO_2, Pd/SnO_2, and $Pt + Pd/SnO_2$) and concentrations to determine the optimum catalyst formulation, (3) long-term performance tests (using an automated-GC reactor) to determine how a catalyst performs with long-term exposure to the test gases, and (4) isotopic studies (using the MS reactor) to determine the interaction of a given catalyst with rare-isotope gases.

A recirculating and a pulsed reactor are also available. In the recirculating reactor a gas mixture is continuously recirculated through a temperature-controlled reactor tube containing a sample of catalyst, and the conversion of CO and O_2 to CO_2 is monitored as a function of time. Gas analysis is performed with a GC. This reactor is used to study the kinetics and mechanism of catalysis for selected catalyst compositions.

With the pulsed reactor, the single-gas or gas-mixture to be studied (in a He carrier) is exposed to the catalyst sample in a series of discrete pulses. The pulses are spaced in time such that the gas exiting the reactor after each pulse can be analyzed by GC. The cumulative gain or loss of each species as a function of time can thus be more finely resolved than with the continuous flow-through and recirculating reactors. The pulsed reactor is used for both reaction and chemisorption studies.

Laser Reactor

A Lumonics model TEA-820 pulsed CO_2 laser (7 Watt, 1-50 pulses/second) is available for catalyst testing under actual laser operating conditions. The laser is operated closed-cycle with an external catalyst bed (in a temperature-controlled oven) and the results are compared with the open-cycle performance of the laser at the same flow rate. It is intended that ultimately the laser will be operated with no heating of the catalyst other than by the laser gas. Gas analysis is performed with a GC in current common-isotope tests. An MS will be used when the laser is operated with rare-isotope CO_2.

RESULTS

The following results have been obtained in studies performed to date.

Common-Isotope Laboratory Studies

(1) Pt on SnO_2 (Pt/SnO_2) has significantly higher catalytic activity for CO oxidation than either Pt or SnO_2 alone (ref. 5). The effect is clearly synergistic and apparently involves separate but complementary roles for the Pt and SnO_2 phases.

(2) The efficiency of Pt/SnO_2-catalyzed oxidation of CO to CO_2 is approximately proportional to catalyst mass until complete conversion is achieved (ref. 5).

(3) The catalyst masss required to achieve complete oxidation of a given concentration of CO is roughly proportional to the flow rate of the gas through the catalyst (ref. 7). This makes possible the extrapolation of results obtained with laboratory reactors to CO_2 lasers.

(4) A technique for achieving much higher Pt loadings than are commercially available has been developed (ref. 16). Platinum loadings as high as 46 percent have been achieved.

(5) The activity for CO oxidation of Pt/SnO_2 catalysts increases with Pt loading until a maximum activity is reached at about 17 percent Pt (Ref. 14). Since Pt loadings between 11 percent and 17 percent and between 17 percent and 24 percent were not tested, the precise optimum loading is somewhat uncertain but it is believed to lie in the range of 15 to 20 percent.

(6) Bimetalic catalysts consisting of Pt and Pd on SnO_2 have a higher activity than catalysts with the same total loading of either metal alone. The optimum Pd loading for maximum catalyst activity is about 5 percent (Ref. 22).

(7) A reductive pretreatment enhances the activity of Pt/SnO_2 catalyts relative to no pretreatment or to pretreatment with O_2 or an inert gas (Ref. 15). Pretreatment consists of a flow of the pretreatment gas (in a helium carrier, for safety and convenience) over the catalyst sample at an elevated temperature prior to exposure of the catalyst to the reaction gas mixture at the selected reaction temperature. Both CO and H_2 are suitable gases for reductive pretreatment (Ref. 15); in this study they were used at a concentration of 5 percent in He.

(8) The temperature at which a Pt/SnO_2 catalyst is pretreated can affect its subsequent activity (Ref. 15). Pretreatment temperatures of 125°C, 175°C, and 225°C resulted in equal catalytic activity, for the catalyst tested, but pretreatment at 100°C yielded somewhat lower activity.

(9) Duration of the pretreatment also affects subsequent catalyst activity (Ref. 15). Catalyst activity after a 20-hour CO pretreatment was found to be lower than after a 1-hour pretreatment. Too short a pretreatment also diminishes catalyst activity. For optimum results the effluent gases from the pretreatment should be analyzed and the pretreatment terminated when no significant yield of oxidation product (CO_2 or H_2O) is detected.

(10) Pretreatment of a Pt/SnO_2 catalyst sample at elevated temperatures--above about 125°C--results in an initial dip in catalyst activity before the steady-state activity is achieved for studies in the flow-through reactors (Ref. 15). No dip occurs if the catalyst is pretreated at lower temperatures. If the catalyst is exposed to moisture following pretreatment but prior to exposure to the reaction gas mixture, or if the reaction gas mixture is humidified, no dip occurs (Ref. 15).

(11) In many cases moisture not only eliminates the initial dip in catalyst activity, it also enhances the activity of the catalyst (Ref. 15). A possible explanation of this phenomenon as well as others described in this section is presented in the next section of this paper.

(12) No initial dip in catalyst activity has been observed in flow-through reactor studies when the Pt loading exceeded 24 percent even at pretreatment temperatures of 225°C. No dip has been observed in studies in the recirculating reactor at any Pt loading or pretreatment temperature.

(13) The activities of Pt/SnO_2 catalysts exhibit some decay with time. Initial activity can be readily restored by outgassing the catalyst either by heating it or by exposing it to an inert gas for about 2 hours (Ref. 23). In either case, restoration of activity has been found to be associated with outgassing of CO_2 from the catalyst but decay in activity occurs again when CO oxidation is resumed.

(14) The yield of CO_2 for a given catalyst sample and set of reaction conditions is increased by addition of O_2 to a stoichiometric mixture of CO and O_2 and decreased by addition of CO to such a mixture (Ref. 22). The reaction has been found to be first order with respect to O_2 concentration. Determination of the reaction order with respect to CO concentration is currently in progress.

Rare-Isotope Catalyst Studies

(1) Reaction of $C^{18}O$ and $^{18}O_2$ on a common-isotope $Pt/Sn^{16}O_2$ catalyst yields about 85 percent $C^{18}O_2$ and 15 percent $C^{18}O^{16}O$ (Ref. 10). This concentration of the mixed-isotope species $C^{18}O^{16}O$ is unacceptable.

(2) A technique has been developed for modifying the surface of common-isotope Pt/SnO_2 so that all reactive surface oxygens are ^{18}O (ref. 10). Reaction of $C^{18}O$ and $^{18}O_2$ over this modified catalyst yielded only $C^{18}O_2$, within experimental error, in a test of 17 days (Ref. 24).

(3) Rare-isotope studies have indicated that some sort of carbonate or biocarbonate species is formed when CO is oxidized on Pt/SnO_2 catalysts (ref. 10).

Surface Characterization Studies

Extensive surface characterization studies have been performed by Hoflund and coworkers at the University of Florida. These studies utilized an ultrahigh vacuum system containing multiple surface techniques including ion scattering spectroscopy (ISS), electron spectroscopy for chemical analysis (ESCA), Auger electron spectroscopy (AES), and electron stimulated desorption (ESD) with pretreatment capabilities at elevated pressures and temperatures. The following results have been obtained:

(1) The surface hydrogen present at a polycrystalline tin oxide film has been studied using ESD before and after annealing the film at 500°C (Ref. 17). Annealing reduces the concentration of surface hydrogen by a factor of 8, and energy analysis of the desorbing ions indicates that at least 3 chemical bonding states of H are present at the surface. Further research is necessary to elucidate the nature of these states.

(2) The reduction by vacuum annealing from 200 to 350°C of a platinized tin oxide film has been examined using ISS, ESCA and AES (Ref. 18). The data show that tin is reduced to metallic form which alloys with the supported platinum.

(3) Since Pt/Sn alloys form in reduced Pt/Sn systems, it is important to characterize the behavior of Pt/Sn alloys. As part of a continuing study of Pt/Sn alloy surfaces, the reduction in H_2 of an air-exposed Pt/Sn alloy surface has been examined using ISS, ESCA and angle-resolved AES (Ref. 19). Initially, a tin-depleted Pt-rich region is covered by a 30Å thick uniform layer of tin oxide. During reduction, oxygen is removed from the surface forming metallic tin and platinum migrates to the surface through vacancies left by the oxygen to alloy with the metallic tin.

(4) An unsupported commercial 2 percent Pt/SnO_2 catalyst has been examined using ISS, AES, and ESCA as a function of pretreatment temperature (air exposed, 75, 100, 125, and 175°C) at 4 and 40 Torr of CO (Ref. 25). During the reduction the O/Sn ratio is decreased, the Pt is reduced from platinum oxides to $Pt(OH)_2$, the surface hydroxyl group concentration is reduced, and a Pt/Sn alloy forms. This is the same catalyst whose activity as a function of reductive-pretreatment temperature is discussed in item (8) of the section on common-isotope studies.

(5) A silica-supported Pt/Sn catalyst developed at NASA has been characterized before and after pretreatment at 125 and 225°C in CO (Ref. 20). The 125°C reduction, which yields a highly catalytically-active surface, converts the Pt oxides primarily to $Pt(OH)_2$. Reduction at 225°C produces a surface which is much less active catalytically. The surface studies show that this is due to coverage of the surface Pt by contaminant species, including silica, and reduction of the $Pt(OH)_2$ to metallic Pt.

Laser Studies

(1) The Lumonics Model TEA-820 laser has been operated closed-cycle with a catalyst bed of 150 g of 2 percent Pt/SnO_2 at 100°C (Refs. 5 and 8). The laser achieved 96.5 percent (± 3.5 percent) of steady-state open-cycle power for 28 hours (1×10^6 pulses at 10 pulses/second). Both the laser and catalyst were fully operational at the conclusion of the test. Additional laser tests are in progress.

(2) Herz and coworkers at the University of California, San Diego, (ref. 21) have developed a computer program which can be used to design catalyst monoliths for specific laser applications. The critical information a user needs to supply is the first-order-overall rate constant and activation energy for the catalyst formulation of interest. After the user supplies other information such as gas composition, gas flow rate and monolith dimensions, the program computes the conversion of oxygen and pressure drop as a function of monolith length. By varying input parameters, the user can investigate various design alternatives. One conclusion of a design study performed with the program is that standard off-the-shelf monoliths are not optimal for use in CO_2 laser applications. This is because standard monoliths have been designed for combustion or emission control applications where reactions occur very fast at high temperature and gas flow-rates are high. Gas flow-rates in lasers are relatively low and reactions occur at low temperatures and thus, are relatively slow. Monoliths optimized for laser applications to provide for minimum monolith size will have thicker layers of active catalyst material than monoliths used for combustion and emission control. The computer program is available through NASA's COSMIC office.

DISCUSSION

A possible explanation of the experimental observations reported in the previous section is as follows. It is postulated that surface OH groups participate in the oxidation of CO chemisorbed on Pt sites. Hoflund and coworkers have observed OH groups on both tin-oxide and platinized tin-oxide surfaces (refs. 17 and 25). Reductive pretreatment of the catalyst enhances the chemisorption of O_2 but pretreatment at elevated temperatures also dehydrates the catalyst surface and thereby significantly depletes the surface concentration of OH. The initial reaction which occurs when the catalyst is exposed to the test-gas mixture further depletes the surface concentration of OH and partially re-oxidizes the surface. This results in the observed decline in catalyst activity. Rehydroxylation of the surface, probably by migration of H (or H^+) from the catalyst bulk, eventually restores the catalyst activity. The sequential decline and increase in catalyst activity results in the observed dip. If the OH concentration at the catalyst surface is restored by humidification of either the catalyst or the reaction gas no dip is observed. Humidification of the catalyst surface may increase the OH concentration above the initial value and the activity of the catalyst may then be enhanced as reported in Reference 15.

Most of the CO_2 formed immediately desorbs from the Pt phase, but a fraction of the CO_2 molecules interact with surface OH sites and are retained, probably as bicarbonate. This bicarbonate eventually undergoes decomposition, but until such decomposition occurs, the chemisorbed-CO_2/bicarbonate species

ties up OH sites and, thus, contributes to the observed decay in catalyst activity. Outgassing of the chemisorbed CO_2 restores the catalyst activity as observed.

CONCLUDING REMARKS

Noble-metal/tin-oxide based catalysts such as Pt/SnO_2 have been shown to be good catalysts for the efficient oxidation of CO at or near room temperature. They are the most promising catalysts for use in closed-cycle pulsed CO_2 lasers whose performance has actually been verified by tests in such lasers. The catalysts require a reductive pretreatment and traces of hydrogen or water to exhibit their full activity. Addition of Palladium enhances the activity of these catalysts with about 15 to 20 percent Pt, 5 percent Pd, and the balance SnO_2 being an optimum composition. Unfortunately, these catalysts presently exhibit significant decay due in part to CO_2 retention, probably as a bicarbonate. Research on minimizing the decay in activity of these catalysts is currently in progress. A proposed mechanism of CO oxidation on Pt/SnO_2-based catalysts is being developed and is discussed in this paper. The mechanism, although at present incomplete, is consistent with experimental results obtained to date.

REFERENCES

1. Herz, Richard D.: Chemical Engineering Design for CO Oxidation Catalysts. Closed-Cycle Frequency-Stable CO_2 Laser Technology, Carmen E. Batten, Irvin M. Miller, George M. Wood, Jr., and David V. Willetts, Eds., NASA CP-2456, pp. 103-112, 1987.

2. Engel, T., and Ertl, G.: Oxidation of Carbon Monoxide. The Chemical Physics of Solid Surfaces and Heterogeneous Catalysis, P. A. King and D. P. Woodruff, Eds., pp. 73-93, Elsevier, New York, 1982.

3. Kiang, San: Transient Isotopic Tracing Technique for the Resolution of the Room Temperature Oxidation of Carbon Monoxide Catalyzed by Commercial Hopcalite Catalyst. Pd.D. Thesis, Columbia Univeristy, 1978.

4. Stark, D. S.; Crocker, A.; and Steward, G. J.: A Sealed 100 Hz CO_2 TEA Laser Using High CO_2 Concentrations and Ambient-Temperature Catalysts. J. Phys. E. Sci. Instrum., vol. 16, pp. 158-161, 1983.

5. Brown, Kenneth G.; Sidney, B. D.; Schryer, D. R.; Upchurch, B. T.; Miller, I. M.; Wood, G. M.; Hess, R. V.; Batten, C.; Burney, L. G.; Paulin, P. A.; Hoyt, R.; and Schryer, J.: Catalytic Recombination of Dissociation Products with Pt/SnO_2 for Rare and Common Isotope Long-Life, Closed-Cycle CO_2 Lasers. SPIE Proc., vol. 663, pp. 136-144, 1986.

6. Rogowski, R. S.,; Miller, I. M..; Wood, G. M.; Schryer, D. R.; Hess, R. V.; and Upchurch, B.T.: Evaluation of Catalyst for Closed-Cycle Operation of High Energy Pulsed CO_2 Lasers. SPIE Proc., vol. 415, pp. 112-117, 1983.

7. Miller, I. M.; Wood, G. M. Jr.; Schryer, D. R.; Hess, R. V.; Upchurch, B. T., and Brown, K. G.: Optimization of the Catalytic Oxidation of CO for Closed-Cycle CO_2 Laser Applications. NASA TM-86421, 1985.

8. Sidney, Barry D.; Schryer, David R.; Upchurch, Billy T.; Hess, Robert V.; Wood, George M.; Miller, Irvin M.; Burney, L. Garland; Brown, Kenneth G.; Van Norman, John D.; and Schryer, Jacqueline: Research on Catalysts for Long-Life Closed-Cycle CO_2 Laser Operation. SPIE Proc., vol. 783, pp. 162-168, 1987.

9. Schryer, David R.; Sidney, Barry D.; Miller, Irwin M.; Hess, Robert V.; Wood, George M.; Batten, Carmen E.; Burney, L. Garland; Hoyt, Ronald F.; Paulin, Patricia A.; Brown, Kenneth G.; Schryer, Jacqueline; and Upchurch, Billy T.: NASA-LaRC Research on Catalysts for Long-Life Closed-Cycle CO_2 Lasers. Closed-Cycle Frequency-Stable CO_2 Laser Technology, Carmen E. Batten, Irvin M. Miller, George M. Wood, Jr., and David V. Willetts, Eds., NASA CP-2456, pp. 113-120, 1987.

10. Upchurch, Billy T.; Wood, George M. Jr.; Hess, Robert V.; and Hoyt, Ronald F.: Rare Isotope Studies Involving Catalytic Oxidation of CO Over Platinum-Tin Oxide. Closed-Cycle, Frequency-Stable CO_2 Laser Technology, Carmen E. Batten, Irvin M. Miller, George M. Wood, Jr., and David V. Willetts, Eds., NASA CP-2456, pp. 193-198, 1987.

11. Batten, Carmen E.; Miller, Irvin M.; Paulin, Patricia A.; and Schryer, Jacqueline: Studies of CO Oxidation on Pt/SnO_2 Catalyst in Surrogate CO_2 Laser Facility. Closed-Cycle, Frequency-Stable CO_2 Laser Technology, Carmen E. Batten, Irvin M. Miller, George M. Wood, Jr., and David V. Willetts, Eds, NASA CP-2456, pp. 193-198, 1987.

12. Sidney, Barry D.: Studies of Long-Life Pulsed CO_2 Laser with Pt/SnO_2 Catalyst. Closed-Cycle, Frequency-Stable CO_2 Laser Technology, Carmen E. Batten, Irvin M. Miller, George M. Wood, Jr., and David V. Willetts, Eds., NASA CP-2456, pp. 211-218, 1987.

13. Brown, K. G.; Schryer, J.; Schryer, D. R.; Upchurch, B. T.; Wood, G. M.; Miller, I. M.; Sidney, B. D.; Batten, C. E.; and Paulin, P. A.: Characterization of Pt/SnO_2 Catalysts for CO Oxidation. Closed-Cycle, Frequency-Stable CO_2 Laser Technology, Carmen E. Batten, Irvin M. Miller, George M. Wood, Jr., and David V. Willetts, Eds., NASA CP-2456, pp. 219-226, 1987.

14. Hess, R. V.; Buoncristiani, A. M.; Brockman, P.; Bair, C. H.; Schryer, D. R.; Upchurch, B. T.; and Wood, G. M.: Recent Advances in Efficient Long-Life, Eye-Safe Solid-State and CO_2 Lasers for Laser Radar Applications. SPIE Proc., vol. 999, pp. 2-18, 1989.

15. Schryer, David, R.; Upchurch, Billy T.; Van Norman, John D.; Brown, Kenneth G.; and Schryer, Jacqueline: The Effects of Pretreatment Conditions on a Pt/SnO_2 Catalyst for the Oxidation of CO in CO_2 Lasers. Submitted to J. Catalysis, 1989.

16. Upchurch, Billy T.; Schryer, David R.; Wood, George M.; and Hess, Robert V.: Development of CO Oxidation Catalysts for the Laser Atmospheric Wind Sounder (LAWS). SPIE Proc., Vol. 1062, 1989.

17. Hoflund, Gar B.; Grogan, Austin L., Jr.; Asbury, Douglas A.; and Schryer, David R.: A Characterization Study of a Hydroxylated Polycrystalline Tin Oxide Surface. Thin Solid Films, vol. 169, pp. 69-77, 1989.

18. Gardner, Steven D.; Hoflund Gar B.; Davidson, Mark R.; and Schryer, David R.: Evidence of Alloy Formation During Reduction of Platinized Tin Oxide Surfaces. J. Catalysis, vol. 115, pp. 132-137, 1989.

19. Gardner, Steven D.; Hoflund, Gar B.; and Schryer, David R.: Surface Characterization Study of the Reduction of an Air-Exposed Pt_3Sn Alloy: Part IV. J. Catalysis (in press).

20. Gardner, Steven D.; Hoflund, Gar B.; Schryer, David R.; and Upchurch, Billy T.: Platinized Tin Oxide Catalysts for CO_2 Lasers: Effects of Pretreatment. SPIE Proc., vol. 1062, pp. 21-28, 1989.

21. Herz, R. K.; Guinn, K.; Goldblum, S.; and Noskowski, E.: Design of Catalytic Monoliths for Closed-Cycle Carbon Dioxide Lasers. Final Report for NASA Contract NAG-1-823, Univ. of Califiornia, San Diego, 1989.

22. Upchurch, Billy T.; Brown, David R.; Miller, Irvin M., and Schryer, David R.: LaRC-Developed Catalysts for CO_2 Lasers. This volume, 1989.

23. Van Norman, John D.; Schryer, David R.; Brown, Kenneth G.; Schryer, Jacqueline; Ohorodnik, Susan K.; and Brown, David R.: Effect of H_2O and CO_2 on CO-Oxidation Catalyst Efficiency. This volume, 1989.

24. Upchurch, Billy T.; Miller, Irvin M.; Brown, David R.; Wood, George M., Jr.; Schryer, David R.; and Hess, Robert V.: Rare-Isotope and Kinetic Studies of Pt/SnO_2 Catalysts. This volume, 1989.

25. Grawdy, Jean E.; Hoflund, Gar B.; Gardner, Steven D.; Yngvadottir, Eva; and Schryer, David R.: Characterization Studies of a Commercial Pt/SnO_2 Catalyst. This volume, 1989.

Status of NASA Laser Atmospheric Wind Sounder (LAWS) Study

Richard G. Beranek, James Bilbro,
William D. Jones, and Daniel E. Fitzjarrald
NASA Marshall

This abstract and paper not available at time of printing.

THE OXIDATION OF CARBON MONOXIDE USING TIN OXIDE-BASED CATALYSTS

Christopher F. Sampson and Norman Jorgensen
United Kingdom Atomic Energy Authority
Harwell Laboratory, Oxfordshire, OX11 ORA
United Kingdom

ABSTRACT

This paper describes the development of a tin oxide/precious metal coated catalytic device for the recombination of carbon monoxide and oxygen resulting from the dissociation of carbon dioxide in a laser system. The study included an evaluation of the method of preparation of the tin oxide sol by a base peptisation route. The particle size, and hence surface area, of the calcined tin oxide depended critically on the preparation route and the pre-treatment conditions. Suitable precious metals and methods of addition were then selected during activity and surface area screening measurements. Subsequent studies covered powders and catalyst coated artefacts which could be doped for enhanced activity with good stability. The principal features of prepared devices are outlined, including some of the physical and mechanical properties. Also discussed are the methods for coating artefacts and the extent of catalysts interaction with the gaseous environment. The paper will show the activity of catalysts at various times and temperatures in simulated and working conditions, together with some speculation about the methods by which the recombination reaction and particle deactivation occur.

PHILLIPS CO OXIDATION CATALYSTS FOR LONG-LIFE CO_2 LASERS: ACTIVITY AND FUNDAMENTAL STUDIES

J. H. Kolts, D. J. Elliott, and F. Pennella
Phillips Petroleum Company
Bartlesville, Oklahoma 74004

ABSTRACT

Four different catalysts have been developed specifically for use by the CO_2 laser industry. Two of the catalysts have been designed for use in situations where high per-unit-volume activity is needed, the other two have been designed for situations where pressure drop across the catalyst must be minimized. A complete description of how the catalysts are tested as well as methods used to determine conversion efficiency will be presented. Activity data as a function of time and reaction temperature will be presented and will be correlated to some of the physical characteristics of the catalysts. In addition the effects of catalyst preparation variables and activation procedures will be discussed. Equilibrium activities for the catalysts (measured after the initial deactivation period) will be shown to be in the range of 1.2 to 2.2 cc CO per minute per gram of catalyst at STP.

In addition to the basic catalyst activity data described above several fundamental aspects of the catalyst will be discussed. Some of these fundamental aspects are: 1) Carbon monoxide and hydrogen chemisorption data and how they correlate to catalyst activity, 2) The role of strong metal support interaction (SMSI), 3) XPS and XRD measurements on promoted and unpromoted CO oxidation catalysts, and 4) The possible effects of solid solutions between precious metals and promoters, and how this affects catalyst activity and chemisorption data.

SYNTHESIS, CHARACTERIZATION AND EVALUATION OF CO OXIDATION CATALYSTS FOR HIGH REPETITION RATE CO_2 TEA LASERS

Thomas P. Moser
Hughes Aircraft Company
Electro-Optical and Data Systems Group
El Segundo, California 90245

ABSTRACT

An extremely active class of noble metal catalysts supported on titania was developed and fabricated at Hughes for the recombination of oxygen (O_2) and carbon monoxide (CO) in closed-cycle CO_2 TEA lasers. The incipient wetness technique was used to impregnate titania and alumina pellets with precious metals including platinum and palladium. In particular, the addition of cerium (used as an "oxygen storage" promoter) produced an extremely active $Pt/Ce/TiO_2$ catalyst. By comparison, the complementary $Pt/Ce/\gamma\text{-}Al_2O_3$ catalyst was considerably less active. In general, chloride-free catalyst precursors proved critical in obtaining an active catalyst while also providing uniform metal distributions throughout the support structure. Detailed characterization of the $Pt/Ce/TiO_2$ catalyst by both SEM and EDX analyses demonstrated uniform dendritic crystal growth of the metals throughout the support, while ESCA analysis was used to characterized the oxidation states of Pt, Ce and Ti. The performance of the catalysts was evaluated with an integral flow reactor system incorporating real time analysis of O_2 and CO. With this system, the transient and steady-state behavior of the catalysts were evaluated. The kinetic evaluation was complemented by tests in a compact, closed-cycle Hughes CO_2 TEA laser operating at a pulse repetition rate of 100 Hz with a catalyst temperature of 75 to 95°C. The $Pt/Ce/TiO_2$ catalyst was compatible with a $^{13}C^{16}O_2$ gas fill.

INTRODUCTION

Long lifetime, high repetition rate CO_2 TEA lasers are required for a number of important applications including advanced rangefinding and chemical detection. The primary life-limiting process of such lasers is the generation of oxygen or some unknown coincidentally formed species in the glow discharge. If such a

species accumulates to a sufficient concentration, the discharge can rapidly degenerate into an arcing process. To prevent arcing, a catalyst can be used to maintain oxygen levels and other deleterious species below consequential levels.

With the increasing demand for high energy, rapidly pulsed CO_2 lasers, considerable attention has been given to the application of CO oxidation catalysts in sealed lasers (1-16). For the most part, however, these investigations have been concerned with the testing of commercial CO oxidation catalysts not necessarily designed for laser applications.

The first extended operation of a sealed TEA laser was reported by Stark et al (1). Operating with high CO_2 levels (eg. 60% CO_2, 40% N_2, 0% He), they demonstrated the continuous operation of a 1 Hz laser aided by a hot (1100°C) platinum wire catalyst. Quantitative details regarding the performance of the platinum wire catalyst were provided by Stark and Harris (2). The hot wire approach was significantly limited in application, however. For high repetition rate devices, both rapid recirculation and cooling of the internal gases are required. Correspondingly, increased catalytic activity would be required to compensate for the increased oxygen production. Under such conditions, a hot platinum wire would consume a prohibitive amount of energy, while introducing an enormous heat removal problem.

With ever stringent engineering constraints posed by laser designs, the practical catalytic solution will likely include a "low temperature" (20 to 100°C) CO oxidation catalyst, preferably in either a monolithic or pellet form. Although highly active at low temperature, Hopcalite (60% MnO_2, 40% CuO) has demonstrated only limited success (3), primarily because of its propensity to form dust and to deactivate by CO_2 adsorption and water contamination. Other catalytic systems include both alumina (Al_2O_3) (4, 5) and tin oxide (SnO_2) (6-15) supported precious metals. In particular, the catalysts which utilize a SnO_2 support have received much attention, primarily because of their reported low temperature capabilities and compatibility with isotopic $^{12}C^{18}O_2$ lasers.

The present investigation involves the fabrication, characterization and evaluation of a new class of precious-metal laser catalysts supported on titania (TiO_2) which use cerium as an "oxygen storage promoter" for improved low temperature activity. As an example, the detailed synthesis, characterization and evaluation of a robust (pellet) $Pt/Ce/TiO_2$ catalyst is presented. Results with a TEA laser using both $^{12}C^{16}O_2$ and $^{13}C^{16}O_2$ are also summarized.

EXPERIMENTAL

Support Material

Titania

The titania support was supplied as 1/8 inch extrudates from Norton Company as a 90/10 mixture of the anatase and rutile phases, respectively. Surface area analysis by the BET method yielded 34 m^2/gram with an average pore diameter of 73 angstroms.

Alumina

The alumina support was supplied as 3.2 mm diameter spheres (Grace LBD) consisting primarily of gamma phase alumina. The BET surface area was 110 m^2/gram.

Catalyst Preparation

The incipient wetness technique was used to impregnate blank titania (TiO_2) and alumina (γ-Al_2O_3) pellets with platinum, palladium, and cerium. Chloride-free catalyst precursors including tetraammineplatinum (II) nitrate, $[Pt(NH_3)_4](NO_3)_2$, tetraammine-palladium (II) nitrate, $[Pd(NH_3)_4](NO_3)_2$, and cerium nitrate, $Ce(NO_3)_3 \cdot 6H_2O$ were used as the source of platinum, palladium, and cerium, respectively. The specific pore volume of the support material was determined by measuring the saturation volume (pore volume as measured for a specific solvent) volumetrically with water. Once this saturation volume was known, a volumetric solution composed of the appropriate metal salts was prepared with a prescribed concentration level. This quantitative solution was then mixed with the appropriate mass of blank support, resulting in the physical adsorption of the solution onto the surface and into the interior of the pellet. A slight excess (ca. 5%) of solution was used in the impregnation procedure to allow uniform and complete saturation. The residual solution was retained for recovery and analysis. The catalyst preparation was completed by slowly drying the "wetted" catalyst pellets in a flowing air hood followed by activation in flowing helium (200°C; 2h), calcination in flowing oxygen (400°C; 4h), and reduction in flowing hydrogen (300°C; 4h). The metal loadings were determined by a material balance, taking into account the concentration of metal in the solution and the saturation volume of the support material.

Catalyst Characterization

BET Surface Area

A Quantasorb Jr. (Quantachrome Corporation) was used to measure surface areas by employing the single point BET method with nitrogen as the adsorbate.

Scanning Electron Microscopy (SEM)

Scanning electron micrographs were obtained with a Cambridge Stereoscan 250 Mk 3 Scanning Electron Microscope equipped with an EDAX PV9100 Energy Dispersive X-ray (EDX) analysis system. Micrographs were obtained with a backscattering detector, while a windowless detector was employed for EDX elemental detection down to the atomic weight of carbon.

Electron Spectroscopy for Chemical Analysis (ESCA)

Information concerning the oxidation states of Pt, Ce, and Ti were obtained by ESCA analysis. A Perkin Elmer 5500 ESCA/SAM with MgK_{α} X-rays was used with a chamber pressure of approximately 10^{-9} torr. Spectra were referenced to the C 1s covalent peak at 284.6 eV.

Catalyst Evaluation

Figure 1 shows the flow scheme for the low flow catalyst test station. A certified gas mixture having a composition of 0.5% oxygen, 1.0% CO, 17% nitrogen, 17% CO_2 and the balance helium was used for routine catalyst evaluation. Other gases including hydrogen, carbon monoxide, oxygen and helium were also deliverable for special processes, such as catalyst conditioning. The combination of high precision rotameters (Fisher Porter Model 10A3555) and individually calibrated mass flow controllers (Tylan Model FC-280) allowed for accurate and reproducible gas flow rates and the synthesis of special gas blends. The system pressure was monitored by an absolute pressure transducer/indicator. For real time gas analysis, a specifically tuned Beckman Industrial nondispersive infrared analyzer (Model 868) was used for CO analysis, while a Beckman oxygen analyzer (Model 755A) monitored oxygen levels.

The reactor was fabricated from standard wall Pyrex tubing having an inner diameter of nominally 0.5 inches and a length of 15 inches (Figure 2). The catalyst pellets were charged to the reactor

together with Pyrex spheres (1/8 inch in diameter) which served to minimize radial temperature gradients. The catalyst zone was held in place by "plugs" of Pyrex wool. The catalyst bed temperature was monitored with a sub-miniature type K sheathed thermocouple. The reactor was oriented vertically.

The catalytic activity for both CO and oxygen disappearance was calculated as:

$$\text{Activity} = \frac{Q\,(X_i^{\text{inlet}} - X_i^{\text{outlet}})}{V_c}$$

where Q = flow rate across catalyst bed (standard cm^3/min)
X_i = mole fraction ($i = O_2$, CO)
V_c = volume of catalyst bed including void volume (cm^3)

Laser Testbed

A sealed modular TE laser was used to investigate catalytic performance. The transmitter used a corona discharge for preionization with transverse gas flow. The modular approach was chosen to allow for both a compact 1 to 3 Hz source or as a 100 Hz device with the straightforward addition of a flow module. The fully integrated, closed-cycle modular laser assembly shown in Figure 3 consisted of, from top to bottom, a potted PFN, discharge module and optical bench, a side mounted catalyst/heat exchanger section, and a tangential fan. A more detailed description of the device was given previously (17).

RESULTS AND DISCUSSION

Role of Catalytic Precursors

The selection of an appropriate chemical complex type for Pt, Pd and Ce proved extremely critical for synthesizing an active catalyst. In particular, catalyst samples prepared with chloride-free metal salts such as tetraammineplatinum (II) nitrate, tetraamminepalladium (II) nitrate and cerium nitrate resulted in deep penetration of the metals into the interior of the titania pellet. By contrast, catalysts prepared with chloride based metals, including

hexachloroplatinic acid-6-hydrate, resulted in "eggshell" metal distributions in the support structure. In all cases, the chloride-free preparations resulted in superior catalytic performance. The relatively lower catalytic activity associated with the chloride-based preparations resulted from poor metal dispersion coupled with the inactive nature of metal sites complexed with chloride ions.

Catalyst Supports and Promoters

Inasmuch as alumina is one of the most common support materials, it provided a basis for comparison with other supported catalyst systems, particularly for metals supported on titania as in the present study.

Figures 4 and 5 show respectively the CO and O_2 disappearance activity for a series of Pt, Pd, Pt/Ce, and Pd/Ce catalysts supported on titania. The 2.0 wt% Pt/2.0 wt% Ce ($Pt/Ce/TiO_2$) catalyst clearly demonstrated the highest activity throughout the 25 to 200°C temperature range. The analogous 2.0 wt% Pd/2.0 wt% Ce ($Pd/Ce/TiO_2$) catalyst was not only less active than the $Pt/Ce/TiO_2$ variety, but also less active than the 4.4 wt% Pd (Pd/TiO_2) catalyst. Furthermore, the 3.8 wt% Pt (Pt/TiO_2) catalyst was the least active of the series. These results suggest a distinct synergistic effect between Pt and Ce which was not apparent between Pd and Ce. Moreover, the simple impregnation of Ce onto TiO_2 yielded an inactive material.

Figures 6 and 7 make a direct comparison between the 2.0 wt% Pt/2.0 wt% Ce on titania ($Pt/Ce/TiO_2$) catalyst and the 2.0 wt% Pt/2.0 wt% Ce on gamma alumina ($Pt/Ce/Al_2O_3$) catalyst. Since the titania and alumina pellets had different particle densities, the activities were normalized on both a volume and mass basis (Figures 6 and 7, respectively). Despite having a much lower surface area (34 versus 110 m^2/gram), the $Pt/Ce/TiO_2$ catalyst was considerably more active than the $Pt/Ce/Al_2O_3$ variety. Whereas the $Pt/Ce/TiO_2$ catalyst demonstrated considerable activity between 25 to 100°C, the $Pt/Ce/Al_2O_3$ catalyst was inactive in the same temperature range.

As with automotive catalysts (18), the addition of cerium apparently helps to balance the relatively weak adsorption of oxygen with the strong adsorption of carbon monoxide. Furthermore, as suggested by the above results, this "oxygen storage" property appears to be directly linked to a chemical interaction between Pt, Ce, and TiO_2.

In-Laser Testing

The modular CO_2 TE laser was tested for extended periods at a 100 Hz repetition rate in a completely sealed condition using the Hughes $Pt/Ce/TiO_2$ catalyst. Typically, the laser was operated for several hours at a time, turned off overnight, and restarted the next day. The test results are as follows:

- -100 Hz repetition rate
- -80 mJ/pulse, no fall off over time
- -1 MW peak power
- -$5x10^6$ total shots
- -75 to 95°C catalyst temperature
- -Operation with $^{12}C^{16}O_2$ or $^{13}C^{16}O_2$

The $Pt/Ce/TiO_2$ catalyst is currently being tested in a higher energy (250 mJ) device at 200 Hz.

Characterization of Hughes $Pt/Ce/TiO_2$ Catalyst

Scanning Electron Microscopy (SEM)

Figure 8 shows both a longitudinal and a transverse view of a sectioned catalyst pellet using a scanning electron microscope. The longitudinal cross section clearly shows a random distribution of Pt and Ce within the pores of the pellet. In addition, the extent of titania reduction or perhaps the density variation throughout the pellet is indicated qualitatively by the dark "band" about the pellet.

Using a backscattering SEM image technique (EDX), a mapping of the Pt/Ce distribution was obtained. Figure 9a clearly shows the dendritic crystal growth of both Pt and Ce in the TiO_2 matrix. Figure 9b shows a close-up view of Figure 9a point A. EDX analysis of the exterior of the pellet (side surface point B, Figure 9a) indicated considerable amounts of Pt and Ce. By contrast, the dark portion of the catalyst pellet as viewed in Figure 8 was void of both Pt and Ce as indicated by the EDX spectrum.

Electron Spectroscopy for Chemical Analysis (ESCA)

Information concerning the oxidation states of Pt, Ce and Ti were obtained by ESCA analysis. This information lends insight into the redox (reduction/oxidation) mechanism functioning at the catalytic surface.

Figure 10 shows the Pt 4f ESCA spectrum for the $Pt/Ce/TiO_2$ catalyst, including both the raw data and fitted curves reflecting the different chemical states of platinum. The Pt $4f_{7/2}$ peak at 70.6 eV and the Pt $4f_{5/2}$ peak at 73.9 eV correspond to metallic platinum (19, 20). The curve fitting analysis indicated the presence of both PtO (oxidation state of Pt^{+2}) and PtO_2 (oxidation state of Pt^{+4}). Likewise, the Ce 3d ESCA spectrum (Figure 11) also indicated multiple oxidation states. The Ce 3d peaks at both 885.3 and 903.6 eV correspond to metallic cerium (21). The fitted Ce 3d peak at 881.2 eV is associated with Ce_2O_3 (oxidation state of Ce^{+3}), whereas the fitted peak at 899.5 eV is associated with CeO_2 (oxidation state of Ce^{+4}). Since it is generally assumed that lattice oxygen is responsible for the catalytic oxidation of carbon monoxide (22), the presence of multiple oxidation states for both Pt and Ce suggests these metal may participate in a redox mechanism.

The corresponding 2p ESCA spectrum for Ti is given in Figure 12. In contrast with the Pt and Ce spectra, the Ti spectrum indicated only a single oxidation state. The Ti $2p_{3/2}$ peak at 458.4 eV and the Ti $2p_{1/2}$ peak at 464.1 eV are associated with the Ti^{+4} oxidation state of TiO_2 (20, 23).

CONCLUSIONS

The development of laser catalysts at Hughes has led to significant improvements in the performance of long-life repetitively pulsed closed-cycle CO_2 TEA lasers. Laser demonstrations in excess of 10^6 continuous shots at 100 Hz were facilitated by a Hughes $Pt/Ce/TiO_2$ catalyst functioning between 75 to 95°C. In addition, the compatibility of this catalyst was confirmed with an isotopic $^{13}C^{16}O_2$ TEA laser.

ACKNOWLEDGEMENTS

The author wishes to thank Dan Demeo and Jerry Meldrum of the Hughes Technology Support Division for catalyst characterization by ESCA and SEM, respectively. In-laser catalyst testing and TE laser development were performed by Wayde Affleck, Dr. David Cohn, Robert Eldridge, and Mike Hasselbeck of the Hughes Advanced Tactical Programs Division and Dr. Tom Watson of the Hughes Industrial Products Division. The catalyst development work was supported by a Hughes independent research and development program.

REFERENCES

1. D. S. Stark, P. H. Cross and M. R. Harris: A Sealed, UV-Preionisation CO_2 TEA Laser with High Peak Power Output. J. Phys. E: Sci. Instrum., **11**, 1978, pp. 311-315.

2. D. S. Stark and M. R. Harris: Platinum-Catalysed Recombination of CO and O_2 in Sealed CO_2 TEA Laser Gases. J. Phys. E: Sci. Instrum., **11**, 1978, pp. 316-319.

3. R. B. Gibson, A. Javan, K. Boyer: Sealed Multiatmosphere CO_2 TEA Laser: Seed-gas compatible System using Unheated Oxide Catalyst. Appl. Phys. Lett., **32**(11), 1978, pp. 726, 727.

4. C. Willis and J.G. Purdon: Catalytic Control of the Gas Chemistry of Sealed TEA CO_2 Lasers. J. Appl. Phys., **50**(4), 1979, pp. 2539- 2543.

5. M. S. Sorem and G. Faulkner: Catalytic Converters for Closed-Cycle Operation of Isotopic CO_2 TEA Laser. Rev. Sci. Instrum., **52**(8), 1981, p. 1193.

6. G. C. Bond, L. R. Molloy, and M. J. Fuller: Oxidation of Carbon Monoxide over Palladium-Tin (IV) Oxide Catalysts: An Example of Spillover Catalysis. J. Chem. Soc. Chem. Comm., 1975, pp. 796-797.

7. D. S. Stark and M. R. Harris: Catalysed Recombination of CO and O_2 in Sealed CO_2 TEA Laser Gases at Temperatures Down to -27°C. J. Phys. E: Sci. Instrum., **16**, 1983, pp. 492-496.

8. D. S. Stark, Z. Crocker, and G. J. Steward: A Sealed 100 Hz CO_2 TEA Laser using High CO_2 Concentrations and Ambient Temperature Catalysts. J. Phys. E: Sci. Instrum. **16**, 1983, pp. 158-161.

9. C. F. Sampson and N. J. Gudde: The Oxidation of Carbon Monoxide using a Tin Oxide Catalyst. Closed-Cycle, Frequency-Stable CO_2 Laser Technology, NASA CP-2456, 1987.

10. H. T. Price and S. R. Shaw: High Repetition Rate Sealed CO_2 TEA Lasers using Heterogeneous Catalysts. Closed-Cycle, Frequency-Stable CO_2 Laser Technology, NASA CP-2456, 1987.

11. D. R. Schryer, B. D. Sidney, I. M. Miller, R. V. Hess, G. M. Wood, C. E. Batten, L. G. Burney, R. F. Hoyt, P. A. Paulin, K. G. Brown, J. Schryer, and B. T. Upchurch: NASA-LaRC Research on Catalysts for Long-Life Closed-Cycle CO_2 Laser. Closed-Cycle, Frequency-Stable CO_2 Laser Technology, NASA CP-2456, 1987.

12. B. T. Upchurch, G. M. Wood, R. V. Hess, and R. F. Hoyt: Rare Isotope Studies involving Catalytic Oxidation of CO over Platinum-Tin Oxide. Closed-Cycle, Frequency-Stable CO_2 Laser Technology, NASA CP-2456, 1987.

13. C. E. Batten, I. M. Miller, P. A. Paulin: Studies of CO Oxidation on Pt/SnO_2 Catalyst in a Surrogate CO_2 Laser Facility. Closed-Cycle, Frequency-Stable CO_2 Laser Technology, NASA CP-2456, 1987.

14. K. G. Brown and J. Schryer: Characterization of Pt/SnO_2 Catalysts for CO Oxidation. Closed-Cycle, Frequency-Stable CO_2 Laser Technology, NASA CP-2456, 1987.

15. B. D. Sidney: Studies of Long-Life Pulsed CO_2 Laser with Pt/SnO_2 Catalyst. Closed-Cycle, Frequency-Stable CO_2 Laser Technology, NASA CP-2456, 1987.

16. P. G. Browne and A. L. S. Smith: Long-Lived CO_2 Lasers with Distributed Heterogeneous Catalysis. J. Phys D: Appl. Phys., 7, 1974, pp. 2464-2470.

17. D. B. Cohn, M. P. Hasselbeck, W. H. Affleck, R. E. Eldridge, T. P. Moser, G. R. Sasaki, T. A. Watson, and P. J. Bailey: Compact High Repetition Rate CO_2 TEA Lasers. SPIE, **1042**, CO_2 Lasers and Applications, 1989, pp. 63-69.

18. S. E. Oh and C. C. Eickel: Effects of Cerium Addition on CO Oxidation Kinetics over Alumina-Supported Rhodium Catalysts. J. Catal., **112**, 1988, pp. 543-555.

19. T. Sheng, X. Guoxing, and W. Hongli: The Nature of the SMSI State of the Pt/TiO_2 System. J. Catal., **111**, 1988, pp. 136-145.

20. G. B. Hoflund, A. L. Grogan, and D. A. Asbury: An ISS, AES, and ESCA Study of the Oxidative Reductive Properties of Platinized Titania. J. Catal., **109**, 1988, pp. 226-231.

21. J. Z. Shyu, W. H. Weber, and H. S. Gandhi: Surface Characterization of Alumina-Supported Ceria. J. Phys. Chem., **92**, 1988, pp. 4964-4970.

22. P. Mars and D. W. van Krevelen: Oxidation carried out by means of Vanadium-Oxide Catalysts. Chem. Eng. Sci., **3**, Spec. Suppl., 1954, pp. 41-59.

23. M. K. Bahl, S. C. Tsai, and Y. W. Chung: Auger and Photoemission Investigations of the $Pt-SrTiO_3$ (100) Interface: Relaxation and Chemical Shift Effects. Phys. Rev. B., **21**(4), 1980, pp. 1344-1348.

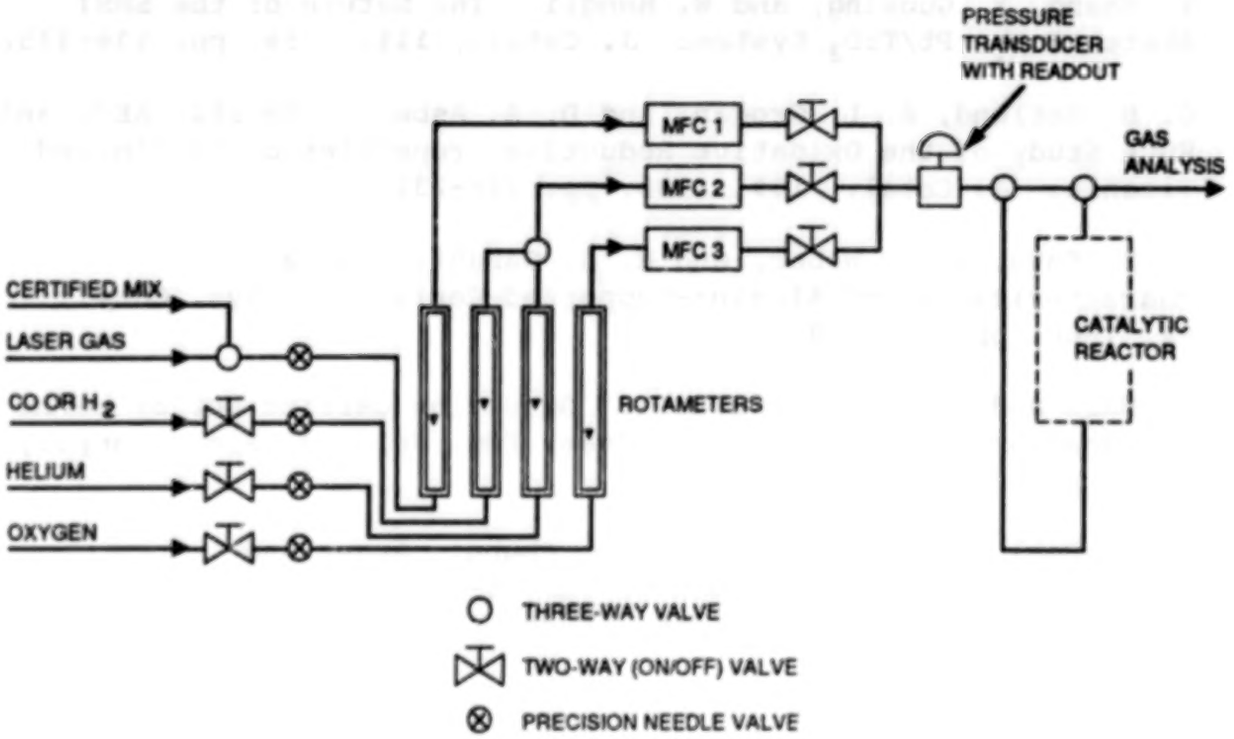

Figure 1. Flow scheme for low flow catalyst test station.

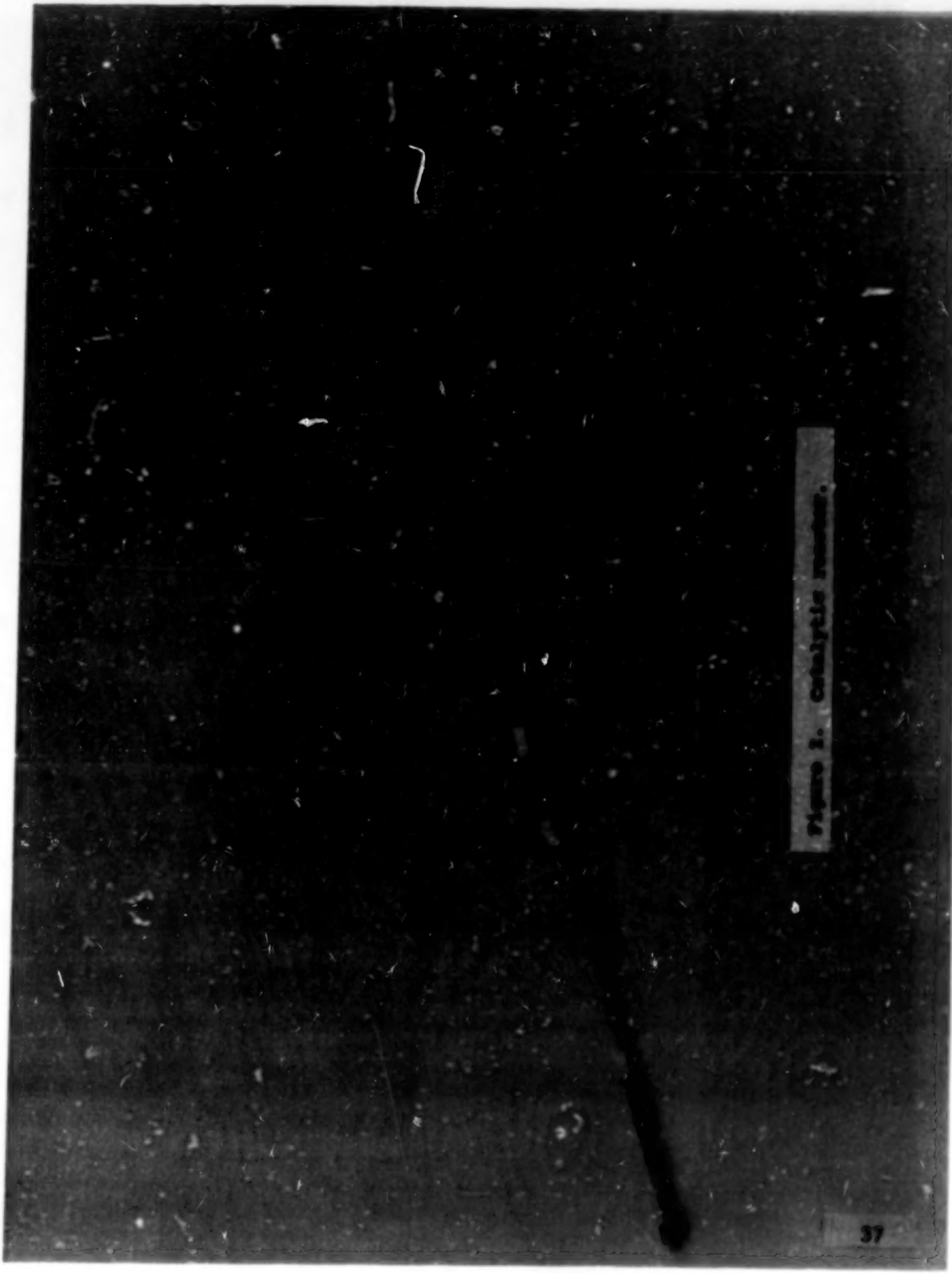

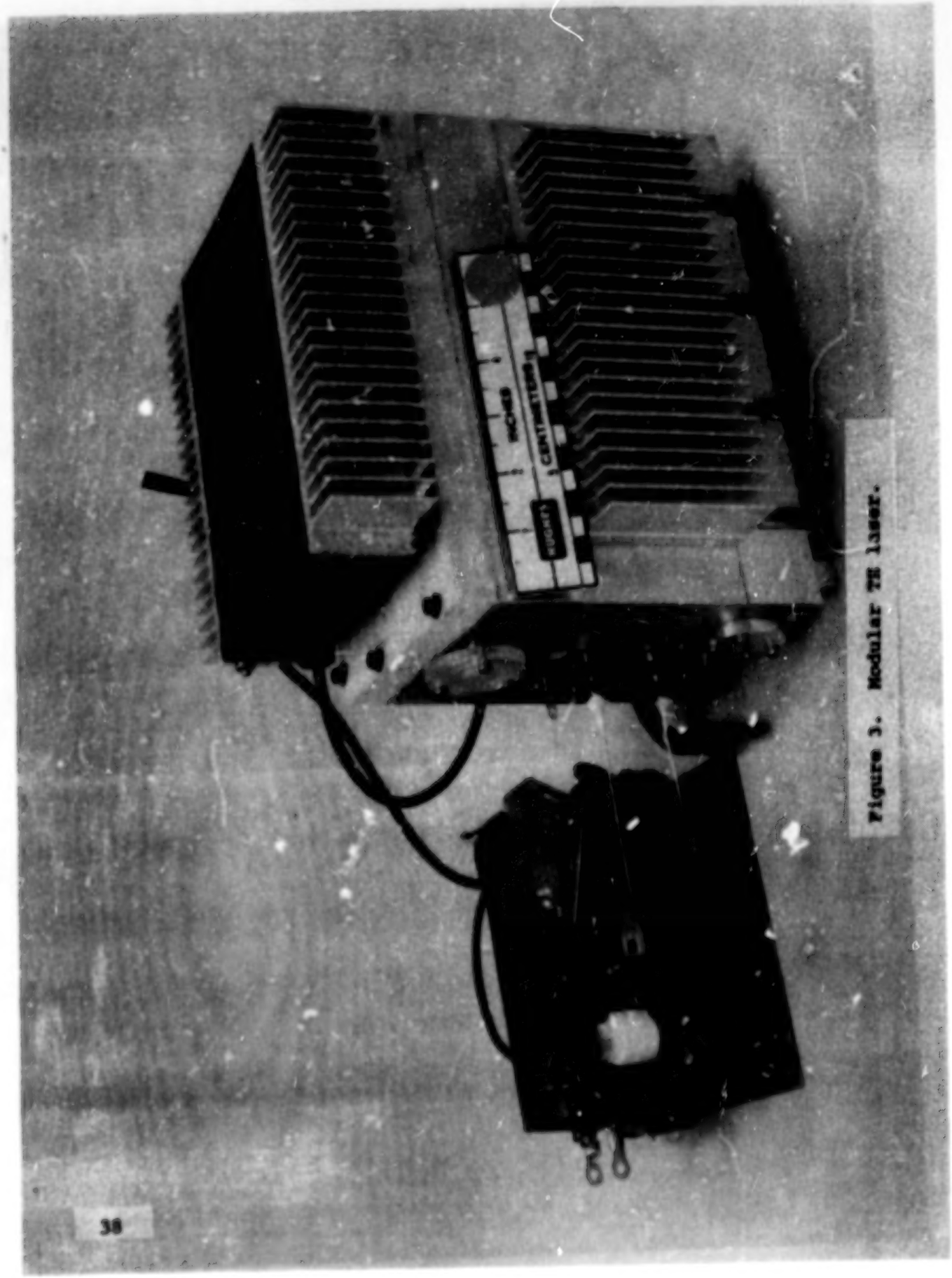

Figure 3. Modular 78 Laser.

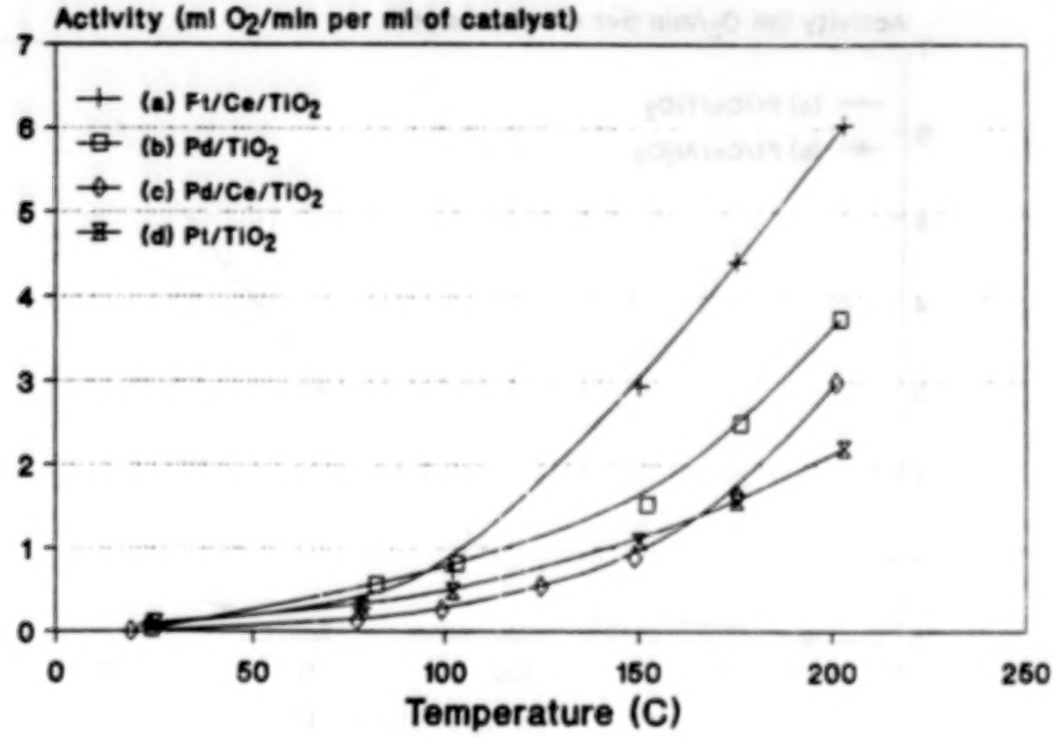

Figure 4. Oxygen disappearance activity for titania supported Hughes catalysts.

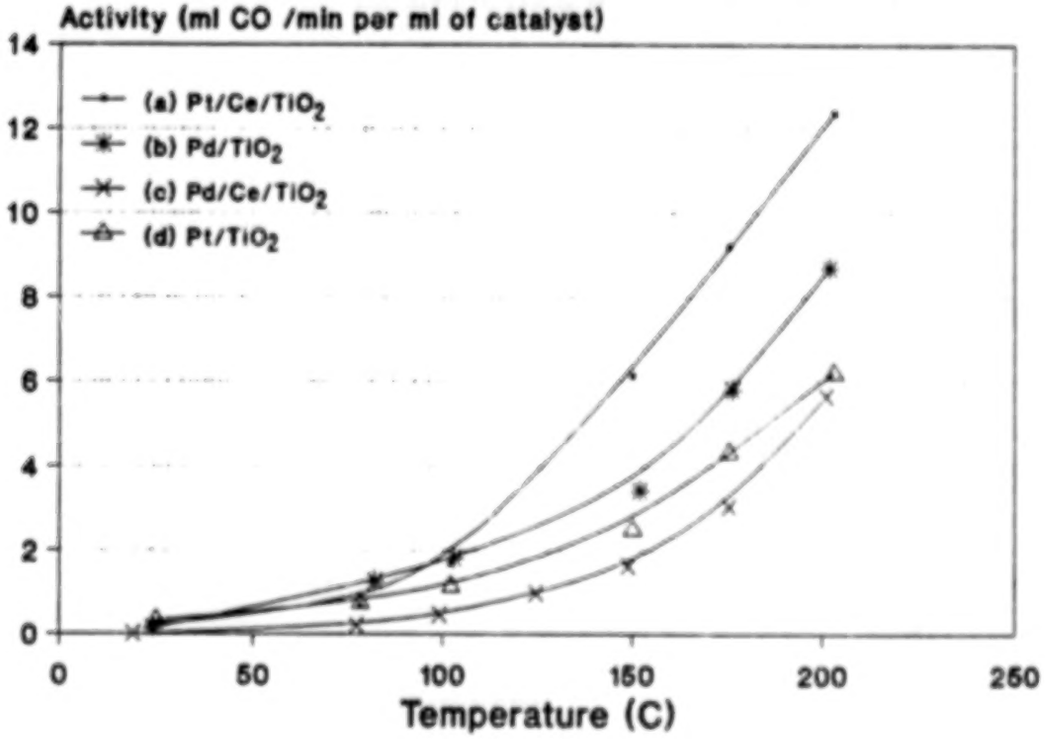

Figure 5. Carbon monoxide disappearance activity for titania supported Hughes catalysts.

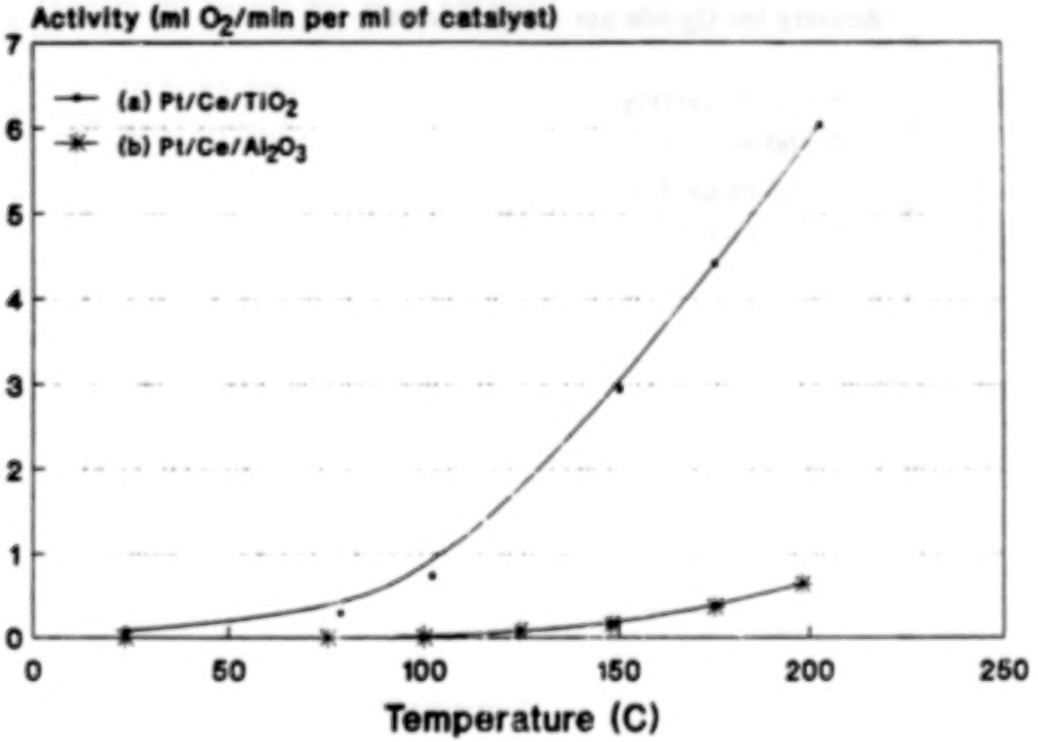

Figure 6. Comparison of alumina and titania supported Hughes Pt/Ce catalysts: Activity normalized on a volume basis.

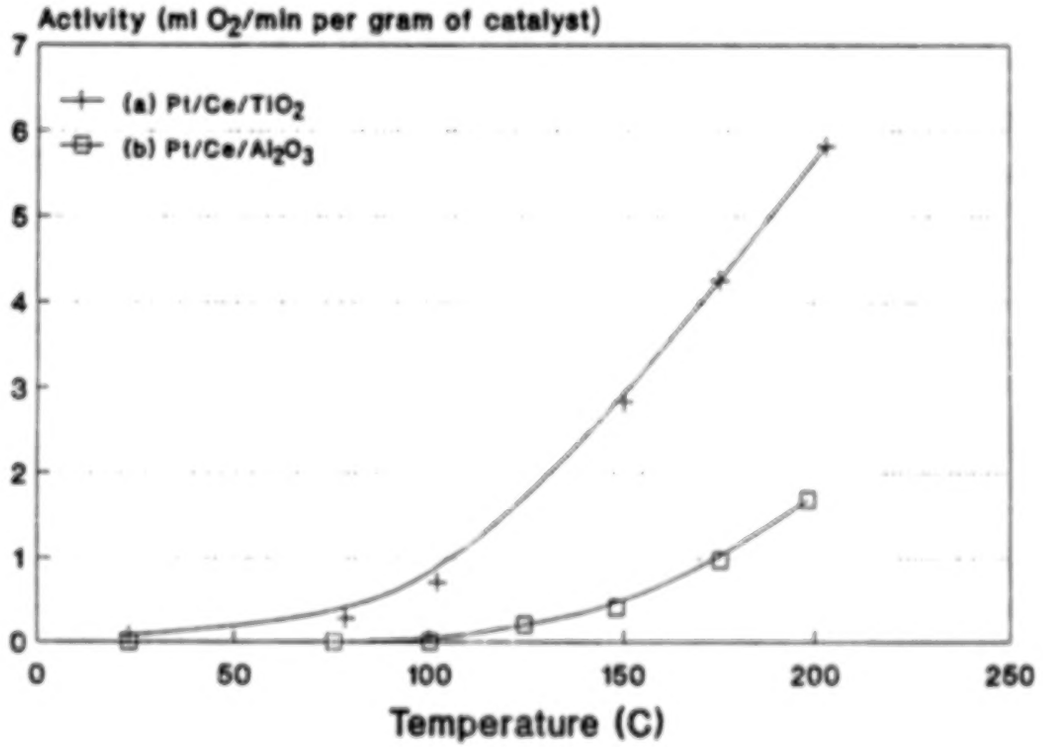

Figure 7. Comparison of alumina and titania supported Hughes Pt/Ce catalysts: Activity normalized on a mass basis.

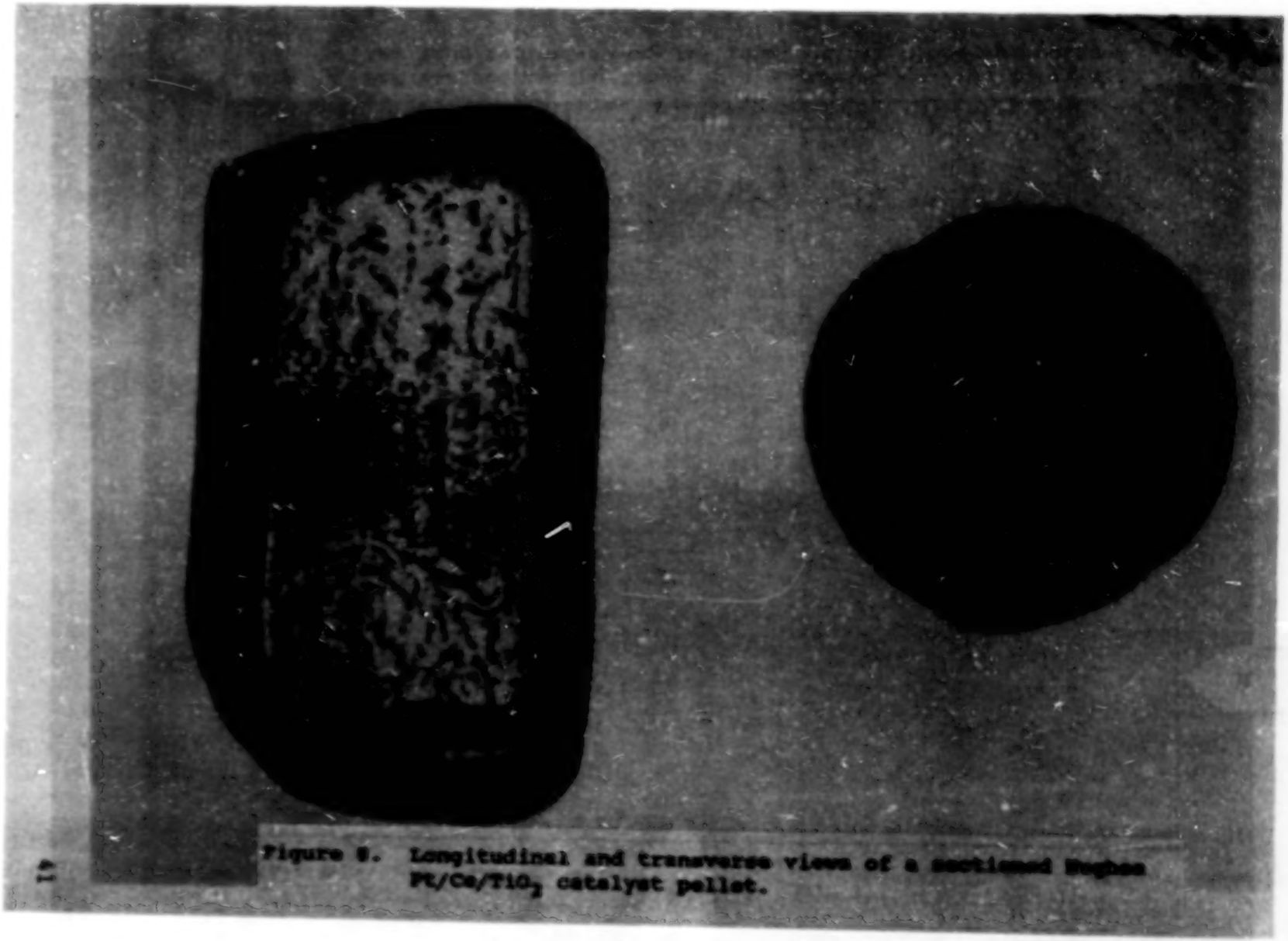

Figure 8. Longitudinal and transverse views of a sectioned Hughes $Pt/Ce/TiO_2$ catalyst pellet.

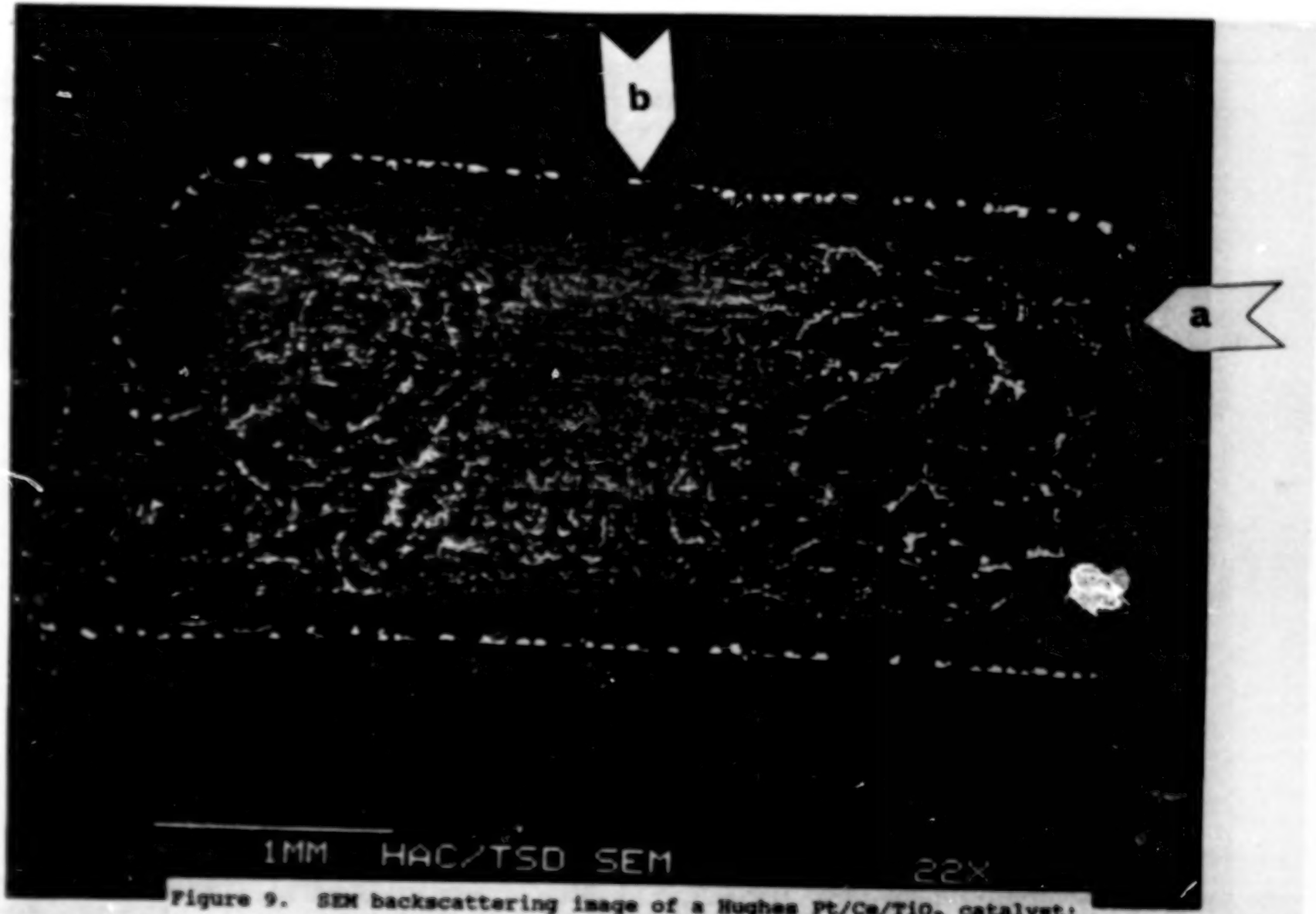

Figure 9. SEM backscattering image of a Hughes Pt/Ce/TiO_2 catalyst: (a) longitudinal view, (b) longitudinal close-up, point A.

Figure 9b.

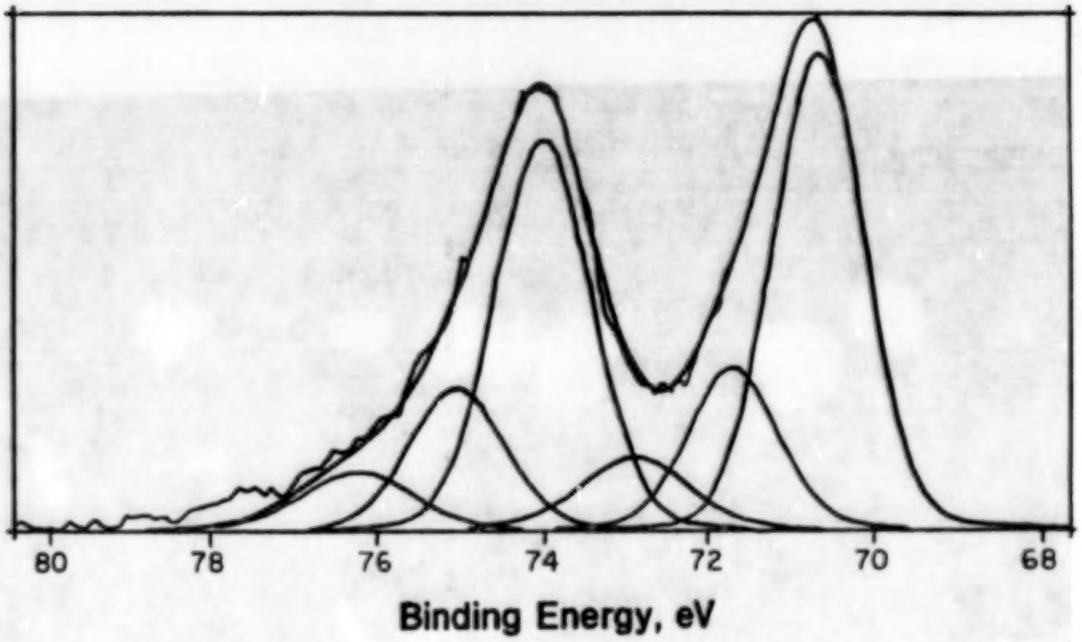

Figure 10. Platinum 4f ESCA spectrum of the Hughes $Pt/Ce/TiO_2$ catalyst.

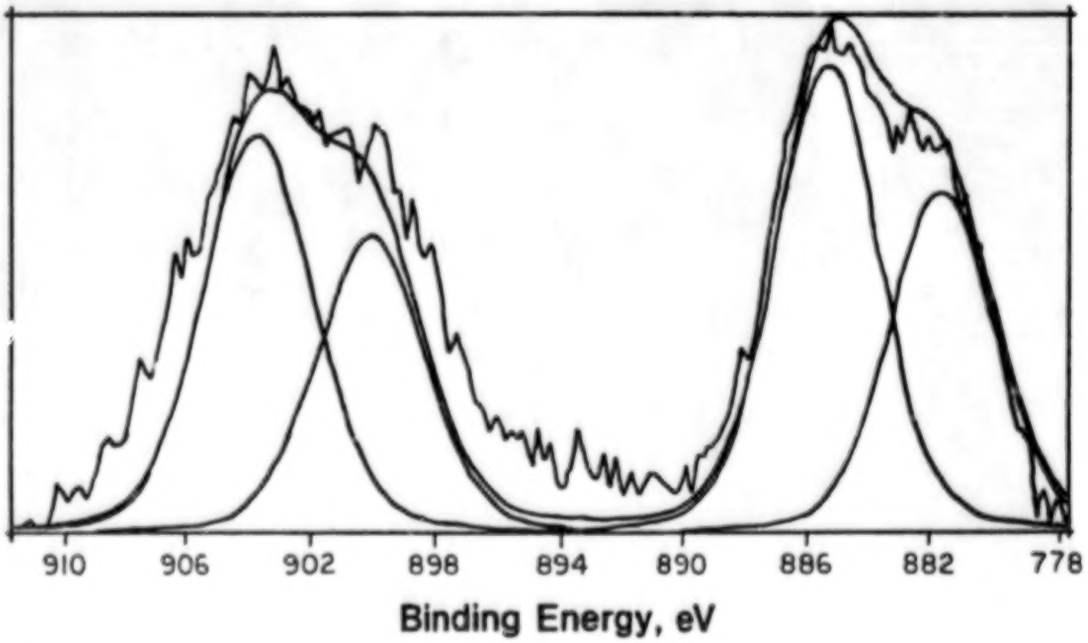

Figure 11. Cerium 3d ESCA spectrum of the Hughes $Pt/Ce/TiO_2$ catalyst.

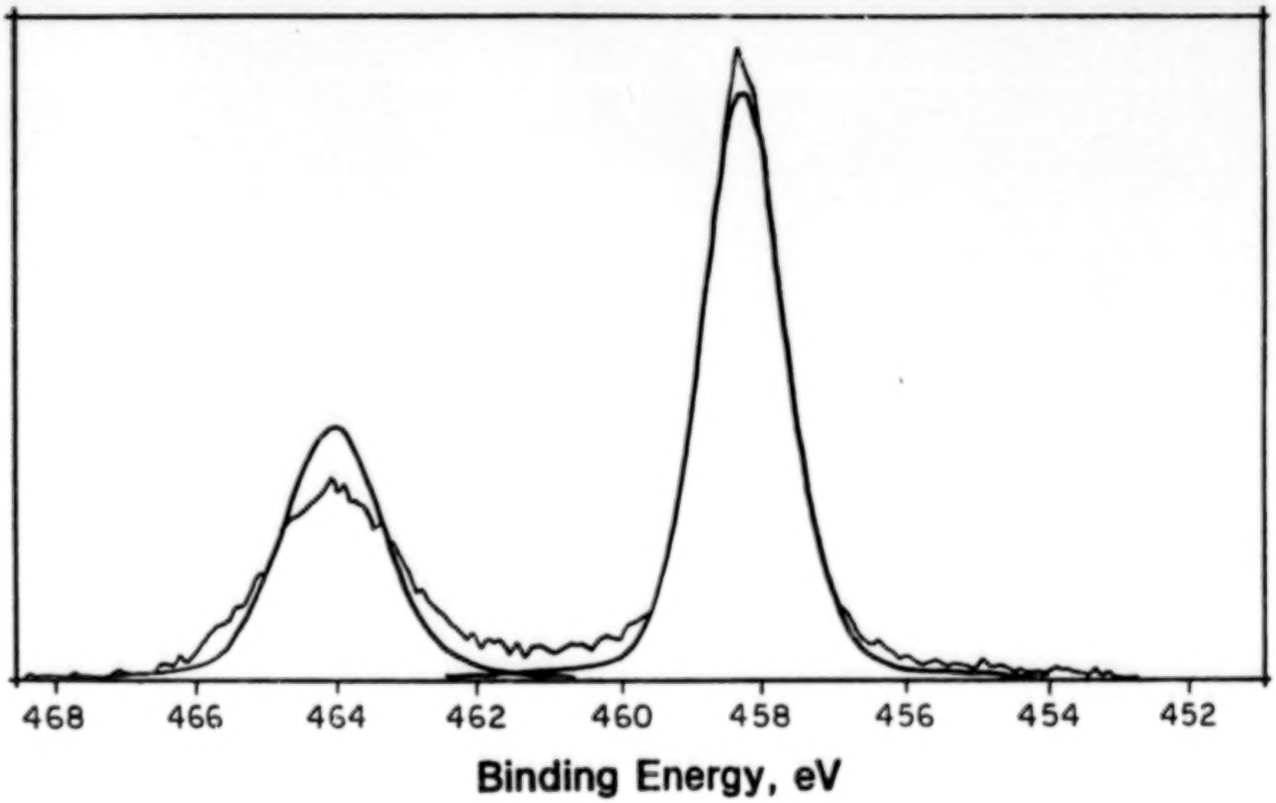

Figure 12. Titanium 2p ESCA spectrum of the Hughes $Pt/Ce/TiO_2$ catalyst.

LARC-DEVELOPED CATALYSTS FOR CO_2 LASERS

Billy T. Upchurch
NASA Langley Research Center
Hampton, VA 23665

David R. Brown
Old Dominion University
Norfolk, VA 23529

Irvin M. Miller
Science and Technology Corporation
Hampton, VA 23666

ABSTRACT

Pulsed CO_2 lasers have many remote sensing applications from space, airborne, and ground platforms. The NASA Laser Atmospheric Wind Sounder (LAWS) system will be designed to measure wind velocities from polar earth orbit for a period of up to three years. Accordingly, this and other applications require a closed-cycle pulsed CO_2 laser which necessitates the use of an efficient CO-O_2 recombination catalyst for these dissociation products which otherwise would degrade the laser operation. The required catalyst must not only operate at low temperatures but also must operate efficiently for long time periods.

The research effort at NASA LaRC has centered around development and testing of CO oxidation catalysts for closed-cycle pulsed and common and rare-isotope CO_2 lasers. We have examined available commercial catalysts both in a laser and under simulated closed-cycle laser conditions with our efforts aimed toward a thorough understanding of the fundamental catalytic reaction and have utilized these data to design and synthesize new catalyst compositions to better meet the catalyst requirements for closed-cycle pulsed CO_2 lasers. In this paper we report syntheses and test results for catalysts developed at Langley Research Center which have significantly better long-term decay characteristics than previously available catalysts and at the same time operate quite well under lower temperature conditions.

ALTERNATIVE CATALYSTS FOR LOW-TEMPERATURE CO OXIDATION

Steven D. Gardner and Gar B. Hoflund
Department of Chemical Engineering, University of Florida
Gainesville, Florida 32611

David R. Schryer
NASA Langley Research Center
Hampton, Virginia 23665

SUMMARY

Materials composed largely of manganese dioxide have been synthesized for evaluation as low-temperature CO oxidation catalysts in CO_2 lasers. The CO oxidation activities of unpretreated MnO_2, Pt/MnO_2, Pd/MnO_2 and CuO/MnO_2 were measured at 75°C in low concentrations of stoichiometric CO and O_2. Significant surface reduction occurs initially as both gas phase and lattice oxygen are utilized in the reaction. The long-term activity of Pt/MnO_2 and Ag/MnO_2 proved superior to a commercially available Pt/SnO_2 catalyst. While more active initially, the Pt/SnO_2 catalyst exhibits an accelerated activity decay whereas the CO_2 yield falls below that of Pt/MnO_2 and Ag/MnO_2 after about 3000 minutes. Perhaps most significant for this application, the CuO/MnO_2 catalyst exhibits negligible activity decay after only 1000 minutes; sustaining a CO_2 yield about half that of Pt/MnO_2 and Ag/MnO_2 over the test period.

The catalysts were further characterized using ion scattering spectroscopy (ISS), Auger electron spectroscopy (AES) and X-ray photoelectron spectroscopy (XPS). The surface and near-surface regions were probed as a function of reaction time. Relative to chemical analytical methods which have previously been used to study MnO_2 surface species, these surface techniques appeared to be more compatible with the unstable nature of MnO_2 surfaces. Although the Ag, Pt and Pd were below XPS detection limits, important information was realized from the surface studies. At least two different oxygen species were indicated possibly suggesting the importance of hydroxyl groups in the reaction. Overall, the results are consistent with a surface reduction/oxidation mechanism which in turn is consistent with the reaction data. Finally, based upon these results and a literature search, several possible catalysts are being considered for applications in CO_2 lasers. The materials include Au/MnO_2, Ru/MnO_2, Au/Fe_2O_3, Au/Ce_2O_3 and a silver-manganese composite oxide. Details of their preparation will be reviewed.

A Comparison of the Dynamics of CO Oxidation on Rh, Pd, and Pt

George W. Coulston and Gary L. Haller
Yale University

This abstract and paper not available at time of printing.

MECHANISTIC STUDIES OF THE CO OXIDATION REACTION ON CATALYSTS FOR USE IN LONG LIFE CO_2 LASERS[1]

Talat Dawood, John R Richmond and Brian W Riley
UOP Limited, Enfield, Middlesex, EN3 7PN, UK.

EXTENDED ABSTRACT

The catalytic recombination of carbon monoxide and oxygen has been studied under conditions expected to be present in a sealed E-beam CO_2 laser system. These conditions are typically a gas inlet temperature of 60°C, a substoichiometric CO/O_2 ratio of ca. 2.5/1 with an oxygen feed rate of ca. 5 micromoles/s, a carrier gas comprising He, N_2 and CO_2 in the ratio of 3:2:1 (termed laser gas mix), near atmospheric pressure and a gas velocity of 4 m/s. Heterogeneous catalysts, based on precious metal supported on tin oxide, have been coated onto ceramic monoliths and tested for catalytic activity and stability after a reduction/passivation step. Two catalyst systems have been chosen. These are $Pt/Pd/SnO_2$ and $Pt/Ru/SnO_2$.

Under the conditions described above, a characteristic decline in catalytic activity is apparent for both systems. In the case of Pt/Ru it has been observed that this process can be reversed by flowing laser gas mix over the catalyst or by effecting a moderate temperature rise of ca. 8°C. Moreover, the reacted catalyst is completely regenerated upon a second reduction/passivation pretreatment. The exit gas temperature has been recognised as a sensitive parameter by which to monitor the activity changes found with these catalysts. A semilogarithmic plot of exit temperature as a function of time has revealed two distinct processes connected with the decline in activity; one process is associated with the depletion of catalytically active sites on the precious metal (Site A), whilst the other is associated with the formation of active sites at the metal-support interface (Site B).

Surface species have been identified using 'on-line' Fourier Transform Infrared (FTIR) spectroscopy. Two characteristic absorption bands have been detected. In the case of Pt/Ru, a distinct band at ca. 2055 cm^{-1} has been identified as linearly adsorbed CO, and a broad, rather weak absorption band at ca. 1890 cm^{-1} identified as bridge-bonded CO; for Pt/Pd, the corresponding absorption bands are found at ca. 2070 cm^{-1} and 1890 cm^{-1} respectively. No marked changes in band intensity could be discerned over a three hour period under reaction conditions.

However, flushing with laser gas mix resulted in significant band shifts as well as an attenuation of the bands, consistent with a lowering of the surface coverage of CO. These effects were more pronounced for the Pt/Pd system. Moreover, in the presence of oxygen alone, the linearly bound species could be removed from the surface in each case. The FTIR studies indicate that high surface coverages of CO are likely under reaction conditions, and that the reactive CO species is linearly bonded to the precious metal surface.

Finally, various poisons and promoters have been added to the catalysts either during preparation or under reaction conditions. In the case of the Pt/Pd system, potassium and manganese act as catalyst poisons at the 1% w/w level. Conversely, in the presence of water (with a relative humidity of 33% at room temperature), manganese stabilises the catalyst. For the Pt/Ru system, the addition of acetone to the feed results in irreversible deactivation. Microreactor pulse experiments have shown that this acetone chemisorbs on the support, and indicate that the poisoning effect of acetone is metal-support related. Conversely, water has been shown to be a promoter and stabiliser under present conditions.

A possible reaction mechanism explaining the experimental observations resulting from this study has been put forward. It is suggested that under reaction conditions dissociated oxygen is transported to the precious metal surface via Site B, and that water promotes this process. Poisoning is accounted for by adsorption of the rate inhibiting species at Site B.

Acknowledgements

The authors would like to thank Professor G Webb and Dr G D McLellan of Glasgow University for their assistance with the FTIR work, and Dr S Tahir of UOP Limited for some assistance with the experimental work.

[1] Support for part of this work is through a contract from SDIO and the UK Ministry of Defence.

EFFECT OF H_2O AND CO_2 ON CO-OXIDATION CATALYST EFFICIENCY

John D. Van Norman[2,3], David R. Schryer[1], Kenneth G. Brown[2], Jacqueline Schryer[2], Susan K. Ohorodnik[2], and David R. Brown[2]

1. NASA Langley Research Center, Hampton, VA 23665

2. Department of Chemical Sciences, Old Dominion University, Norfolk, VA 23529

3. Science and Technology Corporation, 101 Research Drive, Hampton, VA 23666-1340

The effect of H_2O on the activity of Pt/SnO_2 catalyst for CO oxidation has been previously reported.[1] It was reported that when this catalyst, pretreated at 225°C with 5% CO in He, was treated with an humidified inert gas or with a humidified stoichiometric mixture of 1% CO, 0.5% H_2O, 2% Ne in He, no initial dip in activity of the catalyst occurred as noted in the absence of water vapor. A slight enhancement of catalyst activity was also reported.

In this paper we report on the effect of water vapor and carbon dioxide on the activity of not only a Pt/SnO_2 catalyst but also upon a Pt/SnO_2/silica gel catalyst made at NASA Langley Research Center. The presence of the silica gel, a desiccant, modifies the behavior of the catalyst both in the short term and in the long term. Such a catalyst does not exhibit the initial dip in activity reported previously under similar pretreatment conditions nor does it behave in the same way with the addition of H_2O and/or CO_2 to the test gas mixture(s).

Experimental details, results and possible explanations will be presented.

A PROPOSED MECHANISM FOR THE OXIDATION OF CO ON Pt/SnO_2-BASED CATALYSTS

David R. Schryer[1], Barry D. Sidney[2], Gar B. Hoflund[3], Richard K. Herz[4], Billy T. Upchurch[1], Kenneth G. Brown[5], John D. Van Norman[2]

[1]NASA Langley Research Center
Hampton, VA 23665

[2]Science and Technology Corporation
Hampton, VA 23666

[3]University of Florida
Gainesville, FL 32611

[4]University of California, San Diego
La Jolla, CA 92093

[5]Old Dominion University
Norfolk, VA 23508

ABSTRACT

Investigators at NASA-LaRC, Old Dominion University, the University of Florida, the University of California, San Diego, and Science and Technology Corporation have for some time been engaged in a joint study of the oxidation of CO on Pt/SnO_2-based catalysts. A broad summary of this study by Schryer, et al., is presented elsewhere in this volume as are several papers dealing with specific aspects of the study.

One result of this study is that several features of the mechanism of Pt/SnO_2-catalyzed CO oxidation have begun to emerge. Primary among these is the role of surface hydroxyl groups in the oxidation of CO chemisorbed on Pt sites. Although much is still, at best, uncertain or ambiguous and much else is simply unknown, it is now possible to put forth, in some detail, a tentative mechanism which is consistent with a broad range of experimental observations. This proposed mechanism, including detailed reaction equations, will be presented at the conference. Details of the proposed mechanism are not included here in order that the mechanism presented at the conference shall include the most up-to-date results available at that time.

CHARACTERIZATION STUDIES OF Pt/SnO_2 CATALYSTS:

PARTS I AND II

Gar B. Hoflund[1], Jean E. Drawdy[1], Steven D. Gardner[1],
Mark R. Davidson[1], David R. Schryer[2] and Billy T. Upchurch[2]

[1]Department of Chemical Engineering, University of Florida,
Gainesville, Florida 32611
[2]NASA Langley Research Center, Hampton, Virginia 23665

In order to maintain power during the sealed operation of a CO_2 laser, it is necessary to recombine CO and O_2 which are produced during the laser discharge because the O_2 quenches the lasing action. It is desirable to carry out the recombination at low temperature to minimize power and weight requirements. Although numerous materials catalyze the low-temperature oxidation of CO, much effort has been expended in developing highly efficient platinized tin oxide catalysts and examining their catalytic behavior. An effort is also being made to understand the behavior of the catalysts during pretreatment, the composition and chemical nature of the functioning catalytic surface, and the mechanism responsible for production of CO_2. Thus far, two platinized tin oxide catalysts have been extensively studied. These are a 2 wt % Pt supported on tin oxide catalyst produced by Engelhard and 17 wt % Pt/tin oxide catalyst supported on silica and produced at NASA (and referred to as the NASA catalyst). In this study these two catalysts have been examined before and after a reductive pretreatment in CO at various temperature using electron spectroscopy for chemical analysis (ESCA), Auger electron spectroscopy (AES) and ion scattering spectroscopy (ISS).

Reactor studies have shown that the optimum pretreatment temperature in 10 Torr of CO for the NASA catalyst is 125°C and that pretreating at 250°C results in severe loss of catalytic activity. Thus, the NASA catalyst was characterized before and after pretreatment at these two temperatures. ESCA data indicate that the Pt is present initially as PtO_2. Reduction at 125°C converts the PtO_2 to $Pt(OH)_2$ while reduction at 250°C converts the Pt to metallic Pt. ISS data show that the Pt in the outermost atomic layer of the catalyst is mostly covered by substrate species during the 250°C reduction. Both the ESCA and ISS results are consistent with alloy formation during the reduction. The surface dehydration and migration of substrate species over surface Pt and Sn appear to explain why a reduction in CO at 250°C produces an inferior catalyst compared to a CO reduction at 125°C.

The Engelhard catalyst contains less Pt than the NASA catalyst according to the ESCA data, and the Pt initially is present as PtO_2 indicating that this catalyst has been calcined and not prereduced by Engelhard. Reduction in 40 Torr of CO for 1/2 hour at room temperature between 75 and 200°C converts the PtO_2 primarily to $Pt(OH)_2$ and a small amount of metallic Pt. The higher temperature reduction does not convert most of the Pt to metallic form, and this catalyst retains its high activity after such a reduction. During reduction, oxidic Sn is reduced to metallic form which alloys with the Pt. ISS data indicate that the Sn/Pt ratio is much larger for the NASA catalyst than the Engelhard catalyst.

The Utilization of Electron Simulated Desorption to Examine Hydrogen on Low-Temperature Co-Oxidation Catalysts

Mark R. Davidson, et al.
University of Florida

This abstract and paper not available at time of printing.

A STUDY OF THE INTERACTION OF CO, O_2 AND H_2 WITH POLYCRYSTALLINE Pt, A POLYCRYSTALLINE Pt/Sn ALLOY AND PLATINIZED TIN OXIDE

Orlando Melendez[1], Gar B. Hoflund[1] and David R. Schryer[2]

1. Department of Chemical Engineering, University of Florida, Gainesville, Florida 32611, USA
2. NASA Langley Research Center, Hampton, Virginia 23665, USA

In order to understand the mechanism of CO oxidation at low temperature on a platinized tin oxide catalyst, it is useful to examine the interaction of CO, O_2 and H_2 with a reduced platinized tin oxide surface and compare the results with those obtained from polycrystalline Pt and Pt/Sn alloy surfaces. Several surface analytical techniques including ion scattering spectroscopy (ISS), Auger electron spectroscopy (AES), electron spectroscopy for chemical analysis (ESCA), and temperature programmed desorption (TPD) have been used in these studies. The sticking coefficient of CO on polycrystalline Pt has been determined as a function of CO exposure. CO adsorbs rapidly on Pt at room temperature, and saturation coverage appears to be considerably less than a monolayer according to the ISS data. The ISS spectra exhibit peaks due to C, O and Pt after various CO exposures and the C and O peaks are approximately equal in size. This indicates that the CO adsorbs dissociatively since only the O peak would be observed if the CO adsorbs molecularly in the vertical position as found on low-index planes of Pt using ultraviolet photoemission spectroscopy. Further evidence of dissociative adsorption is given by TPD data.

The interaction of O_2 with a cleaned polycrystalline Pt surface has also been examined. ISS data show that the sticking coefficient of O_2 on polycrystalline Pt is very low ($<10^{-4}$). High O_2 pressures (10 Torr) and exposures and a high surface temperature (> 300°C) is required to obtain oxygen coverages of a few percent. It is possible that efficient clean-off reactions by CO and H_2 in the vacuum background gas lower the observed oxygen coverage.

The CO-saturated polycrystalline Pt surface was exposed to various doses of O_2 at room temperature. Very small exposures are efficient in removing the adsorbed C and O to form CO_2. Furthermore, the ISS, O and C peaks decrease simultaneously, but the mechanism of CO_2 formation cannot be ascertained from these experiments.

Related experiments are currently in progress or sputtered Pt/Sn alloy surfaces (Pt-rich alloy surfaces) and reduced platinized tin oxide surfaces. Comparison of the data obtained from these surfaces will be described and should be useful in understanding the mechanism of CO oxidation over platinized tin oxide catalysts.

SURFACE DEFECTS AND CHEMISTRY ON THE SnO_2(110) SURFACE

David F. Cox
Department of Chemical Engineering
Virginia Polytechnic Institute & State University
Blacksburg, Virginia, 24061, USA

SUMMARY

A variety of ultrahigh vacuum (UHV) surface science techniques have been used to characterize the structural, electronic and chemical properties of SnO_2(110), a model catalytic surface. Two types of surface oxygen vacancies have been identified, each associated with different band gap (defect) electronic states. Adsorption experiments show that the interaction of simple gases with this surface occurs primarily through these oxygen vacancies and can show site-specificity to only one of the two types of vacancies.

INTRODUCTION

Tin oxide (SnO_2) is a useful catalytic material most often applied in multicomponent systems. In mixed-oxide systems, tin oxide has found application in catalysts for selective oxidation, ammoxidation, dehydrogenation and isomerization reactions [1-5]. Pure tin oxide typically forms combustion products [6-9], hence its has found an application as a support for Pt in the low-temperature CO oxidation catalyst for pulsed CO_2 lasers.

One of the primary difficulties in characterizing tin oxide surfaces (and hence Pt/SnO_2 catalysts) lies in determining the valence state of the surface tin species. It has been found that neither Auger electron spectroscopy (AES) [10-12] or x-ray photoelectron spectroscopy (XPS) [13] can distinguish between Sn^{+2} and Sn^{+4} because there is no significant change in the core-level binding energies. This distinction is important because it characterizes the redox condition of the tin oxide surface which in turn controls its interaction with gas-phase oxygen. In spite of these difficulties, progress has been made in distinguishing between Sn^{+2} and Sn^{+4} using electron loss spectroscopy (ELS) [13,14]. The ELS technique can clearly give a qualitative indication of the presence of Sn^{+2} species in a SnO_2 matrix. ELS is also sensitive to structural changes in the lattice, however, no clear interpretation other than an oxygen deficiency can be associated with the observed spectral changes [14]. In other words, it is impossible to distinguish between a true SnO surface layer and a partially reduced Sn^{+2} containing SnO_2 structure with oxygen vacancies.

These structural ambiguities in surface characterization can be removed by studying model SnO_2 single crystal surfaces. Surface characterization studies of SnO_2(110) are reviewed here as an example

of the types of information obtainable by studies of well-characterized, model single-crystal surfaces which cannot be obtained from powders or polycrystalline materials. The (110) face was chosen for these studies because it is the most stable, predominant natural growth face for SnO_2. Extended high temperature treatments of tin oxide powders and films leads to a preferential growth of (110) faces [15], hence this particular crystal face is the most likely to be a successful model for realistic SnO_2(110) systems. Also, a perfect (110) crystallographic orientation gives the most "fully oxidized" or "stoichiometric" surface possible because it breaks the fewest number of cation-anion bonds at the surface [16].

BACKGROUND STRUCTURAL INFORMATION

SnO_2 is a wide-band-gap (E_g=3.6 eV), n-type semiconductor with the rutile (TiO_2) structure. When viewed along the [110] direction, the bulk crystal is seen to be composed of charge-neutral units containing three atomic planes [17]. The composition and arrangement of the planes in the unit are $[(O^{-2})(2Sn^{+4} + 2O^{-2})(O^{-2})]$ per (110) unit cell. The charge on each plane is [(-2)(+4)(-2)], and the net charge per three-plane unit is zero. Because this unit has no net dipole moment in the [110] direction the (110) surface is termed nonpolar. The lower surface energy of a nonpolar vs. a polar surface dictates that an ideal, stoichiometric (110) surface will be terminated by a charge-neutral unit. Terminating the (110) surface with a complete, nonpolar, charge-neutral unit corresponds to breaking the smallest number of cation-anion bonds relative to the bulk structure [16]. This termination results in equal numbers of five and six coordinate tin cations in the second atomic layer. The full bulk coordination per cation is six.

Figure 1 illustrates the structure, composition and charges of the individual atomic planes associated with the SnO_2(110) surface. From Fig. 1 it can be seen that the ideal (110) surface is terminated with an outermost plane of oxygen anions which appear as rows in the [001] direction and occupy bridging positions between the second-layer, six coordinate tin cations. Oxygen atoms may also be seen in Fig. 1 in the same plane as the observable tin atoms. For convenience, the two different types of oxygen anions are referred to as "bridging" oxygens and "in-plane" oxygens, respectively.

NEARLY STOICHIOMETRIC SURFACES

The preparation of clean, stoichiometric SnO_2 surfaces for study in UHV is nontrivial. The usual cleaning methods of ion bombardment and high temperature annealing in vacuum preferentially remove surface lattice oxygen, leaving the surface in a reduced condition. Attempts to quantify the surface composition following such treatments typically yields O/Sn ratios less than 2.0, indicative of a less than stoichiometric surface [14]. A clear indication of the electronic consequences of the deviation from stoichiometry is the appearance of defect electronic states in the band gap as seen with ultraviolet photoelectron spectroscopy (UPS).

Surface characterization studies [18] have shown that a nearly ideal SnO_2(110) surface such as that illustrated in Fig. 1 may be reproducibly prepared by sputter cleaning, high temperature annealing in vacuum, and high temperature and pressure oxidation (700 K, 1.0 Torr O_2). The lack of band-gap emission in UPS following such a treatment is a sensitive indicator of a nearly-perfect, stoichiometric (110) surface. Figure 2 illustrates the variations observed in UPS for several surface preparations, including the in-situ oxidation treatment.

Heating the well-oxidized, nearly ideal, stoichiometric (110) surface in UHV removes large amounts of surface lattice oxygen. It has been shown with ion-scattering spectroscopy (ISS) [18] that vacuum annealing a nearly ideal SnO_2(110) surface at 700 K causes a complete removal of the layer of bridging oxygen anions which terminate the surface, leaving a surface terminated by a tin and oxygen containing plane. In addition to the removal of bridging oxygens and the formation of four coordinate Sn^{+2} cations at 700 K, heating in vacuum above 700 K causes the further removal of some in-plane oxygen from the tin and oxygen containing plane of the SnO_2(110) surface [18]. The formation of this second type of oxygen vacancy further lowers the coordination number of the neighboring tin cations from five and four coordination to four and three, respectively. Figure 3 is a ball-model illustration showing a nearly-perfect oxidized surface and a surface formed by removal of the top layer bridging oxygens and several in-plane oxygen anions. The figure illustrates the degree to which the composition changes in these treatments, and shows the variety of different coordination numbers of the tin cations.

The sequential fashion in which surface lattice oxygen can be removed from the oxidized SnO_2(110) surface (bridging oxygen below 800 K, in-plane oxygen above 800 K) makes it possible to tailor this surface in a controlled fashion. The tin cation coordination can be varied from six to three by the proper choice of sample preparation conditions. Associated with these changes in cation coordination, only one surface periodicity is observed in low energy electron diffraction (LEED) when an oxidized surface is used as the starting condition: a (1x1) pattern characteristic of a simple termination of the bulk periodicity. The constancy of the LEED pattern indicates that there is no gross restructuring or reconstruction of the surface associated with the creation of the oxygen vacancies. While there is likely to be some degree of relaxation about the vacancies, the local geometry and coordination is similar to that expected from a simple removal of oxygen atoms from the surface. In essence, the vacancies are created without significantly altering the crystal structure at the surface except by substantial changes in coordination number of the tin cations.

While no changes are observed in the surface geometric structure for these treatments, the surface electronic structure in the band gap undergoes several interesting changes. Associated with the removal of the terminating layer of bridging oxygen anions and the requisite change in coordination of half the surface tin cations from sixfold to fourfold coordination, the appearance of defect electronic states low in the band gap is also observed with UPS. The appearance of these states low in the band gap has been interpreted as the

formation of Sn^{+2} centers associated with the fourfold-coordinated cations [17,18]. For temperatures above 800 K, the formation of threefold-coordinate cations at in-plane oxygen vacancies results in the appearance of a second set of defect electronic states in UPS high in the band gap extending up to the Fermi level [57]. These changes in band-gap electronic structure are illustrated in Figure 4.

HIGHLY OXYGEN-DEFICIENT SURFACES

When ion bombarded and annealed in vacuum, the SnO_2(110) surface undergoes a number of reconstructions as characterized by low-energy electron diffraction (LEED) [19,20]. These reconstructions are driven by the high degree of oxygen deficiency associated with the ion-bombarded surface because of the preferential sputtering of oxygen. The most interesting of these reconstructions is the (4x1) surface which is formed by annealing the ion-bombarded surface near 900 K. This particular reconstruction corresponds to the formation of a reduced SnO(101) coincident overlayer [20] and the reduction of all surface cations to Sn^{+2} oxidation state. Therefore, by the choice of proper surface preparation conditions, a model SnO suboxide surface may also be reproducibly prepared from the SnO_2(110) surface. For annealing temperatures near 1000 K, the surface exhibits a (1x1) LEED pattern which has the same periodicity as the bulk, and hence approaches the same final condition regardless of whether the starting surface condition was ion-bombarded or oxidized.

UPS photoemission studies of the various reconstructions of highly oxygen-deficient SnO_2(110) surfaces show similar band gap features to those observed for the well-defined (1x1) surface [20]. It has been shown that the conclusions regarding the origin of the band gap features on the well-defined (1x1) surfaces can be generalized for more structurally complex situations. Defect electronic states low in the band gap are associated with fourfold-coordinated Sn^{+2} cations. States higher in the gap are characteristic of oxygen vacancies with neighboring threefold-coordinated Sn cations [20].

SITE-SPECIFIC ADSORPTION OF SIMPLE MOLECULES

The interaction of adsorbates with the electronic states in the band gap provides information about the local geometric and electronic properties of the adsorption sites. The effects of O_2, H_2, and H_2O adsorption on the band gap density of states of an ion-sputtered surface are shown with UPS difference curves in Figure 5 [21]. An ion-sputtered surface was chosen for this illustration because it exhibits a large density of states in the band gap when clean. Oxygen adsorption causes a decrease in the photoemission intensity throughout the band gap. Hydrogen adsorption causes a decrease in the defect intensity primarily in states just above the valence band maximum (VBM). A positive change in intensity near the conduction band minimum (CBM) is also seen for hydrogen. This increase is associated with the movement of the Fermi level up in the gap (i.e., downward band bending) and comes from occupied states near the Fermi level for the hydrogen dosed surface. The difference curve

for water shows an increase in the density of states near the Fermi level (as with hydrogen), but a decrease in other states in the top half of the gap. Similar trends are observed for oxygen deficient (4x1) and (1x1) surfaces. The changes in the band-gap density of states caused by H_2, O_2, and H_2O indicate that defects associated with oxygen vacancies play an important role in chemisorption on the (110) surface. Additionally, the gases exhibit some specificity between the different electronic states associated with the defect sites.

The previously described assignments for the types of surface defects associated with the band gap electronic states demonstrate that hydrogen and water are site-specific in their interaction with tin oxide surfaces. The interaction of hydrogen with states low in the gap demonstrates that adsorption occurs at fourfold-coordinated cations similar to those found in the presence of bridging oxygen vacancies. The interaction of water with the states high in the band gap demonstrates the adsorption of water at threefold-coordinated cations similar to those associated with in-plane oxygen vacancies.

SITE-SPECIFIC ^{18}O ISOTOPIC LABELING OF THE LATTICE

As with the use of labeled compounds in thermal desorption spectroscopy (TDS), the use of ^{18}O-labeled lattice oxygen at the SnO_2(110) surface provides a means of investigating the interaction of lattice oxygen in surface reactions. The study of isotopic exchange of oxygen with metal oxide catalysts has been widely used, but isotopic exchange with the well-characterized SnO_2(110) surface provides the unusual possibility of labeling not just surface lattice oxygen in general, but the labeling of only one of two different forms of lattice oxygen at the (110) surface with ^{18}O .

Unlike TiO_2, the diffusion of lattice oxygen through the SnO_2 matrix is slow at temperatures as high as 1000 K, as evidenced by the inability to form a stoichiometric or near-stoichiometric SnO_2(110) surface by simply heating in vacuum after ion bombardment [20]. Therefore, at the 700 K temperatures required for the in situ oxidation treatment [18,20], interlayer mixing of oxygen atoms is expected to be small. Recent ISS results [22] have shown that it is possible to selectively label bridging oxygen positions with ^{18}O since the two forms of surface lattice oxygen can be removed sequentially by heating to different temperatures in UHV. The labeling procedure will make it possible to distinguish between the participation of the two inequivalent forms of lattice oxygen in surface oxidation reactions using TDS.

COMPARISON BETWEEN EXISTING CATALYTIC DATA AND THE SURFACE PROPERTIES OF SnO_2(110)

The previous work on CO oxidation and NO reduction [6-9,23,24] offers insight into the role of SnO_2 in catalyzing oxidation/reduction reactions. The studies using pure tin oxide show that a redox mechanism dominates the chemistry at the surface of SnO_2. CO is converted to CO_2 on oxidized SnO_2 by the removal of

lattice oxygen, a process which reduces and quickly deactivates the catalyst as surface oxygen is consumed. Conversely, NO is converted to N_2 on reduced SnO_2 surfaces through a process which reoxidizes the catalyst. Therefore, the formation and decomposition of oxygenates is dependent on the availability of lattice oxygen at the surface.

There is a close relationship between the $SnO_2(110)$ surface characterization and the existing catalytic data on the selective isomerization of 1-butene to cis-2-butene (cis-/trans-2-butene = 19) over tin oxide powder [5]. Itoh et al. [5] found that the activity and selectivity for cis-2-butene increased dramatically when the catalyst was activated by heating in vacuum to temperatures in the range of 400°C to 600°C (723 K to 823 K). Associated with this change was the appearance of electron-donating paramagnetic centers on the catalyst as seen by ESR. In the presence of 1-butene the ESR signal for this center decreased, indicating a direct interaction between 1-butene and the paramagnetic center. A direct correlation was found between the activity and selectivity of the catalyst and the concentration of paramagnetic centers.

Note that the temperature range and preparation conditions (i.e., heating in vacuum) associated with the catalyst activation is similar to that required to remove in-plane oxygen atoms and expose threefold-coordinated tin cations on the $SnO_2(110)$surface. The electronic properties of the in-plane oxygen vacancies have been described previously in terms of surface color centers [18] which act as electron donors. In the ground state the anion vacancies bind two electrons by their Coulombic wells, and are thus doubly ionizable. The first ionization potential of the defect is small (25 meV [25]), therefore the majority of these centers are singly ionized and contain one unpaired electron as seen in the ESR signal. These similarities suggest that the isomerization reaction over powders occurs in the presence of sites similar to the in-plane oxygen vacancies observed on the $SnO_2(110)$-1x1 surface.

Itoh et al. also observed that the catalyst is poisoned by a number of compounds including H_2O. The UPS results described above for water adsorption on the $SnO_2(110)$ surface have shown that water preferentially adsorbs at in-plane oxygen vacancies on the $SnO_2(110)$ surface. Hence, both the isomerization activity of SnO_2 powders and the poisoning capacity of water can be explained in terms of the properties of the defective $SnO_2(110)$ surface.

REFERENCES

1. F.J. Berry, Adv. Catal. 30(1981)97.

2. D.J. Hucknall, Selective Oxidation of Hydrocarbons (Academic Press, New York, 1974).

3. S. Tan, Y. Moro-oka and A. Ozaki, J. Catal. 17(1970)125.

4. T. Sakamoto, M. Egashira and T. Seiyama, J. Catal. 16(1970)407.

5. M. Itoh, H. Hattori and K. Tanabe, J. Catal. 43(1976)192.

6. M.J. Fuller and M.E. Warwick, J. Catal. 29(1973)441.

7. G.C. Bond, L.R. Molloy and M.J. Fuller, J.C.S. Chem. Comm. (1975)796.

8. G.C. Bond, M.J. Fuller and L.R. Molloy, Proc. Int. Congr. Catal. 6th, 1(1977)356.

9. B. Hori, N. Takezawa and H. Kobayashi, J. Catal. 80(1983)437.

10. C.L. Lau and G.K. Wertheim, J. Vac. Sci. Technol. 15(1978)622.

11. T.W. Capehart and S.C. Chang, J. Vac. Sci. Technol. 18(1981)393.

12. W.E. Morgan and J.R. Van Wazer, J. Phys. Chem. 77(1973)964.

13. R.A. Powell, Appl. Surf. Sci., 2(1979)397.

14. D.F. Cox and G.B. Hoflund, Surf. Sci. 151(1985)202.

15. Z.M. Jarzebski and J.P. Marton, J. Electrochem. Soc. 123(1976)199,299,333.

16. V.E. Henrich, Rep. Prog. Phys. 48(1985)1481.

17. P.A. Cox, R.G. Egdell, C. Harding, W.R. Patterson and P.J. Tavener, Surf. Sci. 123(1982)179.

18. D.F. Cox, T.B. Fryberger and S. Semancik, Phys. Rev. B 38(1988)2072.

19. E. deFrésart, J. Darville and J.M. Gilles, Appl. Surf. Sci. 11/12(1982)637; Solid State Commun. 37(1980)13.

20. D.F. Cox, T.B. Fryberger and S. Semancik, Surf. Sci., in press.

21. D.F. Cox, T.B. Fryberger, J.W. Erickson and S. Semancik, J. Vac. Sci. Technol. A 5(1987)1170.

22. D.F. Cox and T.B. Fryberger, Surf. Sci., submitted.

23. M. Niwa, T. Minami, H. Kodama, T. Hattori and Y. Murakami, J. Catal. 53(1978)198.

24. F. Solymosi and J. Kiss, J. Catal. 41(1976)202.

25. J.W. Erickson and S. Semancik, Surf. Sci. 187(1987)L658.

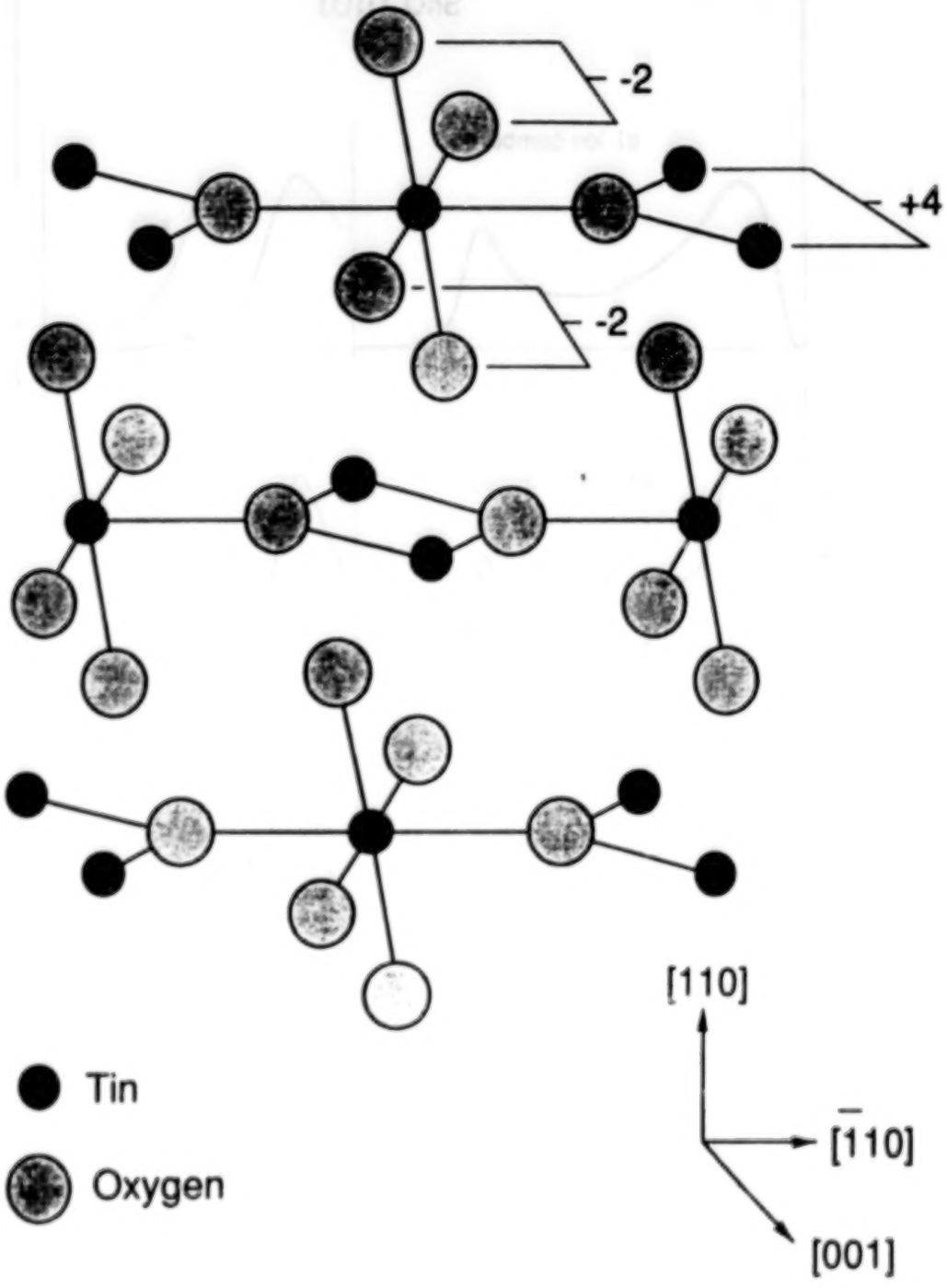

Figure 1. Illustration of the atomic arrangement at the ideal SnO_2(110)-(1x1) surface. The net charge per surface unit cell is shown for each of the three atomic planes composing a charge neutral unit perpendicular to the (110) direction. (Reproduced from Ref.20.)

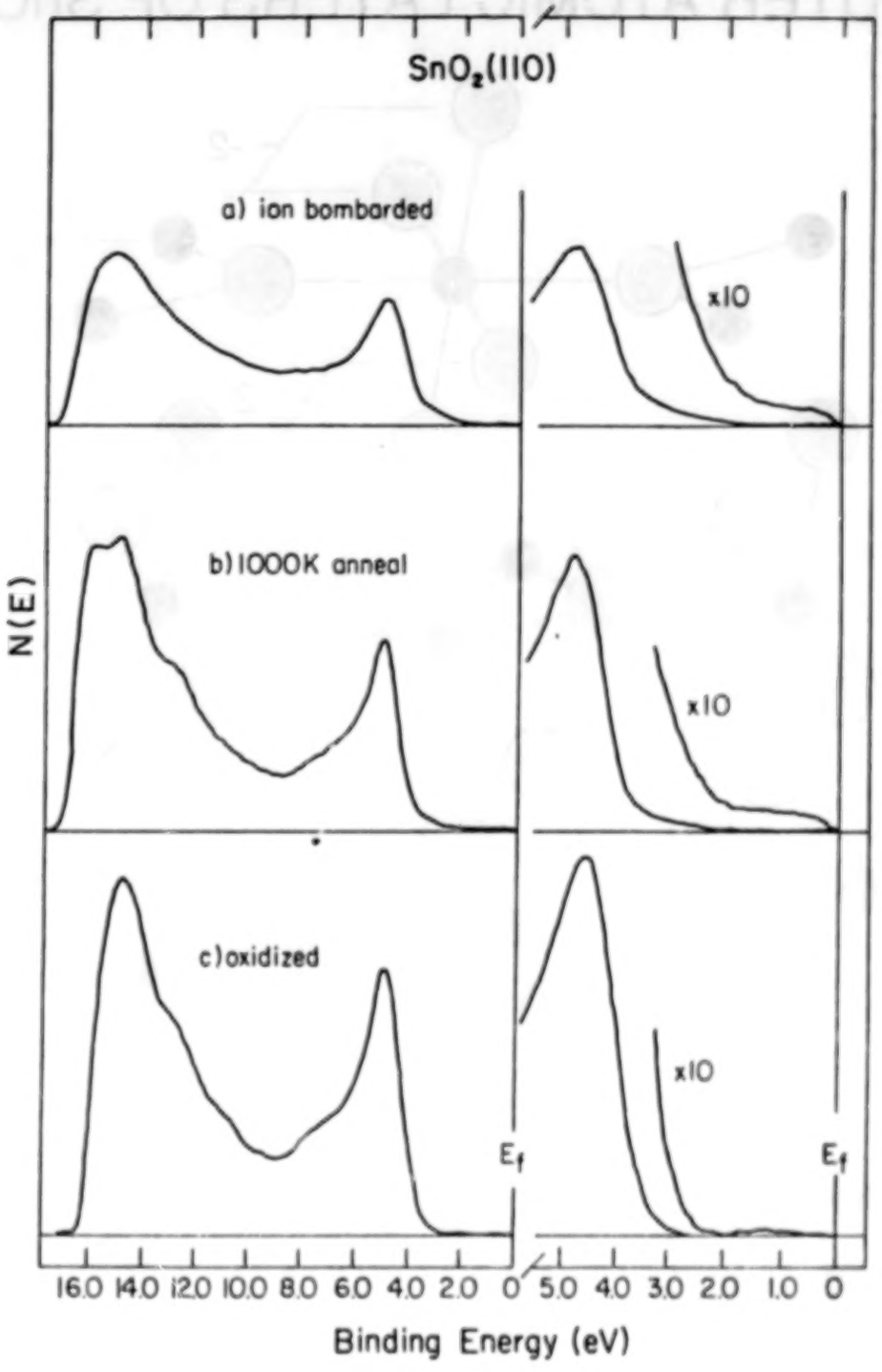

Figure 2. UPS spectra obtained following three different surface preparations: (a) 2-keV in bombardment, (b) ion bombarded and annealed in vacuum at 1000 K, and (c) oxidized in 1.0 Torr of O_2 at 700 K. The panels on the left are complete HeI spectra while the right-hand panels are enlarged views of the band-gap regions and the tops of the valence bands. All spectra are referenced to the Fermi level. (Reproduced from Ref.18.)

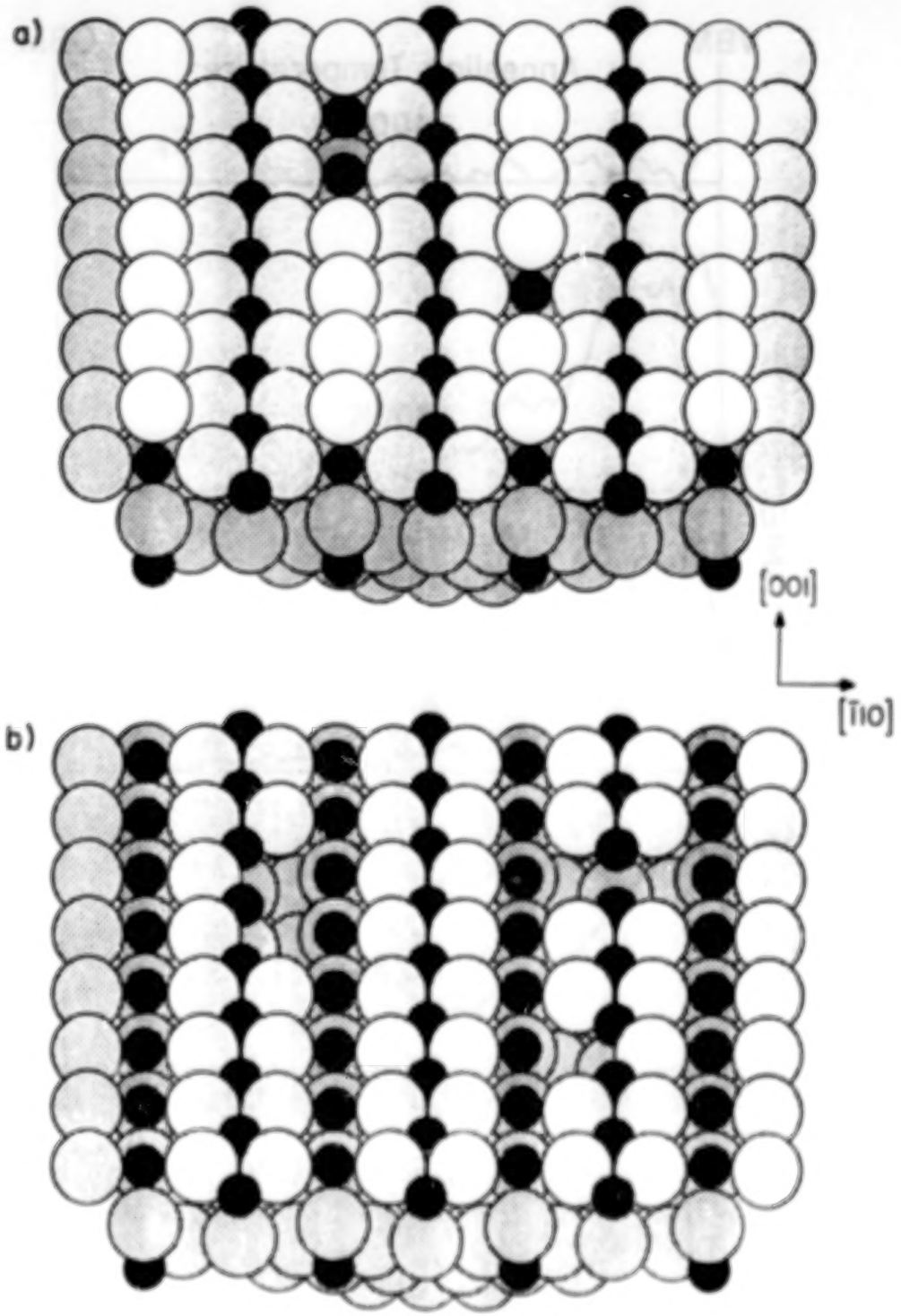

Figure 3. Ball model illustration of the surface viewed 50° off normal along the [001] azimuth. View (a) shows a nearly perfect (110) surface while (b) shows a bare surface following the removal of all top-layer bridging oxygen anions. A few in-plane oxygen vacancies are also shown in (b). (Reproduced from Ref.18.)

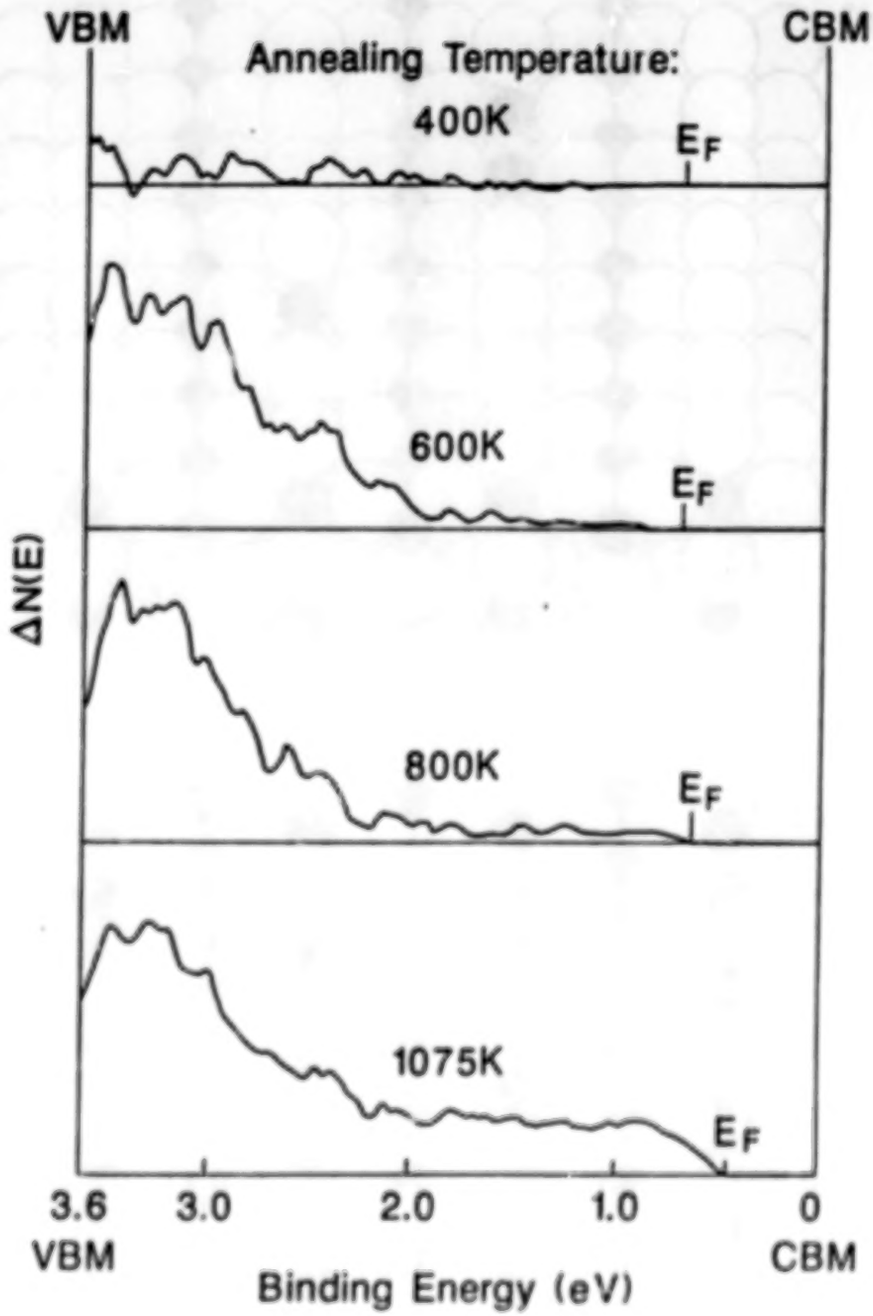

Figure 4. UPS difference curves showing the increase in band-gap (defect) electronic states caused by heating an oxidized surface in vacuum. The curves are referenced to the conduction band minimum (CBM). (Reproduced from Ref.18.)

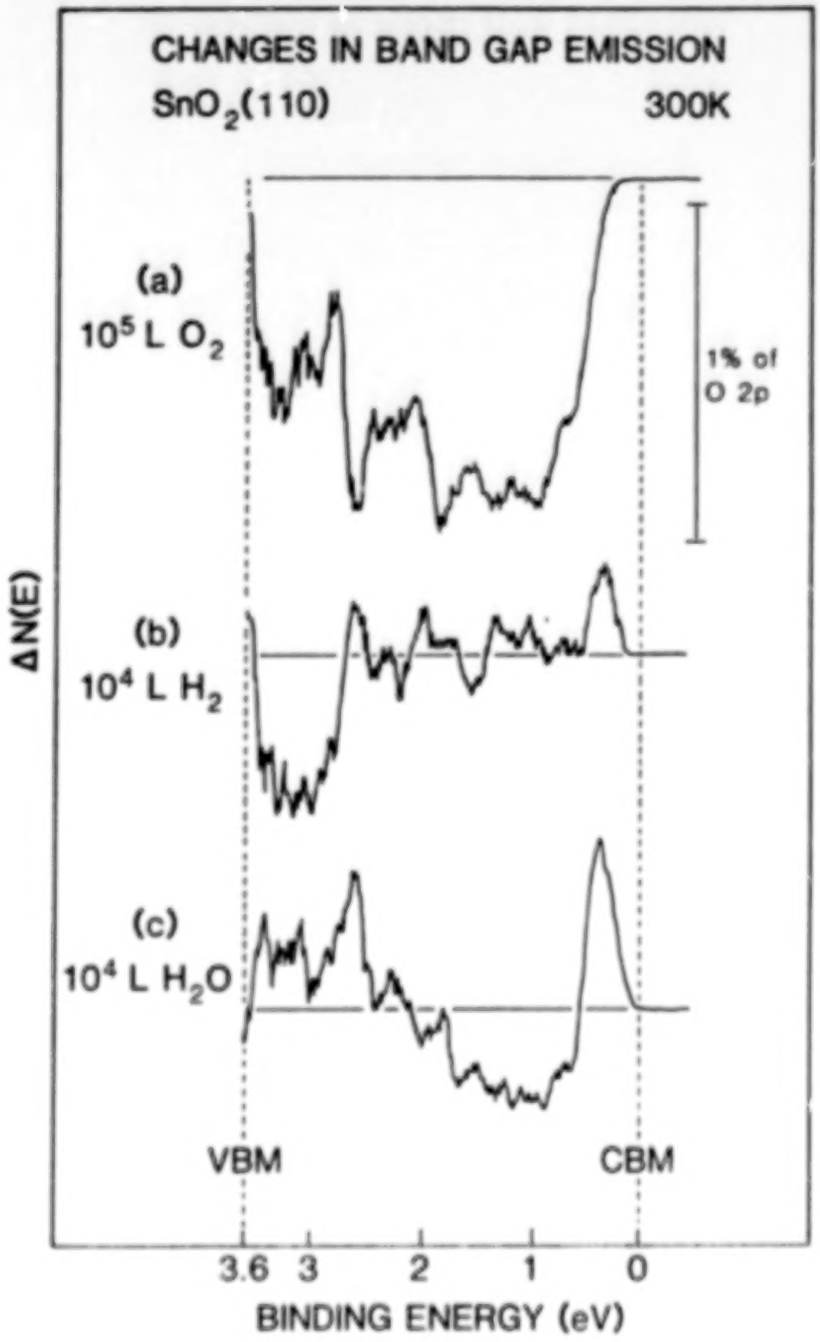

Figure 5. UPS difference curves indicating the changes in the band-gap density of states produced by adsorption of (a) 10^5L O_2, (b) 10^4L H_2, and (c) 10^4L H_2O on an ion sputtered surface. (Reproduced from Ref.21.)

MONITORING OF CATALYST PERFORMANCE IN CO_2 LASERS USING FREQUENCY MODULATION SPECTROSCOPY WITH DIODE LASERS

Liang-guo Wang
Department of Physics, College of William and Mary

Glen Sachse
NASA, Langley Research Center

Closed-cycle CO_2 laser operation with removal of O_2 and regeneration of CO_2 can be achieved by catalytic CO-O_2 recombination. Both parametric studies of the optimum catalyst formulation and long-term performance tests require on line monitoring of CO, O_2 and CO_2 concentrations.

There are several existing methods for molecular oxygen detection. These methods are either intrusive (such as electrochemical method or mass spectrometry[1]) or very expensive (such as CARS, UV laser absorption[2,3]).

We present here a high-sensitivity spectroscopic measurement of O_2 using two-tone frequency modulation spectroscopy (FMS) with a GaAlAs diode laser. Recently frequency modulation spectroscopy has been developed as a powerful method of doing highly sensitive, real-time spectroscopic measurements[4-8]. The theory of single-tone FMS and two-tone FMS have been studied and discussed in detail[4-6]. Since frequency modulation of diode lasers can be achieved by direct injection current modulation, FMS with near infrared diode lasers becomes a very attractive technique to make inexpensive, room-temperature spectroscopic probes for a variety of gases. It has been successfully used for water vapor absorption measurements at wavelengths near 815 nm[9] and methane absorption at wavelengths near 840 nm[10]. With careful selection, an inexpensive commercial laser diode can be obtained that is wavelength tunable from 760-770 nm, where the oxygen A band absorption occurs. This is the $v'=0 \leftarrow v''=0$ band of the magnetic dipole transition from the $x\,^3\Sigma_g^-$ ground electronic state to the excited $b\,^1\Sigma_g^+$ state. This band is known as the O_2 atmosphere band and has been well studied for line strengths, line widths and other spectroscopic parameters[11-14].

We have used a frequency modulation spectrometer, which was built at the University of Virginia, to make the O_2 spectroscopic measurement. Fig. 1 shows the schematic diagram of the frequency modulation spectrometer. A GaAlAs laser (Sharp LT030MF) operating at near 760 nm was mounted on a thermoelectrically cooled/heated block. The laser frequency is varied either by sweeping the injection current of the diode laser or by scanning its temperature with a tunability of 0.12 cm^{-1}/mA (3.6 GHz/mA) or 1.1 cm^{-1}/°C (33 GHz/°C), respectively. In the first case the injection current of the diode laser is swept by an internal function generator to provide straightforward injection-current tuning of the laser frequency. Injection-current tuning gives relatively fast scans (≈120 Hz) which permits us to monitor the FM signal directly on an

oscilloscope. This frequency modulation spectrometer also includes a computer-interfaced temperature controller to provide a slow scan of temperature and hence a slow scan of the frequency of the laser. The temperature controller provides a temperature stability of better than 0.01°C over several hours. A built-in automatic power controller stabilizes the laser output power within 2% when the laser temperature is varied from 10°C to 60°C. The GaAlAs diode laser is injection current modulated at two closely spaced frequencies (1 GHz ± 12 MHz) using capacitive coupling. The two-tone frequency modulated light from the laser is collimated by a 7-mm focal-length lens and passes through a 20-cm-long O_2 sample cell at approximately one atmosphere pressure. The 24 MHz rf beat signal of the two laser modulation frequencies is detected and amplified by using a photodetector (EG & G FND-100) and low-noise rf amplifiers. The signal is then phase detected by a mixer. Finally the signal is directed either through a 100-kHz low-pass filter to be displayed on an oscilloscope (i.e. for injection current tuning) or through a 0.8-Hz low-pass filter to be plotted on a plotter or to be stored into a computer (i.e. for temperature tuning).

Fig. 2 shows two-tone FMS signals of five Oxygen A band absorption lines. The absorption for these lines ranged from 0.8% to 1.2%. The O_2 A band consists of P and R branches. Due to the splitting of the ground electronic state rotational levels, each of these branches is composed of pairs of lines (PP and PQ for P branch; RR and RQ for R branch). The five absorption lines in Fig. 2 belong to the R branch of oxygen A band near 760 nm.

FMS with diode lasers provides high detection sensitivity. Near quantum limit absorption sensitivity of 3×10^{-7} in a 0.8 Hz bandwidth for water vapor absorption lines has been reported[9]. A sensitivity of 10^{-6} can be easily obtained with a little care on eliminating the interference fringes. With a reference cell of O_2, the GaAlAs diode laser can be locked at a particular oxygen absorption line using a electronic feedback circuit. In this way the continuous monitoring of oxygen concentration in an on-line sample cell can be achieved. The minimum detectable (i.e. with S/N of 1) optical depth is estimated to be 5 ppm.meter with a 1 Hz bandwidth.

In conclusion, we have demonstrated a high-sensitivity spectroscopic measurement of O_2 using the two-tone FMS technique with a near infrared GaAlAs diode laser. Besides its inexpensive cost, fast response time, nonintrusive measurements and high sensitivity, this technique may also be used to differentiate between isotopes due to its high spectroscopic resolution.

This frequency modulation spectroscopy technique could also be applied for the on-line monitoring of CO and CO_2 using InGaAsP diode lasers operating in the 1.55 μm region and H_2O in the 1.3 μm region. The existence of single mode optical fibers at these near infrared region makes it possible to combine FMS with optical fiber technology. Optical fiber FMS is particular suitable for making point-measurements at one or more locations in the CO_2

laser/catalyst system.

REFERENCES

1. J. J. Singh, W. T. Davis and R. L. Puster: Proposed Fast-Response Oxygen Monitoring and Control System for the Langley 8-Foot High-Temperature Tunnel. NASA TP-2218(1983).

2. M. P. Lee, P. H. Paul and R. K. Hanson, Opt. Lett. 11, 7(1986).

3. J. E. M. Goldsmith and R. J. M. Anderson, Opt. Lett. 11, 67(1986).

4. G. C. Bjorklund, M. D. Levenson, W. Lenth, and C. Ortiz: Frequency Modulation (FM) Spectroscopy: Theory of Line Shapes and Signal-to-noise Analysis. Appl. Phys. B32, 145(1983).

5. G. R. Janik, C. B. Carlisle, and T. F. Gallagher: Two-Tone Frequency Modulation Spectroscopy. J. Opt. Soc. Am. B 3, 1070 (1986).

6. D. E. Cooper and R. E. Warren: Two-Tone Optical Heterodyne Spectroscopy with Diode Laser: Theory of Lineshapes and Experimental Results. J. Opt. Soc. Am. B4, 470 (1987).

7. N. -Y. Chou and G. W. Sachse: Single-Tone and Two-Tone AM-FM Spectral Calculations for Tunable Diode Laser Absorption Spectroscopy. Appl. Opt. 26, 3584(1987)

8. L. G. Wang, H. Riris, C. B. Carlisle and T. f. Gallagher: Comparison of Approaches to Modulation Spectroscopy with GaAlAs Semiconductor Lasers: Application to Water Vapor. Appl. Opt. 27, 2071(1988).

9. L. G. Wang, D. A. Tate, H. Riris and T. F. Gallagher: High-sensitivity Frequency Modulation Spectroscopy With A GaAlAs Diode Laser. J. Opt. Soc. Am.B, 6, 871(1989).

10. L. G. Wang, unpublished data.

11. D. E. Burch and D. A. Gryvnak: Appl. Opt. 8, 1493(1969).

12. J. H. Miller, R. W. Boese and L. P. Giver: J. Quant. Spectrosc. Radiat. Transfer 9, 1507(1969).

13. L. S. Rothman et al.: The HITRAN database (1986 edition). Appl. Opt. 26, 4058(1987).

14. K. J. Ritter and T. D. Wilkerson: J. Mol. Spectrosc. 121, 1(1987).

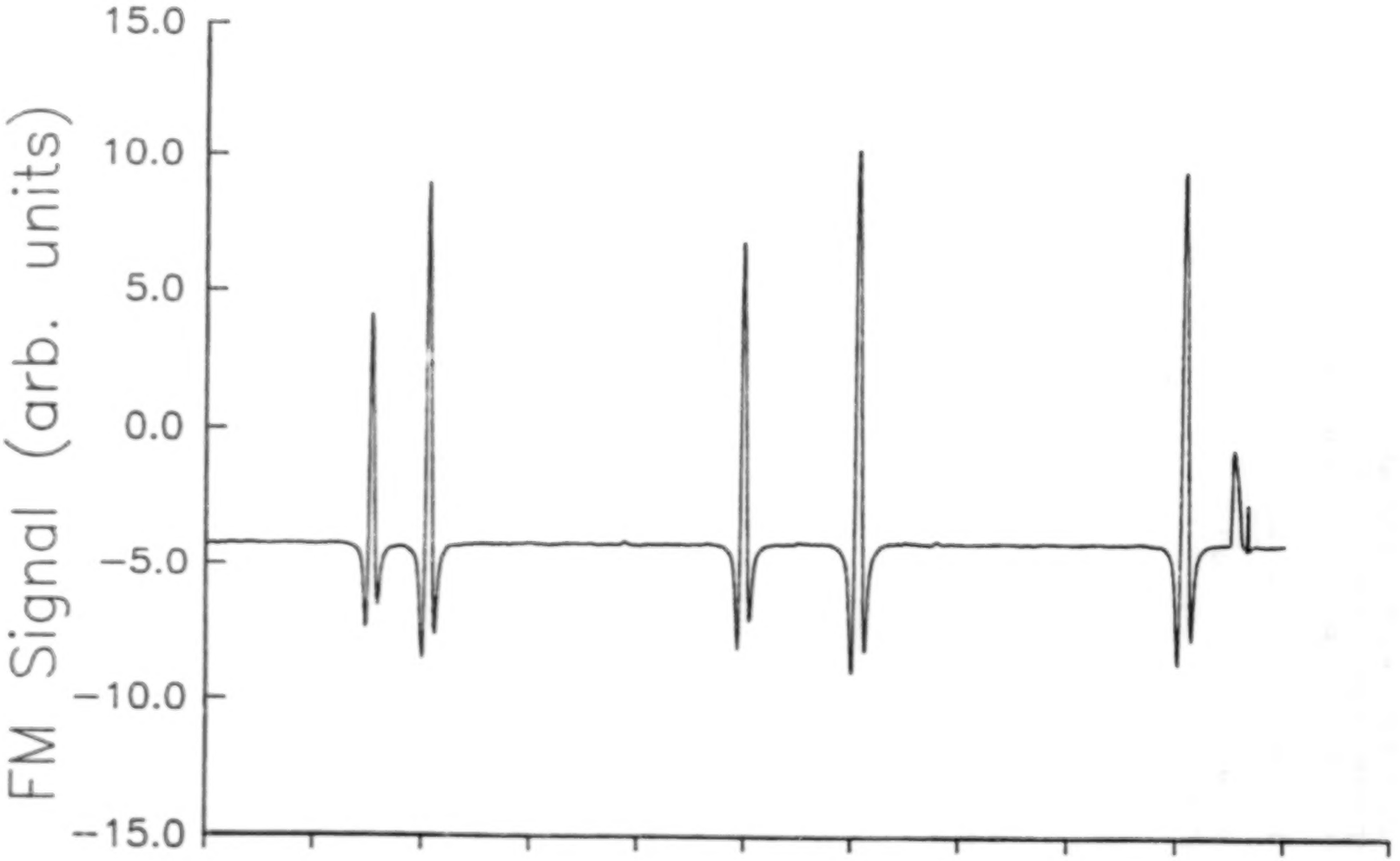

Fig. 2. Two-tone FMS signal of five O_2 absorption lines.

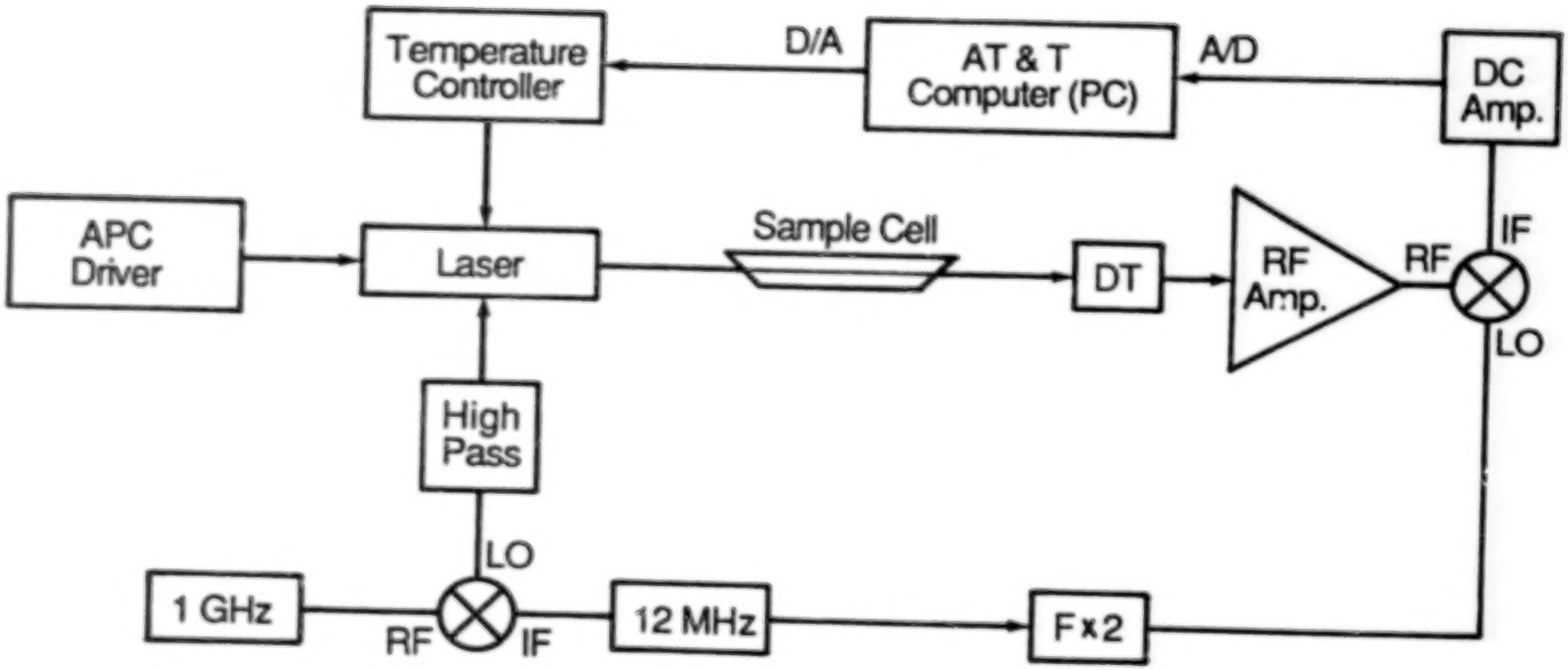

Fig. 1. Experimental setup for two-tone frequency modulation spectroscopy.

IN-SITU ANALYSIS OF CO DURING CHEMISORPTION AND OXIDATION ON GRAPHITE-SUPPORTED Pt BY FTIR-MICROSPECTROMETRY

Valerie A. Shelf and Paul A. Sermon
Department of Chemistry, Brunel University
Uxbridge, Middlesex, UB8 3PH, UK

ABSTRACT

For chemisorption and oxidation on Pt/HOPG (highly-orientated pyrolytic/graphite), reflectance FTIR-microspectrometry reveals a variable state and reactivity for CO. Even for model surface science systems, where surface heterogenity is minimal, surface diffusion may be too slow relative to the reaction rate to avoid segregation of reactants into surface islands under steady-state conditions. Thus in CO oxidation on Pt (where the relevant surface diffusion coefficients are such that $D_o < D_{co}$ then reactant CO islands exist at the perimeters of which the surface reaction is thought to occur. Furthermore CO can chemisorb on metals in linear (atop) and bridge forms to extents which vary with the precise faces predominantly exposed, coverage, etc.

Infra-red has long been used to probe the nature of adsorbed CO on model film and heterogenous surfaces, but it may now be that FTIR-microspectrometry will allow the state of this adsorbate and reactant to be investigated with a spatial resolution of 4.4 μm on model (and real) catalytic surfaces.

Because of its high degree of perfection at an atomic level, highly-orientated pyrolytic graphite (HOPG) has been used as a standard for scanning tunnelling microscopy. Here it has been coated with Pt by vacuum deposition to form a sample of polycrystalline Pt/C which is well defined. Specifically the HOPG sample was sputtercoated with Pt for
30 min., to give a Pt layer 60nm in thickness. No other metallic impurities were detected.

The sample was placed in the FTIR cell within the IRPLAN (Spectra-Physics) IR microscope linked to a Perkin Elmer 1710 FTIR, through which the reactant gases could flow as follows:

(i) in chemisorption 6%CO/N_2 flowed at 23ml/min while heating to 425K at 5K/min and holding at 425K for 45 min before cooling to room temperature

(ii) in CO oxidation where 6%CO/N_2 (21.4ml/min) and 6%O_2/N_2 (21.1ml/min) flowed while heating to 425K at 5K/min and holding isothermally for 2h before cooling to room temperature

Using this IR microscope it was possible to measure reflectance FTIR spectra for selected areas of the surface of the catalyst. All spectra were measured using 50 scans with no subsequent smoothing and with a resolution of $8cm^{-1}$.

In CO chemisorption and oxidation it is thus possible to differentiate linearly-bound and bridge-bound CO by IR.

Reflectance spectra for the surface CO and CO_2 species on Pt/HOPG catalysts in CO chemisorption and CO oxidation have been obtained and analyzed. The area being sampled is 440 μm^2. No significant gas phase bands were noted in this region.

Consistent with analysis of CO on low index crystallographic planes of Pt the

(i) α peak at $1890\pm9cm^{-1}$ is bridge bound CO

(ii) weaker bands at 1933, 1953 and $1982\pm2\text{-}4cm^{-1}$ are γ bands

(iii) β peak at $2082\pm1cm^{-1}$ is linearly-bound CO

In CO chemisorption it is clear that the ratio of α:β peaks varies with analytical position across the Pt/HOPG crystal; so does the extent of observation of γ bands. In other workds the surface is not entirely homogeneous with respect to CO adsorbate. The intensity of the bridge-bound CO band is greater than was expected on Pt. In CO oxidation CO_2 is observed at $2360cm^{-1}$ when the smaller γ peaks are not observed and the α peak is severly reduced relative to the intensity observed in chemisorption of CO alone; suggesting that the α and γ peaks are associated with the most active species in CO oxidation on this Pt, either because they are at the edge of CO islands or because their vibrational characteristics make the transformation to CO_2 easier. In addition, the α peak is shifted to $1887\pm1cm^{-1}$ while the β peak remains at about its earlier position in CO chemisorption: therefore linearly bound CO may be quite unreactive on this surface and unaffected by the presence of O. On Pt/HOPG the apparently more reactive bridge-bound state decreased in intensity on CO oxidation, but the evidence of CO_2 formation and
α/ peak decrease is not uniformly exhibited by the whole surface.

The surface diffusion coefficient D_o of oxygen is thought to be smaller on Pt than that for CO, although both coefficients may be decreased substantially as the surface becomes less energetically homogeneous since the periodic nature of the potential energy surface governs the whole question of surface mobility. This may then be the cause of the spatial difference of CO on the Pt/HOPG seen here in adsorption and catalysis. It may be that reactant islands are important in defining catalysis since the perimeters of these might have highest densities of bridge-bound CO, but alternatively bridge-bound CO may from a vibrational point be more readily converted to CO_2. Nevertheless, the relationship of these results to those obtained for Pt foil in CO oxidation, where active surface grains were seen, may be interesting.

Although since the mid 1950's infra-red has been used to identify adsorbed species on the surfaces of solids and catalysts, it often remains uncertain whether the species detected are the important participants in surface reactions rather than mere spectators, which may numerically exceed the more reactive metastable short-lived participants which are responsible for catalysis.

The present microspectroscopy may be useful in understanding the microchemistry of catalytic surfaces in the sense that here in CO oxidation it suggests that the surface is not uniformly reactive (which is consistent with the presence of reactant islands). Ultimately, this may allow us to understand and control activity-selectivity of such surfaces via fractality-diffusional modes. This new analytical approach could lead to heterogeneous reactions being more effectively and selectively catalysed by surfaces which are even better understood and properly optimised.

Differential-Scanning Calorimetry and Activity-Temperature Hysteresis in CO Titration and Oxidation on Pt and Supported PT Catalysts

Paul A. Sermon, et al.
Brunel University
United Kingdom

This abstract and paper not available at time of printing.

CHARACTERIZATION OF THE SURFACES OF PLATINUM/TIN OXIDE BASED CATALYSTS BY FOURIER TRANSFORM INFRARED SPECTROSCOPY (FTIR)

Joseph T. Keiser and Billy T. Upchurch
NASA Langley Research Center
Hampton, Virginia

ABSTRACT

Transmission FTIR has been used to characterize the surfaces of platinum/tin oxide catalysts and component materials, tin oxide and silica gel. Spectra of the dehydration and reduction of these catalysts will be presented and discussed.

CHEMISORPTION STUDIES OF Pt/SnO_2 CATALYSTS

Kenneth G. Brown, Susan K. Ohorodnik, John D. Van Norman, Jacqueline Schryer, Department of Chemistry, Old Dominion University, Norfolk, Va 23529.

Billy T. Upchurch and David Schryer, NASA Langley Research Center, Hampton, Va 23665

A pulse gas chromatography (GC) apparatus is described which is currently being used to determine the chemisorption of CO, CO_2 and O_2 upon NASA catalysts and their components. This apparatus allows the measurements to be made under the pretreatment conditions that have been determined to be optimum for this catalyst. The dispersion of the catalysts can be determined allowing better comparison of the activity of different catalysts by reducing the data to a turn-over frequency. We may also add water to the sample pulse to determine its effect upon the chemisorption of a particular molecule.

In addition to the GC measurements, the samples are also being analyzed by Diffuse Reflectance Infrared Fourier Transform Spectroscopy (DRIFTS). In this experiment the samples are removed from the GC reactor and immediately placed in the Infrared spectrophotometer. The resultant spectra will then be used to help determine the nature of the adsorbed species and any alterations that may have occurred in the catalyst itself.

DISSOCIATION PHENOMENA IN ELECTRON-BEAM SUSTAINED CARBON DIOXIDE LASERS

Michael R. Harris and David V. Willetts
Royal Signals and Radar Establishment
Great Malvern, Worcestershire WR14 3PS, UK

INTRODUCTION

A number of applications are emerging requiring efficient, long pulse, long-life sealed CO_2 lasers. Examples include the proposed NASA and ESA wind lidars. Electron-beam sustained discharge devices are strong contenders. Unlike self-sustained discharges e-beam sustenance readily provides efficient performance from large volume discharges and offers pulse lengths well in excess of the microsecond or so generally associated with self-sustained devices.

In the case of the e-beam sustained laser, since the plasma is externally maintained and operated at electric field strengths less than that associated with the glow to arc transition, the discharges can be run even in the presence of strongly attacking species such as O_2. Build up of large levels of attacking contaminants is nevertheless undesirable as their presence reduces the current drawn by the plasma and thus the pumping rate to the upper laser level. The impedance rise leads to a mismatch to the pulse forming network with a consequent loss of control over energy deposition, operating E/N, and gain.

Clearly CO_2 dissociation rates, the influence of dissociation products on the discharge and gain, and tolerance of the discharge to these products need to be determined. This information can then be used to assess co-oxidation catalyst requirements for sealed operation.

CARBON DIOXIDE DISSOCIATION

Experimental Apparatus

The equipment used for the oxygen tolerance determination is shown schematically in Figure 1. The electron gun was a cold cathode plasma device run at a pressure of a few tens of microns of helium which was continuously bled in and pumped out by a Roots blower/backing pump combination. This type of gun has been described elsewhere (ref 1); briefly an auxiliary glow discharge is maintained in the drift region and provides ions for acceleration by the pulsed electric field. Secondary electrons emitted from the cathode are accelerated through a capacitative voltage dividing structure to provide an internal gun current of about an amp. The 150kV voltage pulse is delivered by a 6 mesh PFN of total capacitance 0.3μF and total inductance 918μH, switched by a thyratron through the primary of a 10:1 turns ratio pulse transformer. Gun current and voltage could be monitored by inductive loop and resistive division probes and recorded on a storage oscilloscope. The area of the foil separating the main discharge chamber and the gun was 30 x 2cm^2.

The main discharge chamber was constructed almost entirely of Monel, except that Viton O-rings were used for the demountable seals, the foil separating the gun from the main discharge was 25μm aluminium, and insulating lead throughs were made of PTFE. The removable discharge limiters were constructed of alumina. For the majority of the experiments the Monel grid protecting the foil was operated as the anode, so that the cathode material could readily be changed. The

main discharge PFN was a 6 mesh configuration of total capacitance 0.6μF and total inductance 322μH. Voltage and current mointors were provided for the main discharge as for the gun. Figure 2 illustrates the primary current transmitted through the foil; the current could be altered by adjustment of gas pressure in the gun and by control of gun voltage. Figure 3 shows typical main discharge current and voltage waveforms. Note that the current trace is inverted and that the current monitor baseline falls during the pulse.

Continuous analysis of oxygen and carbon monoxide was available using a paramagnetic oxygen analyser and an infrared CO analyser in a flow loop as shown in Figure 1. The oxygen analyser incorporated a pump which resulted in a residence time within the main discharge chamber of about one minute. The device was normally filled by pumping and flushing with the 3:2:1 $He:N_2:CO_2$ gas mixture introduced from a gas manifold before final tap-off. The gas manifold incorporated a range of flow meters for appropriate gases calibrated by a direct water displacement and timing method. Mixtures prepared using these flowmeters were used to check the calibration of the two gas analysers. Main discharge and analyser volume was measured to be 2.28 l by a pressure change method.

Dissociation by Main Discharge

The basic method used to measure this parameter is described below. The main discharge chamber was filled with gas mixture and the gun run at a prf of about 1Hz. The voltage on the main discharge PFN was set to give a value of 4kV/cm atm (1.5×10^{-16} V cm^2) for the operating E/N. As dissociation took place, attaching products were formed which raised the discharge impedance. This caused a mismatch to the PFN so the PFN charging voltage was altered to maintain the E/N at the desired value. Thus the charge passed per shot gradually fell as a consequence of the discharge voltage and duration being held constant and the rise of the main discharge impedance. The result is the nonlinear variation of discharge impedance and oxygen (and CO) concentration with number of pulses shown in Fig 4. A more useful measure of dissociation is as a function of total charge passed and Figure 5 shows such a plot, as crosses, abstracted from the data of Figure 4. It is to be expected that the dissociation rate should depend linearly on CO_2 partial pressure, and thus as oxygen is formed, CO_2 is lost and the dissociation rate falls. Correcting for this loss we obtain the circles as data points in Figure 5 which is thus essentially a dissociation rate at constant CO_2 partial pressure of 0.167 atm. The linear dependence on total charge passed is exactly what would be naively expected, and corresponds to 26.1μmoles of oxygen formed per Coulomb of charge passed by the main discharge, which is equivalent to 2.15 molecules of oxygen produced by each secondary electron crossing the main discharge gap. The $CO:O_2$ stoichiometry was found to about 2.5:1 in all our experiments, similar to results for self-sustained devices. The validity of the assumption that the dissociation rate depends on the CO_2 partial pressure was verified by studying a range of CO_2 concentrations up to 30%. The resultant O_2 generation rates are plotted in figure 6.

Calculations were performed of the bulk dissociation by thermalised secondary electrons. The dissociation in moles per coulomb F is given approximately by (ref 2)

$$F = \frac{G_{PCO_2}}{e\bar{\nu}V_o} Q_{oj} \left[\frac{kT}{e}\right]^{\frac{1}{2}} \left[1 + \frac{\epsilon_j}{kT_e}\right] \exp - \left[\frac{\epsilon_j}{kT_e}\right] \times 6.7 \times 10^7 \qquad (1)$$

where e and m are the charge and mass of the electron, T_e is the glow electron temperature, ϵ_j is the onset energy of the dissociation process of peak cross-section Q_{oj}. $\bar{\nu}$ is the electron drift velocity at the appropriate value of E/N, PCO_2 is the partial pressure of CO_2 in the gas mixture and V_o is the volume containing one mole at the working pressure of one atmosphere. Relevant data on T_e and $\bar{\nu}$ for the 3/2/1 mixture at the appropriate E/N was taken from References (3) and (4) but it

should be noted that Judd's value of T_e of 0.37eV is hardly more than half of Lowke Phelps and Irwin's value of 0.7eV. For all the subsequent calculations we quote both values with the parenthetic note (J) for the 0.37eV and (LPI) for the 0.70eV case. Using values of ϵ_j and Q_{oj} applicable to dissocation (6.2eV and 3.5×10^{-17} cm^2; reference 5) and dissociative attachment (3.9eV and 1.5×10^{-19} cm^2; reference 6), we found similar rates for both processes, but these were in excess of three orders of magnitude lower than experimental findings. This suggests that dissociation is not a bulk process but may be confined to the (cathode) sheath region. This lead us to repeat the dissociation measurement with the gap reduced from 2cm to 1cm and in support of this conjecture it was found that the dissociation rate was unaltered within experimental error. Further measuremets were carried out at halved E/N, and also with the cathode changed from Monel to Dural (a hardened Al alloy), and to 60/40 brass. Also explored was the effect of altering the electrode polarity so that dissociation takes place on the grid rather than on the smoothly profiled electrode. These changes did not significantly alter the dissocation rate either; addition of alumina discharge limiters increased the dissociation rate by about 10%, which we suspect to be due to field distortions caused by the presence of the thick high permittivity limiters. All this evidence is shown in Figures 7 and 8 and points toward dissociation in the sheath region; we have made initial attempts to estimate the magnitude of this process.

It is probably fair to say that the detail of the cathode fall mechanism is not well understood. J J Thomson (ref 7) derived the form of potential fall in a gap which is externally sustained and in which the electron loss process is by recombination. This theory is readily altered to encompass the attachment loss mechanism operative in our device (see below) but unfortunately the assumption that the loss mechanism can be neglected in the sheath leads to preposterous values of cathode fall Φ and sheath thickness L. A much better model has been provided by N G Basov (ref 8) who has adapted the von Engel and Steenbeck treatment of self-sustained discharges for the nonself-sustained case. The assumptions are:

1. Electron emission from the cathode occurs solely by positive ion bombardment, so that

$$j_e = \gamma j_+$$

2. The field varies linearly in the sheath,

$$E(X) = E_o(1-X/L)$$

where X is the distance from the cathode.

Hence from Poisson's equation, ρ is a constant and since

$$\frac{n_+}{n_e} = \frac{j_+ v_e}{j_e v_+} = \gamma^{-1} \frac{v_e}{v_+} \gg 1,$$

$$\rho = \rho_+ = \frac{1}{4\pi}\left[\frac{E_o}{L}\right]$$

3. The positive ion velocity v_+ is constant in the sheath, implying that j_+ is constant and

$$v_+ = \frac{4\pi j_+}{(E_o/L)} = \frac{4\pi j_{tot}}{(E_o/L)} \quad \text{since } \gamma \ll 1.$$

4. The total current density j_{tot} is equated to the value outside the sheath

$$j_{tot} = N_e e \mu_e \left[\frac{E}{p}\right]$$

5. The Holst and Oosterhuis-Seeliger condition holds for balance of electron loss and gain in the cathode fall:

$$\ln\left[1 + \frac{1}{\gamma}\right] = \int_0^L \alpha(X)dX$$

6. The ionisation coefficient α may be written as

$$\alpha/p = A\left[\frac{E}{p} - B\right]^2$$

The results Basov finds are

$$\Phi = \left[\frac{E_o}{p}\right]^2 \frac{Dp^2}{N_e(E/p)}$$

and

$$\frac{E_o}{p} = C\left[\frac{N_e E/p}{p^2}\right]^{1/3} + B$$

and

$$L = \frac{2\Phi}{E_o}$$

Here $D = v_\phi/8\pi\mu_e$ and $C^3 = 3/2DA \ln 1/\gamma$.

We have attempted to use this approximate analysis to examine dissociation in the sheath. Lowke et al (ref 3) give α/p for the 3/2/1 mixture which best fits the Basov formulation near 100V/cm torr for $A = 1.32 \times 10^{-4}$, $B = 0$. γ was set equal to 0.011 and v_ϕ was taken to be 1.3×10^5cm/sec, with μ_e equal to 8×10^5cm^2 torr/sec V. D was thus found to be 4.5×10^4 and C to be 1.045. Φ varied between 200 and 330 V with L varying between 22 and 55μ as N_e was varied over a range 3.5×10^{11}cm^{-3} to 1.4×10^{12}cm^{-3}. Next the gap was divided into ten equal slices and the electron current and thus dissociation evaluated in each slice. It was found that the dissociation increased as E/N fell and electron energy better matched that required for dissociation; the rate maximised at about 70-80% of the distance from the electrode to the negative glow. Agreement with the measurement was not good - calculation was about 50 times less, but is nevertheless much better than that of the bulk process, especially considering the large number of approximations in the analysis. The most disturbing feature of this analysis is the prediction of a

changing dissociation rate as N_e changes as a consequence of oxygen buildup, ie significant curvature should be expected in Figures 5, 7 and 8. It may well be that dissociation is taking place in the negative glow region rather than the cathode fall. It is important to note that the lack of volume scaling indicates that the result should be applicable to any e-beam sustained laser device.

Dissociation by Primary Beam Alone

The results quoted above obviously indicate dissociation by both main discharge and primary electron beam. The latter has a very high energy of about one hundred keV at which dissociative cross-sections are very small. Thus bulk dissociation due to primaries is not expected to be an important process. Exactly the same method was used to assess the effect of the primary beam alone as already described, except that the collector electrode was 'earthed' through a 50ohm resistive current probe. Fiugure 9 illustrates the findings with a linear buildup of oxygen with number of pulses at a rate dependent on current within the pulse. Figure 10 shows that the dependence on current is linear and so the dissociation scales linearly with charge passed. Much more surprising is the independence on the volume exposed to primaries, very similar to the observations on the main discharge. It would thus appear that a surface mediated effect is being observed which was quite unexpected. A further experiment was performed of varying widely the carbon dioxide partial pressure in the gas mixture, starting with a system cleaned by evacuation and repetitive pulsing of the gun and gradually increasing pCO_2. Figure 11 records the results which are absorption isothermal in form, suggestive of a true surface dissociation. However, the rate is amazingly high, at 15mmole/coulomb for the 3/2/1 mixture. This corresponds to 3000 CO_2 molecules being broken up for each primary electron passed which corresponds to a few monolayers/pulse and an overall efficiency of about 20% of total primary beam energy going into dissociation. The primary process appears to be contributing 10-15% of the total cracking observed in the main discharge.

A number of possible mechanisms have been investigated theoretically to account for the large dissociation by the primary beam. These include:

1. Cracking by the fast initial secondaries which have an energy of 30-40eV and thermalise in about 1ns. A bulk effect of 2.4 molecules/electron for a one centimetre gap.

2. Dissociation by thermalised secondaries. At equilibrium, rate of loss by dissociative attachment equals rate of ionisation, so the ionisation and dissociation rates become equal. This is also a bulk process with 13 molecules dissociated/electron crossing a one centimetre gap.

3. Effect of secondary electrons emitted from the electrode surface by the impact of the primary beam or of the fast nonthermalised bulk secondary electrons near the surface. The latter are found to predominate, but the emitted secondaries peak at only 2-3eV energy so the dissociation they give rise to is very small, about 0.1 molecule/primary electron. Although this is a surface mediated effect which is expected to be volume independent, it is of insignificant magnitude.

4. Thermal effects. Thermodynamic data (ref 9) gives

$$\Delta G^{\circ} = -135100 + 41.5T$$

for the process

$$2CO_2 \rightarrow 2CO + O_2$$

Thus $\ln Kp = 6.82 \times 10^4/T - 20.96$

where

$$K_p = \frac{P_{CO_2}^2}{P_{CO}^2 P_{O_2}}$$

Substantial thermal dissociation occurs at $K_p = 1 atm^{-1}$ which corresponds to 3000°C. In the absence of surface conduction and assuming all the primary energy to be deposited in an infinitely thin surface layer, radiative loss limits the surface temperature to 2300°C. In practice, the primary energy is deposited in a thickness of tens of microns and the instantaneous surface temperature rise is limited to a few tens of centigrade degrees. Thus it would appear that this true surface effect is untenable.

We have no explanation at this stage for the large cross section observed. The process might be akin to electron stimulated desorption but the cross sections for ESD are normally quite small. Like the main discharge effect the result we have found should be general for any size of e-beam sustained laser.

DEPENDENCE OF MAIN DISCHARGE CURRENT ON TRANSMITTED PRIMARY CURRENT

A study of the ratio of secondary to primary currents I_s/I_p is of importance for the following reasons. The design process for the main discharge normally sets the operating E/N on efficiency/gain considerations to be about 1.5×10^{16} V cm^2; the current density is then set by specific energy deposition requirements. The transmitted gun current then follows from I_s/I_p which is a powerful influence on gun design.

Figure 12 shows, plotted as circles, the results of measuring this parameter for the 3:2:1 gas mixture. Gun current was altered by varying the helium pressure within the gun and hence its impedance. Gun voltage and hence primary beam energy were maintained constant. The main discharge E/N was also kept invariant. A linear plot results, implying an attachment dominated loss process. In the steady state, the differential equation

$$\frac{dn_e}{dt} = S_o - \beta n_e$$

governing the electron density reduces to $n_e = S_o/\beta$.

Since S_o, the ionisation rate, is proportional to primary current density H_p through the relation (10)

$$S_o = \frac{J_p}{e} \sum_i \sigma_i N_i$$

where σ_i and N_i are the cross section and number density of the ith species present in the discharge, and

$$J_s = n_e e v,$$

we find

$$\frac{I_s}{I_p} - \frac{J_s}{J_p} - \frac{n_e e \bar{v}}{S_o e} \sum_i \sigma_i N_i$$

$$\therefore \frac{I_s}{I_p} - \frac{\bar{v}}{\beta} \sum_i \sigma_i N_i \qquad (2)$$

Taking σ_{N2} to be 1.5×10^{-18}cm^2 and $\sigma_{He} = 0.3 \times 10^{-18}$cm^2,

$$\sum_i \sigma_i N_i$$

is 17.4cm^{-1} for a 1 atm 3/2/1 mixture. $\bar{v}$ is known to be 4.4×10^6 cm sec^{-1} for this mixture and E/N (refs 3, 4). β was evaluated from an overlap integral of the form of equation (1) with the values of Q_{oi} and ϵ_i enjoyed by dissociative attachment to carbon dioxide; a value of 7.7×10^3 (J) and 9.4×10^5 (LP&I) sec^{-1} were found. Thus the predicted value of 3660 (J) is in remarkable agreement, considering the approximations, with the slope of Figure 12 namely 3750. The LPI prediction is for $I_s/I_p = 30$. Inclusion of alumina discharge limiters alters the ratio to 2700, which we presume to result from field distortions arising from inclusion of a substantial thickness of high dielectric constant material.

Composition Dependence of Secondary to Primary Current Ratio

The ratio of secondary to primary currents, was measured for a variety of gas compositions. Figure 12 compares the results of experiments on 3:2:1 and 13:2:1 gas mixtures, these results and a number of others are listed in Table 1. The results can be understood from formula (2) above.

The drift velocity $\bar{v}$ varies weakly with composition, but the attachment coefficient β varies strongly and like the ionisation cross-section, may be written as

$$\beta - \sum_i \beta_i N_i$$

Since the attachment coefficients of nitrogen and helium are much less than that of CO_2, and σ_{He} is very small

$$\frac{I_s}{I_p} \simeq \frac{\bar{v}\sigma_{N_2}}{\beta_{CO_2}} \left[\frac{y}{z} + \frac{\sigma_{CO_2}}{\sigma_{N_2}}\right]$$

for a x:y:z He:N_2:CO_2 gas mixture. It is immediately apparent that M should be constant for a fixed ratio of N_2 to CO_2, independent of the helium content of the mixture. This prediction is well borne out for y = 2, z = 1, and x = 13, 3 and 0. Examining the pure CO_2 ratio, and taking $\beta(CO_2)\bar{v}$ to be about 10^{-21}cm^2 for CO_2 at 4kV/cm atm, we find $\sigma(CO_2)$ to be roughly 3×10^{-17}cm^2, considerably less than $\sigma(N_2)$. Thus to a good approximation,

$$\frac{I_s}{I_p} = \frac{\bar{\nu}\sigma_{N_2}}{\beta_{CO_2}} \left[\frac{y}{z}\right]$$

Taking $\sigma(N_2)$ to be $1.5 \times 10^{-18}cm^2$, we predict I_s/P_p to be about 1500(y/z). For y/z = 2, the prediction of $I_s/I_p = 3000$ compared with a measurement of 3500 is quite satisfactory. It is clear that the ratio can be tailored by control of the nitrogen to carbon dioxide ratio.

Attachment dominated discharges have been found for all the e-beam sustained lasers operated at RSRE. These observations are at variance with the usual assumption of a recombination dominated plasma.

EFFECT OF OXYGEN ON DISCHARGE IMPEDANCE

Having explored the oxygen generation rate, we investigated the effect of oxygen both produced by the discharge, and added directly, on the plasma impedance. It will transpire that the impedance change completely specifies the effects of dissociation products. The data on oxygen added in small amounts in a flowing gas method are shown in Figure 13. The linearity of the impedance - oxygen percentage plot implies that the oxygen also removes electrons by attachment, thus

$$z = \frac{V_s}{I_s} = \frac{V_s}{I_p \sum_i \sigma_i N_i \bar{\nu}} (\beta + N_{o_2}\beta_{o_2})$$

Thus

$$\frac{\partial z}{\partial N_{o_2}} = \frac{V_s \beta_{o_2}}{I_p \sum_i \sigma_i N_i} \qquad (3)$$

where N_{O2} and β_{O2} are the number density and attachment coefficient of oxygen respectively. The measured value of this parameter obtained from the slope of Figure 13 is $1.72 \times 10^{-16}\ \Omega\ cm^3$. Taking the dissociative attachment data of Rapp and Briglia on oxygen (ref 6), we calculate a value of β_{O2} of $1.0 \times 10^{-15}cm^3sec^{-1}$ (J) which is about 400 times smaller than demanded by equation (3) and our data in Figure 13. The LPI calculation yields $5 \times 10^{-13}cm^3sec^{-1}$ which fits our data exactly.

However it is important to recognise that at low electron energies a 3-body process can occur leading to the formation of O_2^- with quite significant cross section

$$O_2 + M + e \rightarrow O_2^- + M$$

Then the attachment coefficient β_{O2} is given by

$$\beta_{o_2} = \sum_i k_i N_i$$

where the k_i's are the electron and gas temperature dependent three body coefficients for each of the neutral species i present in the gas mixture, which have been measured by Chanin et al (ref 11). The values at T_e = 0.36eV are 2 x 10^{-32}, 2 x 10^{-30} and ~ 10^{-33}cm^{6}sec^{-1} for N_2, O_2 and He respectively falling to $\lesssim$ 1 x 10^{-32}, 1 x 10^{-30} and $\approx 10^{-34}$ at T_e = 0.7eV. The values for H_2O and CO_2 are tabulated at a mean electron energy of 0.03eV only, where they are 2 x 10^{-29} and 3 x 10^{-30}cm^{6}sec^{-1} respectively. Thus

$$\frac{\partial Z}{\partial N_{O_2}} = \frac{V_s \sum_i k_i N_i}{I_p \bar{\nu} \sum_i \sigma_i N_i}$$

The k_i and σ_i for i = He may be neglected; if these coefficients are also neglected for CO_2, oxygen and water, we find

$$\frac{\partial Z}{\partial N_{O_2}} = \frac{V_s k_{N_2}}{I_p \bar{\nu} \sigma_{N_2}} = 2.7 \times 10^{-16}\ \Omega\ \text{cm}^3 \quad (0.36\text{eV})$$

$$\lesssim 1.3 \times 10^{-16}\ \Omega\ \text{cm}^3 \quad (0.7\text{eV})$$

in good agreement with the experimental determination. It is difficult to justify the neglect of the k_i's for O_2, H_2O and CO_2 except for the fact that the latter pair are ill-determined; at face value the oxygen k_i should introduce significant curvature into the graph of Figure 13. The influence of discharge-produced oxygen is shown in Figure 14. Here we have plotted the discharge resistivity rather than impedance with allows ready scaling to other discharge dimensions or for the presence of discharge limiters. It is apparent that the dissociation products influence the discharge in the same way as deliberately added oxygen, the impedance doubling at an oxygen concentration of about one per cent. This fact is consistent with the observation that carbon monoxide has no influence on the discharge impedance.

GAIN MEASUREMENTS

Methodology

The optical arrangement used to measure the gain in the amplifier is shown in Figure 15; it relies on the usual method of probing with a low power cw laser. The output from this cw laser was transmitted by variable attenuators of CaF_2 and then double passed through the gain medium. The probe beam was focussed onto the surface of a room-temperature CMT photoconductive detector whose output voltage was amplified and displayed by a storage oscilloscope. Although the oscilloscope was restricted to a maximum bandwidth of 1MHz it was confirmed that this response was more than adequate for the long pulse observations of interest. A removable mirror allowed the operating transition of the cw laser to be examined using a wavelength monitor; the probe laser was set on the 10P(20) line for all measurements by adjustment of its cavity length, by control of the voltage on the piezoelectric transducer to which one vacity mirror was attached. Two periscopes, omitted from the diagram for clarity, changed the height of the probe beam out of the plane of the diagram in passing through the lead X-ray shield around the gain cell. The polarisation of the cw probe was roughly parallel with the main discharge electric field.

Results

A typical example of a gain measurement is shown in Figure 16. The chopped signal shows the probe power and zero power baseline in the absence of gain. The continuous trace shows the time variation of the amplified probe laser power in the presence of pulsed gain; since the amplifier could not be DC coupled the change in probe power is observed, ie the baselines of the chopped and cw signals are different and this was borne in mind when calculating the gain. Addition of optical attenuation did not alter the gain, confirming that a small-signal measurement had been successfully achieved. The small-signal gain was measured for the 3/2/1 gas mixture as a function of main discharge current at various values of E/N and the influence of oxygen on the gain was also examined. Figure 17 illustrates a graph of the peak small signal gain against main discharge current, in which the gun conditions were held constant and the secondary current was varied by changing the impedance by the deliberate addition of oxygen. The behaviour observed, in which the gain levels off with increasing curent, is quite typical of such systems (ref 12). In Figure 18 similar data on single pass gain is presented for three different values of E/N in a flowing gas 3/2/1 mixture wherein the main discharge current was altered by variation of the primary beam current. Note that all the quoted values of E/N are nominal since they do not allow for voltage drops in electrode sheaths. Figure 19 shows how the gain varies with main discharge current at a constant E/N of 1.5×10^{-16} V cm^2. The main discharge current was altered by three different means: (i) variation of primary current, (ii) deliberate addition of oxygen in a flow gas configuration, (iii) sealed operation in which dissociation products were allowed to accumulate. It can be seen that there is no significant different between these cases which proves that dissociation products influence the gain only through the impedance change caused by the presence of oxygen. This result is unsurprising since it is known that neither oxygen nor carbon monoxide absorb at 10.59μm.

SIGNIFICANCE OF RESULTS TO AMPLIFIER DESIGN PHILOSOPHY

Discharge Impedance

Since the effects of discharge impedance mismatch to the PFN are of overriding significance in understanding the device operation, we will briefly explore these here. We assume a PFN imepdance of Z with a discharge impedance MZ, where M can be greater or less than unity and equals one at match. Then the discharge current I and voltage V during the conduction stage are given by

$$I = \frac{V_o}{Z(1+M)}$$

$$V = \frac{V_o}{1 + \frac{1}{M}} = \frac{MV_o}{1+M}$$

The total capacitance C_o of the PFN is related to the pulse length τ by $C_o = \tau/2Z$ which ensures that at match, (M=1) the PFN is completely discharged. In the general mismatched case the charge lost $I\tau$ is obviously

$$I\tau = Q_{lost} = \frac{V_o \tau}{2(1+M)} = \frac{2ZC_o V_o}{Z(1+M)} = \frac{2Q_o}{1+M}$$

Thus Q_r, the charge remaining on the PFN at the end of the pulse is

$$Q_r = Q_o - Q_{lost} = \left[\frac{M-1}{M+1}\right] Q_o$$

and so V_r, the voltage remaining on the device at the end of the pulse is

$$V_r = \frac{Q_r}{C_o} = \frac{Q_o}{C_o}\left[\frac{M-1}{M+1}\right] = V_o\left[\frac{M-1}{M+1}\right]$$

Similarly, the energy E deposited by the discharge is

$$E = IV_T = \frac{2C_o MV_o^2}{(1+M)^2}$$

which at match equals $\frac{1}{2}C_oV_o^2$; thus the fraction F of energy deposited compared with the matched case is given by

$$F = \frac{4M}{(1+M)^2}$$

In Figure 20 the voltage multiplication factor 2M/1+M, fractional voltage remaining V_r/V_o = M−1/M+1, and F are plotted vs the impedance multiplication factor M, which is a function of oxygen present in the discharge. Clearly for M = 1.5 which corresponds to ½% oxygen, V/V_m = 1.2, V_r/V_o = 0.20 and F = 0.96. This means that the operating E/N would exceed the design value for 0% oxygen by 20%, a residual E/N of 40% $(E/N)_{design}$ would remain after the pulse, and 96% of design energy would be delivered to the plasma. Although we have yet to elaborate on the residual voltage, these figures suggest that even without any measures being taken to counteract the oxygen produced, a level of ½% should be tolerable.

It is instructive to compare the energy deposited in Figure 20 with the small signal gain of Figure 18. For a matched design E/P of 4kV/cm atm, at 170 A secondary current the gain equals 1.92% cm^{-1}; for M = 1.86, we find an actual E/P of 5.2kV/cm atm, F = 0.91, and I = 119A so that the gain becomes 2.35% cm^{-1}. As the discharge moves out of match the gain changes along the broken line in Figure 18. Thus as the energy deposition falls the small signal gain g_o rises. This happens because the output energy g_oE_sL depends also on the saturation parameter E_s wich we have not investigated.

Discharge Stability

The design E/N is well below the region of the attachment instability, so an arc will develop in the main discharge only if the instantaneous value of E/N gets too high. The previous section deals with the effect of impedance matching on the field E during and after the conduction phase; thus information is also required on the gas density N. The latter changes during the period of energy deposition due to gas heating and consequent expansion, which lowers N and raises E/N. Clearly such a rapid expansion must be adiabatic, and with the assumption of reversibility has been treated by Baranov and Breev (ref 13) who find for the ratio of densities before and after expansion

$$\frac{N'}{N} = \left\{1 + (\gamma - 1)\frac{\epsilon}{p_o V}\right\}^{-\frac{1}{\gamma}}$$

where ϵ/V is the energy density imparted to the gas at initial pressure p_o and γ is C_p/C_v. The assumption of reversibility is obviously very questionable for an explosive expansion, and we find (14) for the irreversible abiabatic expansion that

$$\frac{N'}{N} = \left\{1 + \frac{\gamma-1}{\gamma} \cdot \frac{\epsilon}{p_o V}\right\}^{-1}$$

For our constant current and voltage discharge, ϵ increases linearly with time during the conduction phase and is essentially constant thereafter. For typical energy loadings of 150J/1, N falls near the end of the pulse by a factor of 1.5 times its initial value. With this preamble we are now in a position to consider in more detail the conditions under which an arc can form.

1. Arcs near end of conduction phase

During the main discharge the voltage and thus field remain constant but the density progressively falls. Thus arcs are most likely to form near the end of the discharge by an avalanching process called the glow the arc transition. The value of E/p necessary for this process to occur is much less than that in an unionised gas, ie the static breakdown field. Near the end of the conduction phase the initial value of E/N will have risen by $(1+(\gamma-1)\epsilon/\gamma p_o V)$ which is thus a function of the energy loading and particularly nonuniformities in the latter. In our device, assuming the nonuniformity to be zero, the glow-arc transition sets in at about 10kV/cm atm, ie at ϵ/V = 200 J/1 atm and initial E/N = 6 kV/cm atm. Note that E/N dependence on gas composition through the $(1-\gamma^{-1})$ term.

2. Arcs due to gun failure

Should the gun current cease before the PFN has discharged the impedance matching analysis has to be modified. The worst case applies for early gun failure, when the gas will have hardly expanded and the charge on the PFN fallen insignificantly, so the value of E/N immediately after cessation of gun current might be almost as high as that applicable before the gun was switched on, namely twice the design E/N for the matched case. However, this field is now present in the conducting medium, which can undergo the glow-arc transition as previously explained. We have not observed this failure mode working at E/p of 4 kV/cm atm but obviously it could set in for mismatches or design E/p's of 5 kV/cm atm or above. It could be beneficial to deliberately mismatch with M > 1 to guard against main discharge arcs arising from gun failure.

3. Post conduction phase arcs

For a matched case, no voltage remains on the PFN at the end of the conduction phase and obviously further discharges cannot occur. For mismatched cases, voltages do remain which are most noticeable for M < 1, and furthermore gas expansion has taken place. For example, for M = ½, a voltage reversal takes place at the end of the conduction phase so that there is set up a field equal in magnitude but opposite in sign to that prevailing during the main discharge. Gas expansion has occurred so that E/N at the end of the pulse is the same as that in the post conduction phase or afterglow. Since electron density decays in the afterglow, the situation here is more akin to static breakdown than the glow-arc transition. Hence since a type I arc has not occurred for M > ½ the post conduction phase should be stable. For M < ½ the residual voltage is greater than that during

conduction and could lead to breakdown, depending on the PFN risetime. Such mismatches should not be encountered since they require inordinately high PFN charging voltages and dissociation products increase the value of M. For these reasons we have not encountered post conduction phase arcs.

Discharge stability is thus governed by the design E/N and energy loading, but especially by matching criteria for the PFN and discharge impedance.

SUMMARY

1. The oxygen concentration was found to rise linearly with charge passed, at a rate of 30 μmole/Coulomb. This dissociation rate was independent of volume, implying effects in the cathode fall or negative glow regions. The result should therefore be applicable to any size of device, and is roughly one hundred times less than for self-sustained devices.

2. Discharge limiters altered the above figure by about 50%, probably due to field distortions.

3. The $CO:O_2$ ratio departed from 2:1 stoichiometry, as is typical of self-sustained devices, to a value of about 2.5:1.

4. CO does not attach and was found to have negligible effect on the discharge impedance.

5. The discharge impedance was found to rise linearly with oxygen partial pressure, doubling at 1% added oxygen. This arises from electron attachment.

6. The secondary current was found to depend linearly on the primary current, implying electron loss by attachment rather than recombination. $I_s:I_p$ was found to depend mainly on the ratio of readily ionised N_2 to electro-negative CO_2 in the gas mixture. For X:2:1 $He:N_2:CO_2$ mixtures $I_s:I_p$ was found to be about 3500.

7. Dissociation by the primary beam alone contributes about 10% of the total dissociation observed. It scales linearly with charge passed, the oxygen concentration rising at 15 millimoles/coulomb of primary current.

8. Like the main discharge effect, this rate did not change with volume, implying some kind of surface mediated phenomenon. The result should therefore be applicable to any size of laser.

9. Dissociation by primaries was measured as a function of CO_2 partial pressure to further investigate the process. The dependence was nonlinear, with an absorption isothermal shape suggesting a true dissociation process, perhaps akin to electron stimulated desorption.

10. The primaries appear to dissociate CO_2 with amazing efficiency, around 10%. 3000 CO_2 molecules are cracked by each primary electron. The process is not understood.

11. Gain measurements have been carried out on the P(20) line. Small signal gain was a sublinear function of E/N and main discharge current. Oxygen, produced by the discharge or deliberately added, influenced the gain only through changes in secondary current brought about by impedance alteration.

12. Dissociation has been shown to influence discharge stability only through impedance changes caused by oxygen formation.

REFERENCES

1. A Crocker et al, Electron Lett 8, 460 (1972).
2. C Webb in Inst Phys Conf Ser No 29 (1976).
3. J J Lowke et al, J Appl Phys 44 (10) 4669 (1973) and O P Judd, J Appl Phys 45 (10) 4572 (1974).
4. M C Cornell et al, J Appl Phys 54 (4) 1723 (1983).
5. K K Corvin and S J B Corrigan, J Chem Phys 50 2570 (1969).
6. D Rapp and D D Briglia, J Chem Phys 43 (5) 1480 (1965).
7. J J Thomson, "Conduction of Electricity through gases" (Cambridge 1933).
8. N G Basov et al, Sov Phys Tech Phys 17 (12) 1976 (1973).
9. J D Gilchrist, "Extraction Metallurgy", Pergamon (1967).
10. O P Judd in Inst Phys Conf Ser No 29 (1976).
11. L M Chanin et al Phys Rev Lett 2 344 (1959); Phys Rev 128 219 (1962).
12. J C Comly et al, IEEE J Quant Electron QE17 1786 (1981).
13. V Yu Baranov et al, Sov J Quant Electron 7 1059 (1977).

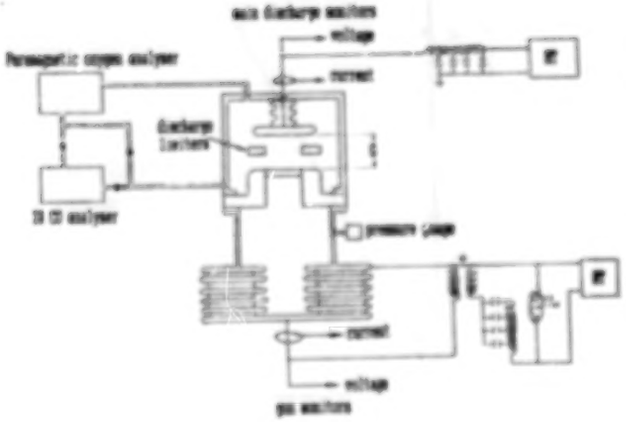

Fig.1 Schematic diagram of experimental apparatus.

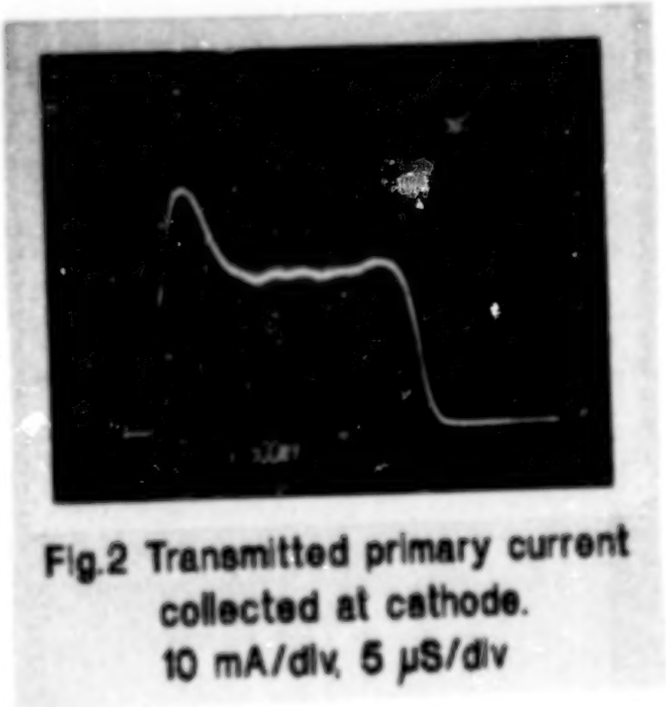

Fig.2 Transmitted primary current collected at cathode. 10 mA/div, 5 μS/div

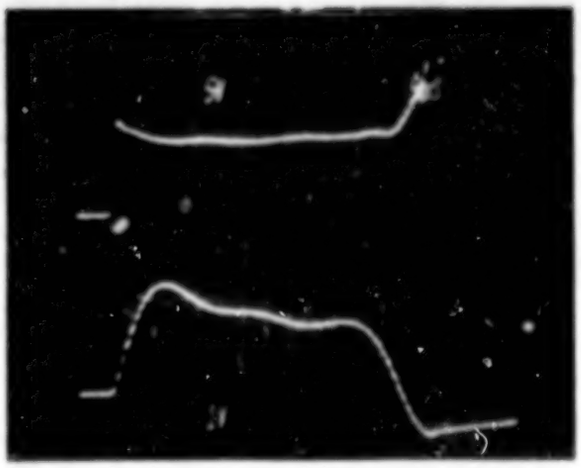

Fig.3 Main discharge voltage & current waveforms. 5 KV/div, 45 A/div, 5μS/div.

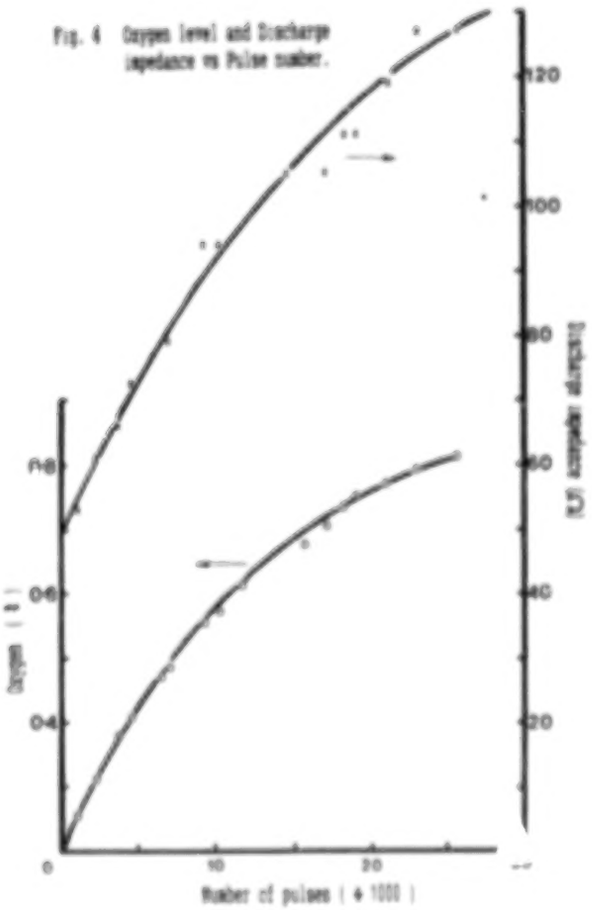

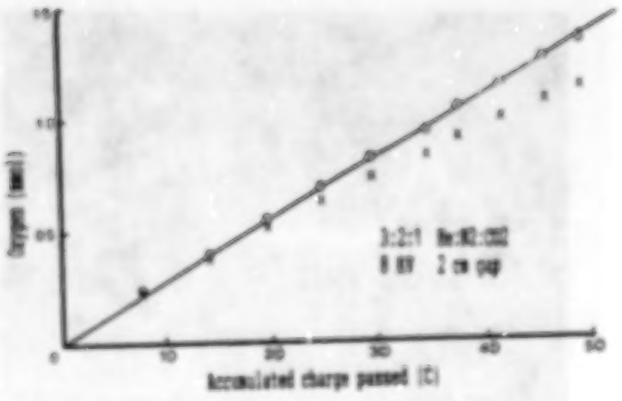

Fig. 5 Oxygen generation vs accumulated charge passed.

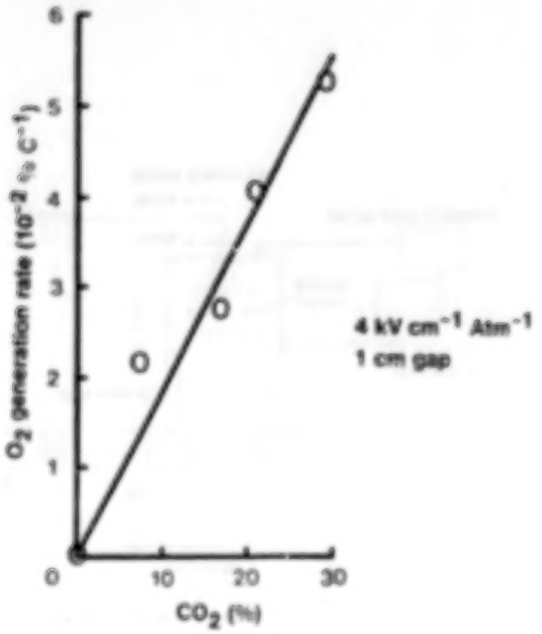

Fig. 6 Dependence of oxygen generation rate on carbon dioxide concentration.

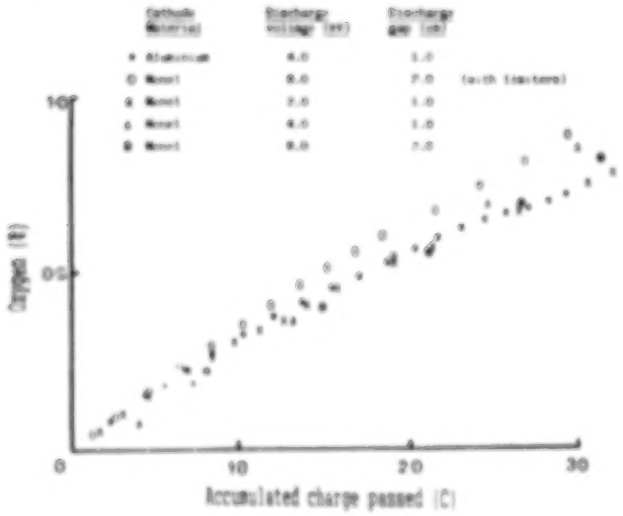

Fig. 7 Production of oxygen on discharge

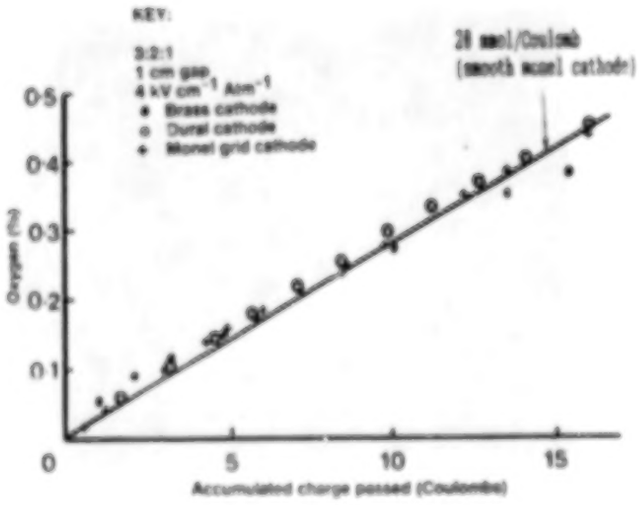

Fig. 8 Dependence of oxygen generation rate on cathode material and form.

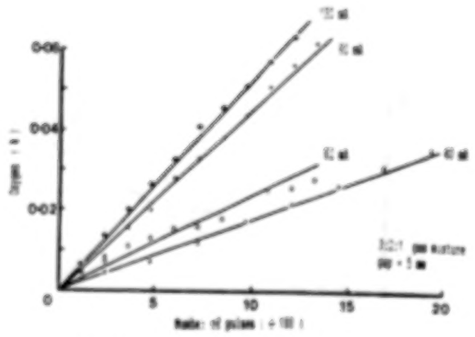

Fig. 9 Oxygen generation by transmitted primaries.

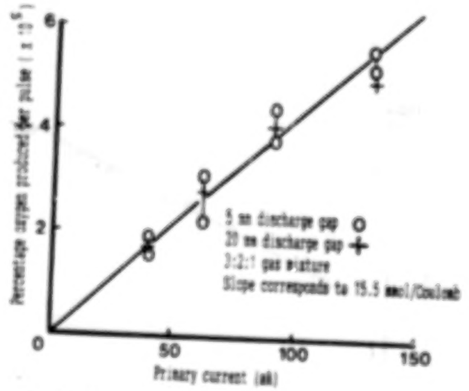

Fig. 10 Oxygen generation rate vs Transmitted primary current.

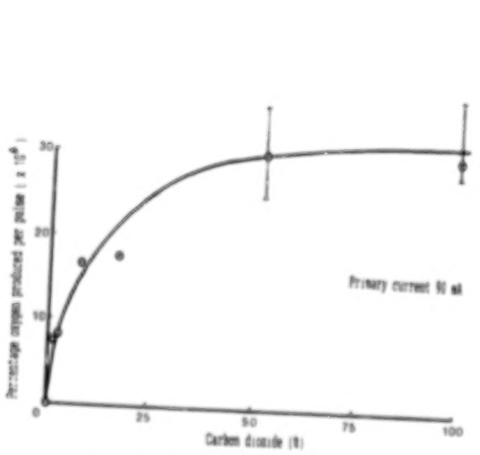

Fig. 11 Dependence of primary beam oxygen generation rate on carbon dioxide concentration.

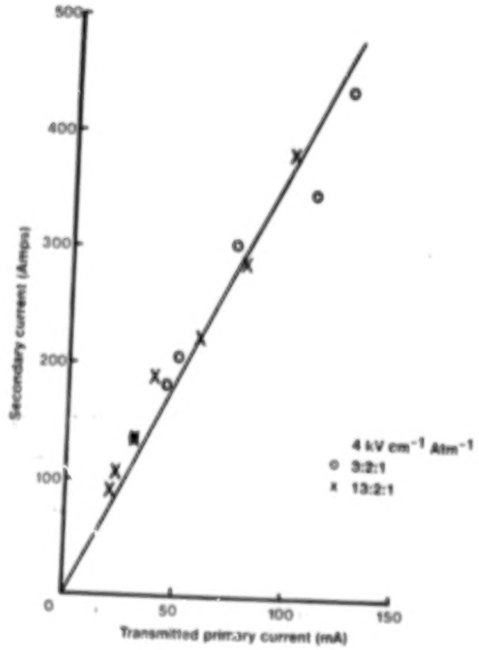

Fig. 12 Dependence of secondary current on transmitted primary current.

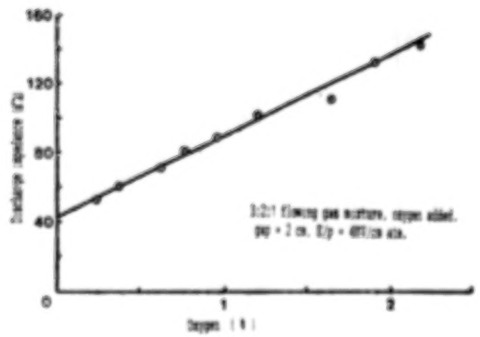

Fig. 13 Influence of oxygen on discharge impedance.

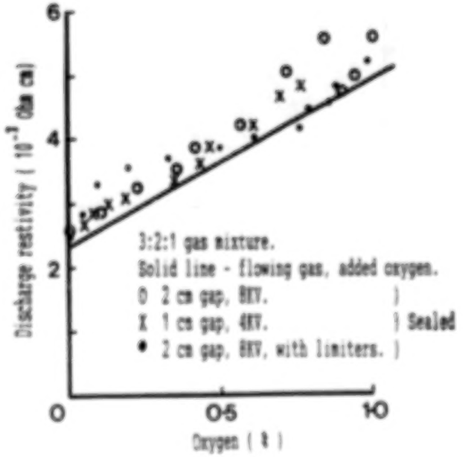

Fig. 14 Influence of oxygen on discharge restivity.

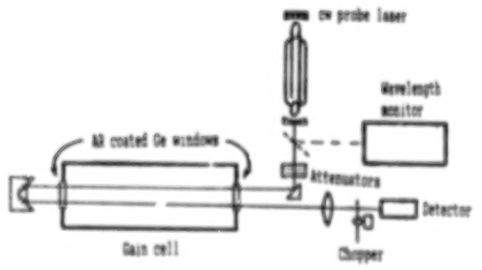

Fig. 15 Experimental arrangement for gain measurement.

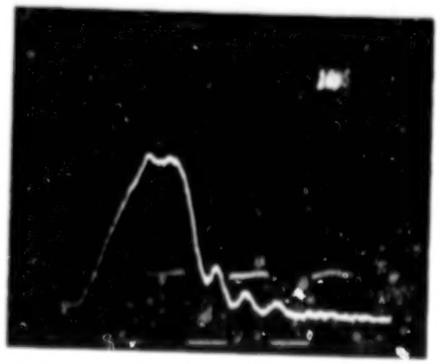

Fig 16 Measurement of small signal gain.
Chopped signal 2mS/div
Gain signal 10 μS/div
3:2:1 He:N_2:CO_2 +1% O_2
10P(20)

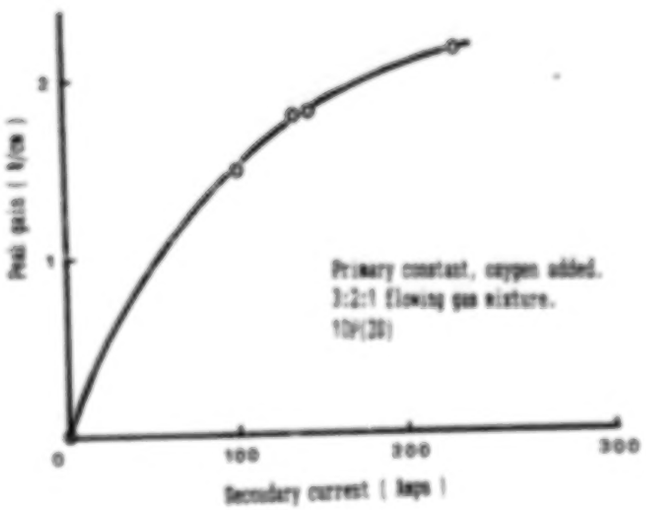

Fig. 17 Dependence of small signal gain on secondary current.

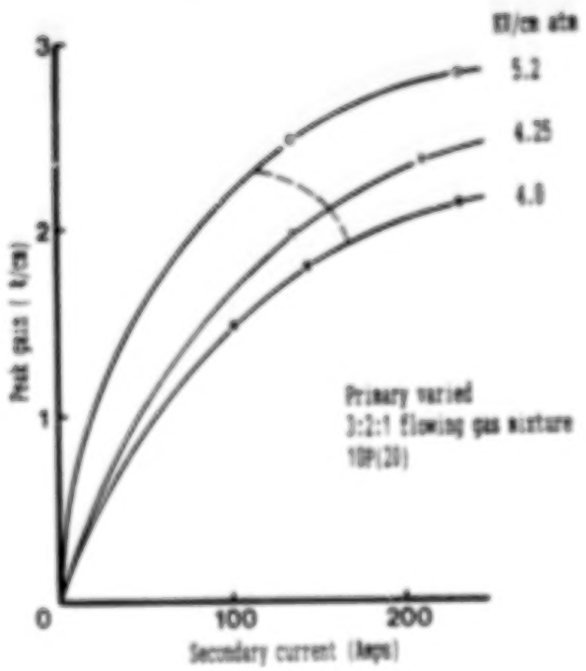

Fig. 18 Dependence of small signal gain on secondary current and electric field.

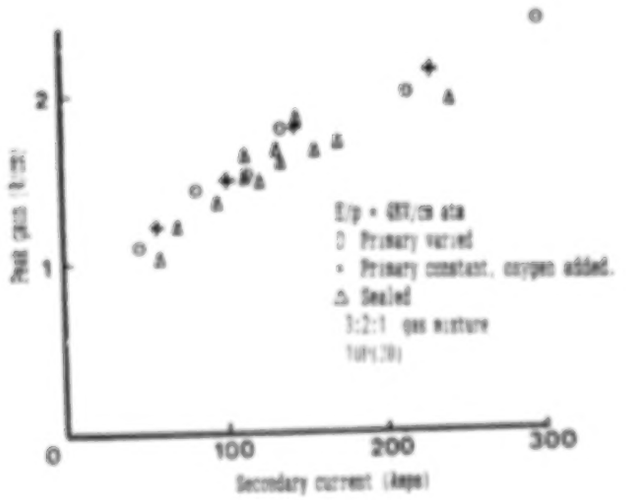

Fig. 19 Dependence of small signal gain on secondary current.

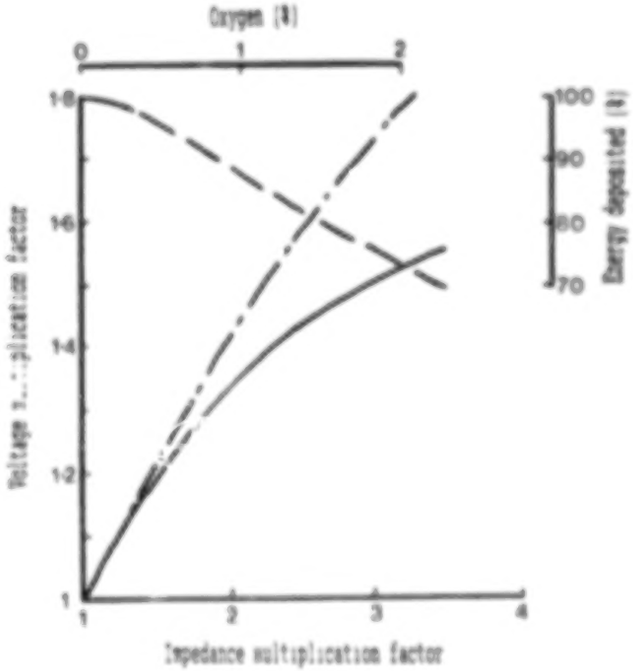

Fig. 20 Effect of increasing discharge impedance on input energy deposition.

E-BEAM SUSTAINED CO_2 LASER AMPLIFIER

M. J. Brown, S. R. Shaw, and M. H. Evans
Applied Physics Division, GEC Avionics Limited,
Borehamwood, Hertfordshire, WD6 1RX, United Kingdom

ABSTRACT

The design features of an e-beam sustained CO_2 amplifier will be described. The amplifier is designed specifically as a catalyst test-bed to study the performance of room temperature precious metal CO-oxidation catalysts under e-beam sustained operation.

The amplifier has been designed to provide pulse durations of 30 ms in a discharge volume of 2 litres. With a gas flow velocity of 2 m/s, operation at repetition rates of 10Hz is accomodated. The system is designed for sealed-off operation and a catalyst bed is housed in the gas circulation system downstream from the discharge region. CO and oxygen monitors are used for diagnosis of gas composition in the amplifier so that catalyst performance can be monitored in-situ during sealed lifetests.

A COMPACT, RUGGED, HIGH REPETITION RATE CO_2 LASER INCORPORATING CATALYST

P. Schwarzenberger and X. Matzangou
Applied Physics Division, GEC Avionics Limited
Borehamwood, Hertfordshire, WD6 1RX, United Kingdom

ABSTRACT

The principal design features and operating characteristics of a high repetition rate CO_2 laser are outlined. The laser is a completely sealed unit, the gas seal being formed by a metal enclosure which also provides electromagnetic screening of the device. There is an output window incorporated to allow the laser beam to exit, and a military standard high voltage connector to provide connections to the discharge circuit. The laser discharge is formed between two modified Rogowski profile electrodes with a discharge volume of $11cm^3$. A tangential fan, powered by a military standard motor, circulates the gas within the enclosure at a high speed. Catalyst is mounted in the region of the fan intake. A rugged mounting scheme has been introduced for the resonator optics, and parallelism between the cavity optics is retained over a wide temperature range. The size of the laser head is 300mm x 100mm x 90mm, and the weight is 3.9kg. Typically, the output power of the laser is 870kW with an energy of 64mJ.

The laser has been tested over a temperature range from $-35^{\circ}C$ to $+65^{\circ}C$ as a sealed unit, with catalyst installed, and stable operation has been demonstrated for two minute periods at 30Hz, one hour at 10Hz and one second bursts at 50Hz, at a range of temperatures. It should be noted that these duty cycles are associated with the fact that there is no active gas cooling in the laser. To conclude, a laser/catalyst system has been successfully demonstrated in a compact, rugged unit over a wide range of temperatures.

ABSTRACT: A COMPUTER PROGRAM FOR THE DESIGN OF OPTIMUM CATALYTIC MONOLITHS FOR CO_2 LASERS

Keith Guinn, Seth Goldblum, and Richard Herz
AMES/Chemical Engineering, B-010
University of California at San Diego
La Jolla, CA 92093

Pulsed CO_2 lasers have many applications in aeronautics, space research, weather monitoring and other areas. Full exploitation of the potential of these lasers is hampered by the dissociation of CO_2 that occurs during laser operation. The development of closed-cycle CO_2 lasers requires active CO-O_2 recombination (CO oxidation) catalysts and design methods for implementation of catalysts inside lasers. This paper will discuss the performance criteria and constraints involved in the design of catalyst configurations for use in a closed-cycle laser and will present several design studies performed with a computerized design program that we have written. Trade-offs between catalyst activity and dimensions, flow channel dimensions, pressure drop, O_2 conversion and other variables will be discussed.

This work was performed under a grant from the NASA Langley Research Center, Technology Utilization and Applications Office. The FORTRAN computer program is available through the NASA COSMIC Program.

APPLICATIONS OF LOW TEMPERATURE CO OXIDATION CATALYSTS TO BREATHABLE GASES

Ehsan Noordally, and John R Richmond
UOP Limited, Enfield, Middlesex, EN3 7PN, England

SUMMARY

Modifications of tin oxide/precious metal catalysts described for use in CO_2 lasers have also been developed for use in other applications; namely as low temperature CO oxidation components in fire escape hoods/masks for mines, aircraft, hotels and offices and in sealed environments such as hyperbaric chambers and submarines. Tin oxide/Pt/Pd catalysts have been prepared on a variety of carbon cloth substrates for application in fire escape hoods. These show high and stable CO oxidation capability (10^4 ppm CO reduced to 10^1 ppm CO) at GHSV of 37,000 h^{-1} and water saturated inlet gas at body heat (37°C) and below.

Water vapour plays an important role in the surface state/performance of tin oxide catalyst. Water resistant formulations have been produced by the introduction of transition metal promoters, Mn is one such promoter.

Tin oxide/titania/Pt/Pd catalysts have also been developed for CO oxidation in the North Sea diving environment and are currently in use in a variety of hyperbaric chambers and diving vehicles. Ambient temperature operation and resistance to atmospheric water vapour has been demonstrated and they offer viable alternative to hopcalite or heated catalyst systems.

A new range of non-tin oxide based low temperature CO oxidation catalysts is described. They are based on CeO_2, Fe_2O_3 promoted with precious metals. Preliminary data on selected materials in the form of both carbon cloth artefacts and shaped pellets are presented. They are expected to be applicable both to the breathable gas application area and to CO_2 lasers.

INTRODUCTION

The study of the heterogeneous oxidation of CO has been fruitfully researched by many investigators in heterogeneous catalysis and is still on going, as is evident at this workshop. Active catalysts have been prepared from simple oxides and

multicomponent oxides, largely from transition metals, groups III and IV of the periodic table. Many of these oxides contain small amount of precious metals in order to achieve low temperature catalytic oxidation. Several catalysts have thus far been commercially developed and although these are of considerable theoretical and practical significance, they do not all possess sufficient activity to warrant their use in for example gas masks for effective removal of CO from air. For this purpose only the most powerful, highly reactive, oxidising catalysts can be utilized.

Catalysts used in breathable gas systems must initiate the oxidation of CO without an appreciable induction period. The reaction must proceed at the high space velocity required for breathing purposes and under all environmental conditions likely to be encountered in use. The catalyst must have a sufficiently long life and in static systems preferably be regenerable. The catalyst artefact must be sufficiently porous to offer very little resistance to air flow, i.e. low pressure drop across the catalyst bed, and have sufficient chemical stability to withstand prolonged storage at temperature up to 60^{o}C. The ideal catalyst would be one that would be capable of reacting completely with CO in low as well as high gas/air concentration within the temperature range of 0-40^{o}C, and not be poisoned by water vapour or small amounts of impurity likely to be encountered in contaminated air.

APPLICATIONS

A major use of low temperature CO oxidation catalyst is in respiratory protection. The latter is necessary where the prevailing breathable environment is not capable of supporting life because of contamination with CO. The most usual circumstances are those involving fires and toxic gases encountered both by the public and fire rescue services. Low temperature CO oxidation catalysts reported here have been developed for this specific purpose, where CO removal down to ppm level is required for air purification, and where the catalyst is :

1. In granular form and is fitted as part of a life support system either with or without supplemental oxygen.

2. Deposited on carbon cloth, and incorporated in a smoke hood filter device.

These commercial low temperature tin oxide catalysts have found actual and potential use in :

1. Diving industry
2. Underground shelters as static systems and
3. Smokehoods or portable self-rescue breathing sets.

Diving Industry

Oil explorations in offshore locations have given rise to the need and development of extended duration diving techniques. Using helium/oxygen mixture as the breathable gas, divers can work for several weeks at depth of up to 300 m. During this time the breathing gas is scrubbed clean of contaminants like CO_2, CO and NO_x produced during respiration and welding operations. Removal of these toxic compounds together with close monitoring of the oxygen levels, ensures a high level of diver safety. $Pt/Pd/SnO_2/TiO_2$ with trace quantities of manganese provides the CO scrubbing capability.

Typically hydrocarbon and sulphur compounds are removed by appropriate adsorbents upstream the CO oxidation catalyst.

Underground Shelters

The provision by civil authorities, of the safe shelters for the majority of the population in the event of a catastrophe or war is becoming a more acceptable practice. A major consideration in the design of such structures is environmental control equipment to prevent the build up of toxic gases such as CO produced from smoking, fires and CO_2 from respiration. The Pt/Pd on tin oxide is an appropriate catalyst for this application; it has high tolerance to water vapour, and is regenerable.

Smokehoods

Fire in a confined area such as a mine, aircraft, or a hotel room frequently incapacitates and kills more from the smoke, poison gases and choking particles emitted than from the heat generated.

Oxygen levels often remain as high as 15-16% until just before the "flash-over" point when the fire ball moves through the whole of the confined area. Emergency self-rescue devices or smokehoods can therefore utilise catalytic oxidation of the CO to deal with that particular toxic component.

Filter self-rescue systems generally consist of adsorptive sections to remove toxic components such as HCN, other acid gases and hydrocarbons together with a catalytic system for the oxidation of carbon monoxide.

Rebreather systems typically provide supplemental oxygen by chemical means or pressure bottles, together with CO_2 and H_2O removal by appropriate adsorbents in the recirculating gas.

The filter systems need to cope with potentially high ambient CO levels and current draft standards are based on challenge gases containing 1% CO. Rebreather systems also have to deal with CO arising from potential leakage into the mask from face and neck seal and from exhalation but these levels will be lower.

Process Applications

Air fed to air separation plants and compressors producing pressurised air for breathing purposes require incoming air to be free of CO (and usually CO_2). Carbon dioxide, water and other contaminants can usually be adequately removed by the appropriate regenerable adsorbents but carbon monoxide is not normally adsorbed sufficiently well.

Oxidation of trace CO can be achieved with catalysts described in this paper at typical compressor exit temperature of 50-100°C thus eliminating the need for additional pre-heat. Their ability to work at high relative humidity also eliminates the need for water vapour removal from the feed gas.

POTENTIAL TECHNOLOGY TRANSFERS OF RESEARCH ON LOW-TEMPERATURE CARBON MONOXIDE - OXYGEN RECOMBINATION CATALYSTS

Edward J. Poziomek
Artech Associates
80-4 Cosey Beach Avenue, East Haven, CT 06512

SUMMARY

Results from research on catalytic recombination of CO-O_2 for stable closed-cycle operation of CO_2 lasers hold much promise for a variety of technology transfers. Expansion of CO_2 laser remote sensing applications toward chemical detection and pollution monitoring would certainly be expected. However, the catalysts themselves may be especially effective in low-temperature oxidation of a number of chemicals in addition to CO. It is therefore of interest to compare the CO-O_2 catalysts with chemical systems designed for chemical sensing, air purification and process catalysis. Success in understanding the catalytic mechanisms in the recombination of CO-O_2 could help to shed light on how catalyst systems operate. New directions in low-temperature oxidation catalysts, coatings for chemical sensors and sorbents for air purification could well emerge.

INTRODUCTION

There are a number of applications for CO-O_2 recombination catalysts. An important one is the achievement of long-term, closed-cycle operation of CO_2 lasers. The lasers are used for remote-sensing applications such as observing and predicting atmospheric behavior. The ability to understand catalyst performance and to control frequency stability is critical. CO_2 can dissociate in the laser discharge to CO and O_2. The loss of CO_2 results in a corresponding loss of laser power. The buildup of O_2 can cause discharge instabilities. A catalyst is needed to facilitate recombination of the CO-O_2. It is critical that the mechanisms involved in the catalytic recombination be understood. The challenges are multifold and include the need for studies of the catalytic process as well as the physical and chemical properties of the catalyst. An excellent review of approaches toward efficient recombination catalysts appeared in the proceedings of a workshop held at the NASA Langley Research Center in 1986 (ref. 1). A review of recent advances was presented in 1988 (ref. 2).

Pt/SnO_2 appears to be the most promising catalyst system for the recombination of CO and O_2 in CO_2 lasers (ref. 3). A systematic study of Pt, Pd/SnO_2 catalysis has been underway for several years. There are many parameters including catalyst preparation, catalyst surface area, effect of CO_2 concentration, catalyst pretreatments, catalyst distribution and quality control of test procedures, to mention several. Considerable progess has been made toward high activity systems for combining CO and O_2 to form CO_2 in high powered lasers. This will be discussed at the International Conference on CO Oxidation Catalysts for Long-Life CO_2 Lasers in October 1989 at the NASA Langley Research Center, Hampton, VA.

As pointed out during the international conference in 1986, the immediate United States interest in the development of pulsed CO_2 lasers is for the NASA Marshall Space Flight Center's Windstat program (involving the measurement of wind) (ref. 4). However, it was mentioned that the potential for technology transfer to industrial, medical, defense and other research applications is significant. Industrial process control, laser ranging, communication, frequency stability and reliable long-term unattended operation were mentioned as being most important. United Kingdom

interests relate heavily to military applications, however, there is also a policy of technology transfer to industry (ref. 5).

The purpose of the present paper is to more specifically outline the potential technology transfers from the research on low-temperature CO-O_2 recombination catalysts. Major areas discussed include:

- Remote sensing
- Chemical sensors
- Air purification
- Process catalysis.

REMOTE SENSING

An appreciation of the utility of lasers in meteorology, and earth and atmospheric remote sensing can be obtained by reviewing the proceedings of a recent conference on the subject (ref. 6). The titles of the sessions reflect the scope:

- Advances in laser technology for remote sensing
- Laser remote sensing for meteorology applications
- Laser remote sensing for surface applications
- Laser remote sensing of trace species
- Laser remote sensing of velocity fields.

Titles in the session on trace-species sensing follow:

- Remote active spectrometer
- Measurement of atmospheric trace species and rocket fuels using CO_2 lidars
- Development of an active imaging system and its application to the visualization of gas clouds
- Multiwavelength and tripled CO_2 lidars for trace gas detection
- Analysis of laser diagnostics in plumes
- CO_2 laser photoacoustic detection of trace toxic compounds in the ambient air
- Stratospheric ozone measurements with a ground-based, high power lidar
- CO_2 DIAL measurements of toxic gases.

Chemical analysis at a distance is of special interest for many reasons. Recent progress in the possibility of a chemical warfare treaty highlights the need for chemical monitoring and verification procedures. The war on drugs could benefit from stand-off sensors to locate and identify organic vapors from suspected drug-processing facilities. Also, many environmental situations require a variety of chemical sensors including stand-off systems. Use of differential absortion lidar for pollution mapping is a good example. Table I lists molecules of interest in air pollution and their absorption wavelengths corresponding to wavelegths of line-tunable CO_2 lasers.

Achievement of long-term, closed cycle operation of CO_2 lasers should significantly expand the use of remote sensing especially in the detection, identification and monitoring of pollutants.

CHEMICAL SENSORS

The first SnO_2 semiconducting gas sensor was marketed over two decades ago for the detection of combustible gases. Applications have been extended to the sensing of ammonia, hydrogen sulfide, thiols, ethanol, hydrogen, CO, arsine, acetic acid and other compounds. A recent review on the development of SnO_2 sensors is available (ref. 8), as well as an outline of what was published on conductometric sensors during the 1985-1987 period (ref. 9). The mechanism of detection in air is usually a catalytic oxidation at the surface of the oxide inducing an increase in conductance. The operating temperature for a particular sensor would most likely be found in the range of 200-400°C. Recent advances relate to selectivity and include a combustible gas detector having insensitivity to reductive gases (ref. 10). Several patents (mostly to Japanese companies) have appeared for CO detection using semiconducting oxides.

SnO_2 is the most frequently used material for semiconducting gas sensors. Few other materials have been put into practical use. The sensitivity of the sensor for CO can be improved significantly by adding Pt or Pd; silanization with trichlorosilane enhances the selectivity for H_2S (ref. 9). There appears to be more interest at the presnt time in studying SnO_2 to increase its performance rather thna to search for new materials. Increasing selectivity, sensitivity, reliability and long-term stability are the goals.

Applications of SnO_2 gas sensors include:

- Toxic gas detection (CO, NH_3, H_2S, etc.)
- Combustion monitoring
- Gas-leak detection
- Air quality monitoring
- Fermentation control
- Ventilation control
- Fire detection (CO)
- Breath analyzer (alcohol).

These and some new applications such as detection of odors (e.g., in testing for freshness of foods) are discussed briefly in reference 8.

The SnO_2 and other catalysts emerging in the research on CO-O_2 recombination for the CO_2 laser application should be considered candidates for semiconducting oxide sensors and vice versa. A low-temperature SnO_2 system developed in the laser work could dramatically expand the utility of semiconducting oxides in chemical sensing.

AIR PURIFICATION

Catalysts for removal of CO from air at room temperature are commercially available. Hopcalite, a co-precipitate of oxides of manganese and copper, is a classic example. As pointed out by Sampson and Gudde (ref. 11), the main difference between CO oxidation for air purification and for laser control lies in the gas composition. The CO and O_2 concentrations are much higher and the CO_2 concentrations much lower in the air purification application than in the laser recombination one. However, the operating requirements are very similar.

It is of interest to compare the CO-O_2 recombination catalysts with other systems known to react with CO. For example, the current U.S. Department of Defense sorbent for air filters in chemical defense is whetlerite. This is an activated charcoal which has been impregnated with a mixture of copper, silver and chromium. It functions through a combination of physical adsorption and chemisorption. Descriptions of some of the chemistry and characteristics of whetlerite are available (ref. 12, 13). It is known that CO is oxidized at room temperature in air using whetlerite (ref. 14, 15). The activation energy for the oxidation was estimated to be 14.6 kJ mol^{-1} (ref. 16). The oxidation of CO has also been proposed as a nondestructive test for predicting the residual chemical life of whetlerite (ref. 17, 18). The chemical reactivity of whetlerite involves both hydrolysis and oxidation. However, the mechanisms are complicated; complete details have not been worked out. Several analogies can be drawn between the Pt/SnO_2 oxidation of CO in the laser application and the chemisorption processes in air purification using whetlerite. It is pertinent to compare the proposed reaction mechanisms for the respective systems. Success in understanding the catalytic process in the recombination of CO-O_2 could help to shed light on how other oxidation catalysts work including whetlerite.

New or modified sorbents for air purification could emerge as a result of the research on CO-O_2 recombination catalysts. Low temperature oxidation catalysts for CO have been investigated with other toxics for air purification. (ref. 19).

PROCESS CATALYSIS

A product review on process catalysts showed that nearly every segment of the catalyst business is growing (20). The value of catalysts consumed in pollution abatement uses this year is expected to exceed the value of catalysts consumed in petroleum processing. However, the physical volume of catalysts used in pollution control is actually quite small because of the high activity and cost of Pt and other metals of the Pt group used as catalysts. Automotive catalysts accounted for 43% of all U.S. consumption of platinum group metals in 1987. A major problem is still the stability of the noble-metal catalysts and the catalyst supports (21). Environmental catalysts should lead value growth among other catalysts into the next century, however, research is underway to find catalysts that are less expensive than the noble metal ones.

It has been estimated that almost 25% of the total production volume of the top 20 chemicals worldwide depends upon selective oxidation catalyzed by solid metal oxides (22). The most selective catalysts contain a cation with an empty or full outermost *d* orbital. This includes Sn(IV) which has a $4d^{10}$ orbital.

The work on Pt/SnO_2 for CO-O_2 recombination should lead to new insights on catalytic oxidation mechanisms as well as materials which may be relvant to various aspects of process catalysis.

REFERENCES

1. Batten, C. E.; Miller, I. M.; Wood, G. M., Jr.; Editors,: Closed-Cycle, Frequency-Stable CO_2 Laser Technology, NASA Conference Publication 2456 (Proceedings of a workshop sponsored by the National Aeronautics and Space Administration and held at the Langley Research Center, Hampton, Virginia, 10-12 June 1986). Published 1987.

2. Hess, R. V.; Buoncristiani, A. M.; Brockman, P.; Bair, C. H.; Schryer, D. R.; Upchurch, B. T.; and Wood, G. M.: Recent Advances in Efficient Long-Life, Eye-Safe Solid-State and CO_2 Lasers for Laser Radar Applications. Proceedings of SPIE Symposium on Fiber Optics. Optometrics and Other Laser Applications. Boston, MA. September 1988.

3. Rogowski, R. S.; Miller, I. M.; Wood, G.; Schryer, D. R.; Hess, R. V.; and Upchurch, B. T.: Evaluation of Catalysts for Closed-Cycle Operation of High Energy Pulsed CO_2 Lasers. SPIE Proceedings, vol. 415, 1983, p. 112.

4. Wood, G. M., Jr.: Reference 1. pp. 1-2.

5. Willetts, D. V.: Reference 1. pp. 7-8.

6. Sokolowski, M. M., Chair: Conference on Laser Applications in Meteorology, and Earth and Atmospheric Remote Sensing. Los Angeles, CA. SPIE Proceedings, vol. 1062; January 1989.

7. Fredriksson, K. A.: Differential Absorption LIDAR for Pollution Mapping. In: Laser Remote Chemical Analysis. Measures, R. M., ed. John Wiley & Sons. New York. 1988. pp.273-332.

8. Takahata, K.: Tin Dioxide Sensors - Development and Applications. In: Chemical Sensor Technology, Vol. 1. Seiyama, T., ed. Elsevier. New York. 1988. pp. 39-55.

9. Janata, J; and Bezegh, A; Chemical Sensors. Anal. Chem., vol. 60, no. 3, 15 June 1988, pp.62R-74R.

10. Otani, H.: Combustible Gas Detector Having Insensitivity to Reductive Gases. Japanese Patent JP 86195339 A2. 29 August 1986. (Chem. Abstr., vol. 106, no. 2, p. 6835e.)

11. Sampson, C. F.; and Gudde, N. J.: The Oxidation of Carbon Monoxide Using a Tin Oxide Catalyst. Reference 1. pp. 65-69.

12. Poziomek, E. J.; Mackay, R. A.; and Barrett, R. P.: Electron Spin Resonance Studies with Copper/Silver/Chromium Impregnated Charcoals. Carbon, vol. 13, 1975, p. 259.

13. Deitz, V. R.; Robinson, J. N.; and Poziomek, E. J.: Electron Transmission Microscopy of Charcoals Impregnated with Ammonium Salts of CuII and CrVI. Carbon, vol. 13, 1975, p. 181.

14. Meier, E. P.; Luckan, S. K.; and Poziomek, E. J.: Reaction of Carbon Monoxide with Impregnated Carbons. Carbon, vol. 11, 1973, p. 417.

15. Lutchko, J. R; and Stoneburner, G. R.: U.S. Patent 3,545,915, 8 December 1970.

16. Deitz, V. R.; and Poziomek, E. J.: Temperature-Reversible Oxidation of Carbon Monoxide by New and Weathered Whetlerite. Carbon, vol. 24, no.4, 1986, pp. 463-468.

17. Deitz, V. R.; Poziomek, E. J.; and Baker, J. A.: Nondestructive Analysis of the Chemical Reactivity of Copper/Chromium/Silver Impregnated Charcoals. Anal. Letters, vol. 16, no. A8, 1983, pp. 643-653.

18. Hui-ping, Z.; Dai-yun, C.; and Fang, G.: The Non-Destructive Test Method of Chemical Reactivity of Impregnated Carbon Bed. Proceedings of the 3rd International Symposium on Protection Against Chemical Warfare Agents. Umea, Sweden. 11-16 June 1989, pp. 257-262.

19. Collins, M. F.: Characterization of the LTC Catalyst: Performance Against Common Air Pollutants. Reference 1. pp. 153-163.

20. Greek, B. F.: Process Catalysts Enjoy Surging Market. Chem. Engr. News, 29 May 1989, pp. 29-56.

21. Haggin, J.: Catalysis Gains from Auto Emission Work. Chem. Engr. News, 15 May 1989, p.23.

22. Campbell, I. M.; Catalysis at Surfaces. Chapman and Hall. New York. 2nd Edition. 1988. p.169.

ACKNOWLEDGEMENT

Part of this work was performed by the author as an American Association for the Advancement of Science (AAAS) Science and Engineering Environmental Fellow in the Office of Modeling, Monitoring Systems and Quality Assurance, U.S. Environmental Protection Agency, Washington, DC. The support of AAAS and the U.S. Environmental Protection Agency is gratefully acknowledged.

TABLE I. - ABSORPTION WAVELENGTHS FOR MOLECULES OF INTEREST IN AIR POLLUTION STUDIES (REF. 7)

Compound	Wavelength
Carbon Monoxide	4.709 4.776
Nitric Oxide	5.263
Sulfur dioxide	8.881 9.024
Ammonia	9.220
Freon-11	9.261
Ozone	9.505 9.508
Freon-113	9.604
Benzene	9.621
Methyl hydrazine	10.182
Ethyl mercaptan	10.208
Ethyl chloride	10.275
Ammonia	10.333
Ethylene	10.533
Sulfur hexafluoride	10.551
Trichloroethylene	10.591
1,2,-Dichloroethane	10.591
Hydrazine	10.612
Vinyl chloride	10.612
1,1-Dimethylhydrazine	10.696
Freon-12	10.719
Perchloroethylene	10.742
1-Butene	10.787
Perchloroethylene	10.834

PERFORMANCE OF ALUMINA-SUPPORTED Pt CATALYSTS IN AN ELECTRON-BEAM-SUSTAINED CO_2 LASER AMPLIFIER*

D.L. Cunningham, P.L. Jones, C.I. Miyake, and S.E. Moody
Spectra Technology, Inc.

SUMMARY

The performance of an alumina-supported Pt catalyst system used to maintain the gas purity in an electron-beam-sustained (636) isotope CO_2 laser amplifier has been tested. The system characteristics using the two-zone, parallel flow reactor were determined for both continuous- and end-of-day reactor operation using on-line mass spectrometric sampling. The laser amplifier was run with an energy loading of typically 110 J-ℓ/atm and an electron-beam current of 4 mA/cm^2. With these conditions and a pulse repetition frequency of 10 Hz for up to 10,000 shots, increases on the order of 100 ppm O_2 were observed with the purifier on and 150 ppm with it off. The 1/e time recovery time was found to be approximately 75 minutes.

INTRODUCTION

Purification of gas mixes used in isotopic or long-life carbon dioxide lasers has become an increasingly active area of investigation. For ground-based applications where power and size requirements are not limiting factors, traditional catalyst technology may be employed, such as the well-developed alumina-supported platinum catalysts. In the present work, we have used an alumina-supported Pt catalyst to provide either on-line continuous or "end-of-day" purification of 13:2:1 He:N_2:$^{13}CO_2$ laser gas mixtures used in a large-scale laser amplifier.

The laser amplifier system (CORA) is an atmospheric pressure, electron-beam-sustained, pulsed discharge device with the parameters of Table I. The design emphasizes the use of clean and stable materials for maintaining the purity of the isotopic CO_2 used in the 6200-ℓ device. The catalyst system is incorporated into the amplifier by attaching it to an ancillary system that provides purging of the anode triple point and the electron-beam drift regions of the gain module assembly. Approximately 9 ℓ/sec are removed from the gain module, of which 3 ℓ/sec are sent through the catalyst bed housed in a separate unit.

The catalyst system was built to our specifications by Applied Photonics, Inc. It consists of a two 30" Iconel retort tubes each containing 4 to 5 mesh-size platinized

* Work supported by MIT/Lincoln Laboratory Contract Number BX-2332

pellets layered between stainless steel strainer elements. The tubes each have a surface area of approximately 7500 cm^2, are separately heated, and are arranged in a parallel flow configuration. Based upon vessel size and flow rates the time required to pass a module volume through the purifier is approximately 34 minutes. Typically the catalyst zones are held at 600 ± 5 °C during operation with the gas entering and leaving the purifier at room temperature.

Initial treatment of the catalyst after receipt from Applied Photonics was to heat the catalyst to 800 °C in steps which maintained a 100 mTorr or better vacuum above the catalyst. The catalyst was then held at 800 °C for one hour after outgassing was complete and allowed to cool. The system was flushed with a laser mix using $^{12}CO_2$, evacuated, and the heating process repeated to 300 °C. At this point the purifier was again flushed with laser gas, evacuated again, and the catalyst heated to 800 °C under a continuous flow of laser gas. The laser gas was discarded, the complete system pumped to 5 x 10^{-5} Torr and refilled with a clean gas mix. Initial experiments were performed with carbon-12 carbon dioxide. The quality of the laser gas in the module was monitored using a quadrupole mass spectrometer and the discharge behavior of the gas. Since the discharge diagnostics included color video as well as current and voltage monitors, it was very easy to spot changes in the gas composition either by changes in the discharge color or the presence of bright spots in enhanced field regions of the discharge, as well as by changes in the discharge impedence.

The quadrupole mass spectrometer was a Dycor 200M, 0-200 amu gas analyzer with computer control and data acquisition. The position available for sampling from the gain module was not directly on the flow loop, so the mixing time of the flow loop with other regions needed to be considered in measurements involving real-time monitoring of the gas composition. The mixing time was observed to be the order of 30 minutes. The pressure at the QMS was maintained at a tolerable level by providing a differentially-pumped sample volume. The first aperture was a small-diameter, thin-walled hole in a copper disk while the second was provided by a sampling valve provided by Dycor. A mechanical forepump was used as the differential pump. Calibration of the spectral intensities was made using the known composition of the commercial laser gas mixes and assuming constant ionization efficiencies. Examples of the data are shown in Figure 1.

RESULTS AND DISCUSSION

The first round of experiments involved running the system with the catalyst cold. The gas was sampled before and after the accumulation of 14,000 shots at 3-kJ energy loading per shot. The O_2 concentration rose 208 ppm from 135 ppm to 343 ppm; an oxygen generation rate of 30 ppm - L/kJ for the device. This was lower than expected based upon DVT studies in a single-shot device using similar materials. The reason is due the the ability to effectively electron-beam scrub the insulator surfaces of the discharge volume in the CORA device. We found that electron-stimulated desorption from the insulator surfaces produced large quantities of oxygen and water and that 15,000 shots of the electron beam (order 2 mA/cm^2 and 150 keV

at the insulator) and simultaneous flushing of the gas were required to produce a clean discharge and stable gas composition.

The catalytic purifier was then heated and the laser gas cycled for several hours. The plotted data in Figure 2 show that the oxygen concentration decayed with a 1/e time of 75 minutes.

For our application, use of the purifier at all times is desired. A typical run of the system is several short bursts of a few thousand shots within an hour of a 10,000 shot run at 10 pps and full energy loading; a run time of just over 17 minutes. The amplifier then requires a two-hour cool-down period. Under these conditions continuous on-line purification maintains a stable initial gas composition. For example, running the purifier at 600 °C while operating through the accumulation of 32,000 shots in one day resulted in a change in O_2 concentration, as measured within a half hour of the final firing, of 20 ppm over that at the beginning of the day. The gas composition recovered completely by leaving the purifier on a longer time. An estimated "dynamic" production rate, which ignores the issues of gas mixing times, is 20 ppm - L/kJ. This is two thirds of the rate of oxygen production during a run without the purifier operating.

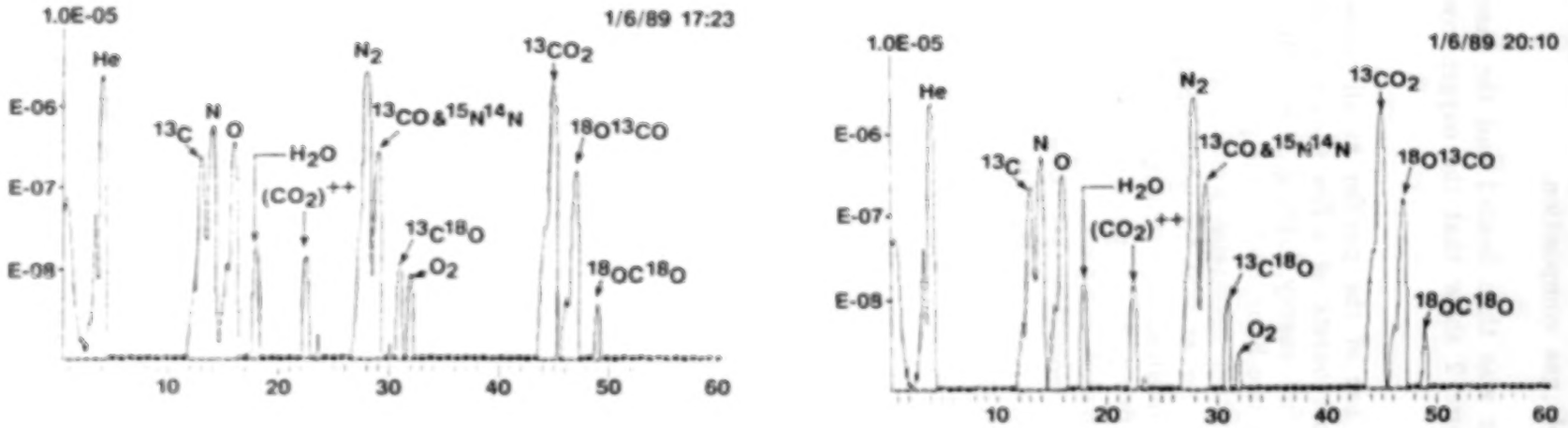

Figure 1. Mass Spectra for ^{13}C Isotope Showing Reduction in O_2 by Catalyst

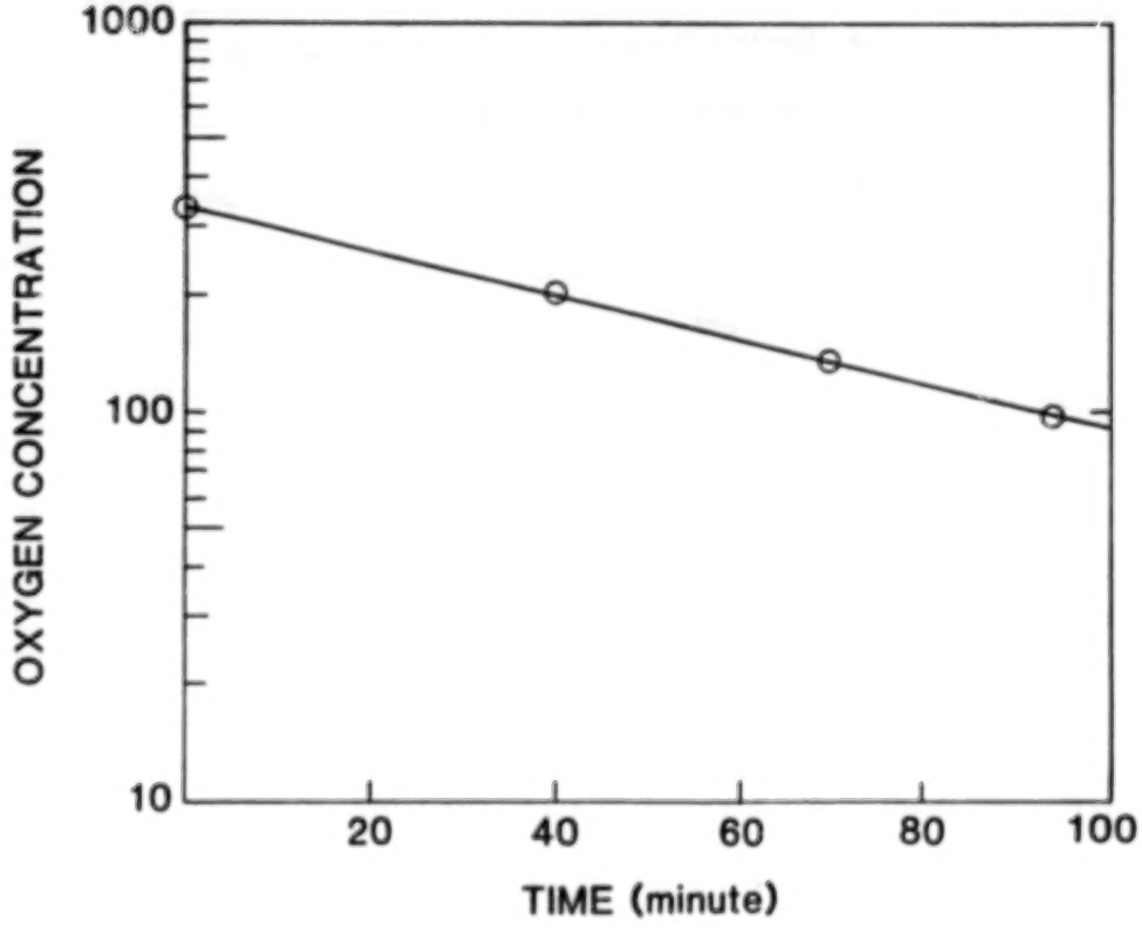

Figure 2. Purifier Performance: Gas Cleanup After 14,000 Shots

Table I

CORA WIDEBAND AMPLIFER - GENERAL INFORMATION

- Electron-Beam-Sustained Pulsed Discharge
- Gas Mix: 13:2:1 $He:N_2:CO_2$
- Clean System, Designed for $^{13}CO_2$ Isotope
- Parameters
  - 10-pps burst-mode operation of 10,000 shots
  - ~110-J/ℓ-atm energy loading
  - ~5-mA/cm^2 electron beam
  - 25-kV, 3.5-kA discharge
  - ~2.5-m active length
  - 2.5 ms^{-1} transverse flow through cavity
  - 2400 ℓ flow loop volume
    6200 ℓ total volume

NASA
National Aeronautics and Space Administration

Report Documentation Page

1. Report No.	2. Government Accession No.	3. Recipient's Catalog No.
NASA CP-10037		

4. Title and Subtitle	5. Report Date
CO Oxidation Catalysts for Long-Life CO_2 Lasers	October 1989
	6. Performing Organization Code

7. Author(s)	8. Performing Organization Report No.
David R. Schryer, Compiler	
	10. Work Unit No. 146-74-06-70

9. Performing Organization Name and Address	11. Contract or Grant No.
NASA Langley Research Center Hampton, VA 23665-5225	
	13. Type of Report and Period Covered
12. Sponsoring Agency Name and Address	Conference Publication
National Aeronautics and Space Administration Washington, DC 20546-0001 and Royal Signals and Radar Establishment Malvern, Worcester WR14 3PS, United Kingdom	14. Sponsoring Agency Code

15. Supplementary Notes

16. Abstract

This publication presents a collection of papers and extended abstracts of papers submitted for presentation at the "International Conference on CO Oxidation Catalysts for Long-Life CO_2 Lasers" held at the NASA Langley Research Center October 17-19, 1989. The conference was jointly sponsored by NASA and the Royal Signals and Radar Establishment (UK). The papers encompass a wide range of topics related to the development and testing of low-temperature, high-efficiency CO-oxidation catalysts with primary emphasis on their applicability to long-life, closed-cycle CO_2 lasers.

17. Key Words (Suggested by Author(s))	18. Distribution Statement
CO_2 Lasers CO Oxidation Catalysts	Unclassified - Unlimited Subject Category: 36

19. Security Classif. (of this report)	20. Security Classif. (of this page)	21. No. of pages	22. Price
Unclassified	Unclassified	145	A07

NASA FORM 1626 OCT 86 For sale by the National Technical Information Service, Springfield, Virginia 22161-2171

END

DATE

FILMED

AUG 16 1990